UNIVERSITY OF BRASILIA

POST GRADUATION PROGRAM IN CHEMISTRY

RECONSTRUCTION OF NEOGENE SEA SURFACE TEMPERATURES IN CEARA RISE (SOUTH ATLANTIC) BASED ON ALKENONES

Juliana Pinheiro Pires

Supervisors:

Prof. Dr. Fernanda Vasconcelos de Almeida

Dr. Jung-Hyun Kim

Brasilia – DF

2015

JULIANA PINHEIRO PIRES

RECONSTRUCTION OF NEOGENE SEA SURFACE TEMPERATURES IN CEARA RISE (SOUTH ATLANTIC) BASED ON ALKENONES

Dissertation submitted to the Institute of Chemistry, University of Brasilia, as a partial requirement for obtaining title of Master in Chemistry.

Area of concentration: Analytical Chemistry.

Supervisors: Prof. Dr. Fernanda Vasconcelos de Almeida and Dr. Jung-Hyun Kim.

Brasilia - DF

2015

APPROVAL SHEETF

Communicate the approval of the Dissertation Defesnse of Master of the student Juliana Pinheiro Pires, registration nº. 13/0086053, entitled "Reconstruction of Sea Surface Temperatures Neogene In Ceara Rise (South Atlantic) Based On Alkenones " presented at PADCT room of the Institute of Chemistry (IQ) of the University of Brasilia (UnB) on March 5, 2015 .

Prof. Dr. Fernanda Vasconcelos de Almeida
President of the sink (IQ/UnB)

Prof. Dr. Valéria Regina Bellotto
Titular Member (IQ/UnB)

Prof. Dr. Poliana Dutra Maia
Titular Member (FUP/UnB)

Prof. Dr. Marly Eiko Osugi
Substitute Member (IQ/UnB).

March 5, 2015

I dedicate this thesis to my parents Roberto and Maria Geralda,
who gave me unconditional support and do not measure efforts to
the realization of my dreams.

Dedico essa dissertação aos meus pais Roberto e Maria Geralda,
pelo apoio incondicional e por não medirem esforços para
a realização dos meus sonhos.

ACKNOWLEDGMENTS

Thank first to God for giving me strength and wisdom to walk the paths of graduation and master and overcome the difficulties.

To my parents, who were with me in the moments that I most needed and advised me in the most difficult moments. You are responsible for the person I have become. I love you.

To my sister Luciana and my boyfriend Jonatan, who endured my moments of anxiety and stress. Without the love, friendship and fellowship of you, I could not conclude this important stage of my life.

To the teacher Dr. Fernanda, who welcomed me in the laboratory and was always willing to listen and help me. Thank you for being my supervisor and giving me all the support necessary for the conclusion of this master.

To my supervisor Dr. Jung- Hung Kim, for sharing her experience and wisdom.

To Elsbeth Van Soelen, for all patience, attention and dedication and for being my partner in all stages of this master. Thank you.

To the AQQUA teachers, Valéria, Jez, Fernando, Ana Cristi and Alexandre, for being always available to help and answer questions.

To my colleagues in AQQUA Group, especially Angela, Gabriel, Tati, Rosy, Carla, Victor, Milena and Daniel, for sharing great moments of relaxation, laugh and for be always willing to help me.

To CNPq, for financial support.

To the ClimAmazon Project for financial support.

To UNB and the Institute of Chemistry.

And to all who were part of this history.

Thank you!

AGRADECIMENTOS

Agradeço primeiramente a Deus, por ter me concedido força e sabedoria para trilhar os caminhos da graduação e do mestrado e vencer as dificuldades.

Aos meus pais, que estiveram ao meu lado nos momentos que mais precisei e me aconselharam nos momentos mais dificeis. Vocês são os responsáveis pela pessoa que me tornei e devo aos dois tudo que já consegui. Amo vocês.

À minha irmã Luciana e ao meu namorado Jonatan, que aguentaram meus momentos de ansiedade e de estresse. Sem o carinho, a amizade e o companheirismo de vocês, eu não conseguiria concluir esta etapa tão importante de minha vida.

À professora Dra. Fernanda, que me acolheu no laboratório e sempre esteve disposta a me ouvir e ajudar. Obrigada por ser minha orientadora e me dar todo o suporte para que esse mestrado se realizasse.

À minha coorientadora Dra. Jung-Hung Kim, pela experiência e sabedoria.

À Elsbeth Van Soelen, por toda paciência, atenção e dedicação e por ser minha companheira em todas as etapas dessa dissertação. Muito obrigada.

Aos professores do AQQUA, Valéria, Jez, Fernando, Ana Cristi e Alexandre, por estarem sempre dispostos a ajudar e tirar dúvidas.

Aos colegas do Grupo AQQUA, especialmente Angela, Gabriel, Tati, Rosy, Carla, Victor, Milena e Daniel, por proporcionarem ótimos momentos de descontração, boas risadas e estarem sempre dispostos a me ajudar.

Ao CNPq e ao Projeto ClimAmazon, pelo auxílio financeiro.

À UnB e ao Instituto de Química.

E a todos que fizeram parte dessa história.

Muito Obrigada!

“The real voyage of discovery consists not in seeking new landscapes, but in having new eyes.”

Marcel Proust

“A verdadeira viagem de descobrimento não consiste em procurar novas paisagens, mas em ter novos olhos.”

Marcel Proust

ABSTRACT

PIRES, J. P. **Reconstruction of Neogene sea surface temperatures in Ceara Rise (South Atlantic) based on alkenones.** 2015. Dissertation (Master in Chemistry) – University of Brasilia, Brasilia, 2015.

The Ceara Rise is a seismic peak located in the Atlantic Ocean and receives both marine and terrigenous sediments. These sediments are important for understanding the paleoclimatic and paleo-environmental conditions in the ocean. With the goal of reconstructing the past sea surface temperature (SST), the lipid biomarkers n-alkanes and alkenones were analyzed in sediments of Ceara Rise. The quantification of both biomarkers was performed by Gas Chromatography with Flame Ionization Detector (GC-FID). For the n-alkanes, analytical curves, which resulted in acceptable figures of merit by official norms and the National Institute of Metrology, Quality and Technology (Inmetro) were built. Because there is no alkenone standard commercially available for the construction of analytical curves for alkenones, the quantification was done by comparison of the areas of analytes to the area of a standard ketone commercially available. The quantification by comparison areas was validated by T-Test, in which the values of concentration of n-alkanes obtained for this quantification method were compared with the calculated concentrations from analytical curves, which led to satisfactory results. The n-alkanes were evaluated according to the proxies Carbon Preference Index (CPI) and Average Carbon Length (ACL). The results suggest that the main source of organic matter in the studied sediments originates from terrigenous material transported by rivers and by wind action. The , proxy that use the concentration of alkenones to calculate the SST, was used for climatic reconstruction of the region. The concentration range of alkenones was 0.001 to 0.516 µg g-1. According to the result of proxy, the estimated lowest temperature was 22.5 °C, toward the end of Early Miocene, while the highest temperature, 28.5 ° C, was held at half the Early Oligocene.

Keyword: Ceara Rise, Sediments, CPI, ACL, and SST

LIST OF FIGURES

LIST OF TABLES

LIST OF ABBREVIATIONS AND ACRONYMS

ANVISA	National Health Surveillance Agency
ACL	Average Chain Length
AQQUA	Grupo de Automação, Quimiometria e Química Ambiental
Be	Berilium
C-22	*N*-docosane
C-23	*N*-tricosane
C-24	*N*-tetracosane
C-25	*N*-pentacosane
C-26	*N*-hexacosane
C-27	*N*-heptactosane
C-28	*N*-octacosane
C-29	*N*-nonacosane
C-30	*N*-triancontane
C-31	*N*-hentriacontane
C-32	*N*-dotriacontane
C-33	*N*-titriacontane
C-34	*N*-tetratriacontane
C-35	*N*-pentatriacontane
$C_{37:2}$	Alkenone with 37 carbons and two unsaturations
$C_{37:3}$	Alkenone with 37 carbons and three unsaturations
$C_{37:4}$	Alkenone with 37 carbons and four unsaturations
$C_{38:2}$	Alkenone with 38 carbons and two unsaturations
$C_{38:3}$	Alkenone with 38 carbons and three unsaturations
CRA	Core Recovery A
CRB	Core Recovery B
CO_2	Carbon Dioxide
CV	Coefficient of Variation
CPI	Carbon Index Preference
DCM	Dichloromethane

DSDP	Deep Sea Drilling Project
Et	Ethyl
FID	Flame Ionization Detector
GC	Gas Chromatograph
GDGT	Glycerol Diakyl Glycerol Tetraethers
ICH	International Conference of Harmonization
INMETRO	Instituto Nacional de Metrologia, Qualidade e Tecnologia
IS	Internal standard
KYR	Thousand years
LOD	Limit of Detection
LOQ	Limit of Quantification
Ma	Million Years Ago
mbsf	Meters below sea floor
Me	Methyl
MeOH	Methanol
Na_2SO_4	Sodium Sulfate
N_2	Nitrogen gas
NOAA	National Oceanic and Atmospheric Administration
ODP	Ocean Drilling Project
OLR	Out of Linear Range
pA	Picoampere
R	Correlation Coefficient
RT	Retetion Time
SD	Standard of Desviation
SST	Sea Surface Temperature
TLE	Total Lipid Extract
UCM	Unresolved Complex Mixture
UnB	Universidade de Brasília
	Unsaturation Ketone Index

SUMARY

1. INTRODUCTION

Studies based on past climate change are frequently used to understand current climates trends and also making forecasts. The main climate data refer to rainfall patterns and temperature variations (VILLALBA *et al*., 2009).

The tools proxies are equations that relate proportions of molecules with different environmental conditions. They play an important role in the reconstruction of temperature profiles and are widely used in paleoenvironmental studies as a natural register of environmental changes (CASTAÑEDA *et al*.,2008; MANN *et al.*, 2008). Among the various proxies applied to achieve this goal, those using organic molecules considered biomarkers have shown great potential for application in determining the surface temperature of the sea.

The determination of sea surface temperature (SST) is one of the fundamental parameter for the reconstruction of past climate conditions, as well as for understanding the hydrological cycle and wind systems. (EGLINTON *et al*., 2008).

Considering these aspects, the present study aims to evaluate the temperature changes on sediment core from the Ocean Drilling Program (ODP) 154, site 925 using lipid biomarkers. Site 925 sediment samples were retrieved in the Ceara Rise (South Atlantic), located 800 kilometers east of the mouth of Amazon River. The sediments contain organic matter derived from both terrestrial and marine sources. Therefore, core site 925 will provide valuable information which can help to link paleoenvironmental and paleoclimatic conditions on land to those in the ocean.

This study is part of the international project CLIM-AMAZON, the joint Brazilian-European research facility for climate and geodynamic research on the Amazon River basin sediments. The main objectives of this project were:

i. to set up the analytical structure for the extraction and analysis of lipid biomarkers in sediment samples in the analytical chemistry laboratory at the Chemistry Institute in the University of Brasilia (UnB), AQQUA group;

ii. to analyze *n*-alkanes and alkenones, two types of lipid biomarkers, in marine core sediments of Ceara Rise (South Atlantic) at different core depth levels;

iii. to generate analytical data for reconstruct the past sea surface temperatures from the Miocene to the Holocene in the Ceara Rise.

2. BIBLIOGRAPHIC REVIEW

2.1 CENOZOIC CLIMATE EVOLUTION

The Cenozoic, the most recent era, covers the period from 65.5 million years ago (Ma) to present (Appendix A). This era is divided into three sub-periods: Paleogene (65.5 - 23 Ma), Neogene (23 – 2.5 Ma, the sub-period containing the Miocene and Pliocene epochs) and Quaternary (2.5 Ma to the present day) (HELMOND, 2010).

The Cenozoic presents a complex climatic evolution and this information is obtained mainly from the study of deep-sea sediment cores. In general, climate changes over time are driven by shift in the distribution of sunlight (LISIECKI *et al.*, 2007), tectonic processes (FEARY *et al*., 1990) and orbital cycles (ZACHOS *et al*., 2001).

Due to the high temperatures recorded during the early Cenozoic, the planet was characterized as 'Greenhouse World' (HELMOND, 2010). The concentration of greenhouse gases, mostly from volcanic emissions, is among the facts that led to this high temperature, because the partial pressure of gases such as carbon dioxide (CO_2) affects the level of precipitations, the stability of the ice sheets and atmospheric and oceanic circulation. In a period of less than 10,000 years in the transition between the Paleocene and Eocene (~ 55 Ma), an increase of approximately 5 °C was recorded (ZACHOS *et al*., 2008). This warming trend has spread from the early Eocene (~ 50 Ma), period in which there were records of extreme high temperatures, until the Oligocene (~ 33 Ma) (PEARSON *et al*., 2007).

From then, the lowering of the concentration of greenhouse gases has shown that climatic evolution was characterized by a global cooling trend, and this coincided with the appearance of glaciers in Antarctica (PEARSON *et al.*, 2007). The trend to lower temperatures, which persisted until the late Oligocene (FEARY *et al.*, 1990; ZACHOS *et al*., 2001), could be demonstrated by increase in the

concentration of oxygen isotopes ($\delta^{18}O$), parameter used to study changes in volume of ice and water temperature (LISIECKI *et al*., 2007; PEARSON *et al.*, 2007; ZACHOS *et al*., 2001;. ZACHOS *et al.*, 2008). Cooling happened milder in the tropics but, at the poles, led to a decline of 5-10 °C in SST (PEARSON *et al*., 2007).

In the middle Miocene (15 Ma) and early Pliocene (6 Ma) small intervals of heat were registered, resulting in a reduction in the volume of glaciers. However, it is observed that the general trend in the Cenozoic was the global cooling, due mainly to the expansion of ocean passages and thermal isolation of Antarctica (FEARY *et al*., 1990; ZACHOS *et al*., 2001; LISIECKI *et al*., 2007).

The climatic changes that occurred during the Neogene are especially important because they resulted in significant impacts on the fauna and flora, giving rise to modern climatic regimes and biomes (PETER *et al*., 2004).

It is estimated that at the end of the century, the concentration of CO_2 in the atmosphere will be similar to what occurred in the warm period of the early Pliocene, in which the SST was 3 ° C warmer than the currently registered. Thus, understanding climate changes that occurred in the Neogene is of fundamental importance to predict the futures climate trends (HAYWOOD *et al*., 2009).

The regional impact of such changes, for instance on the Amazon basin, is yet unclear. The marine sediment cores, which contain both terrestrial and marine organic matter allow understanding the relationship between the oceanic and climatic conditions, from the Miocene to the present day. This is possible through the analysis of organic material recovered outside the Amazon Basin in Ceara Rise (South Atlantic). Climatic variations in this region may also serve to understanding climate dynamics that affect various parts of the globe (BOOT, *et al*., 2006).

2.2. LIPID BIOMARKER PROXY FOR CLIMATE RECONSTRUCTION

Proxies can relate the variation of temperature with environmental changes through a calibration, which allows to estimate the climatic conditions over the years (CASTAÑEDA *et al*., 2008; MANN *et al*., 2008).

The determination of SST is one of the fundamental parameters for the reconstruction of past conditions, as well as for understanding the hydrological and wind systems (ENGLITON *et al*., 2008; KIM *et al*., 2009). SST also influences air temperature, once the land surface has a lower specific heat than the water bodies (FRITZSONS *et al*., 2008).

For the determination of SST, there are temperature proxies that were developed from the study of geochemical properties, such as the ratio of isotopes of carbon or oxygen, primary tool for climatic reconstruction of the Cenozoic (FEARY *et al*., 1991; ZACHOS *et al*., 2001). However, proxies that use information at the molecular level are more specific because they do not require many additional data to the definition of profiles (VILLALBA *et al*., 2009; CASTAÑEDA *et al*., 2008; EGLINTON *et al*., 2008; EIGENBROD *et al*., 2010). The biological markers, known as biomarkers, are the major organic molecules used for this form of proxy.

Biomarkers are complex organic molecules derived from living organisms, especially plants and bacteria, which may be deposited with the sediments and provide environmental information from the time they were deposited. Their concentration depends on factors such as ocean temperature and light level (CASTAÑEDA *et al*., 2008; EGLINTON *et al*., 2008; SMITH *et al*., 2013; BLYTH *et al*., 2008; MEYERS *et al*.,2003; SACHS *et al*., 2013; SPERA *et al*., 2012). They are widely applied in the stratigraphic temporal resolution because

they possess a high degree of preservation (CASTAÑEDA *et al*.,2008; EGLINTON *et al*., 2008; BLYTH *et al*., 2008).

One of the major organic biomarkers for studying paleotemperatures variation are alkenones, long chain ketones which have 37 carbons with two, three or four unsaturations ($C_{37:2}$, $C_{37:3}$ and $C_{37:4}$, respectively) or 38 carbons with two or three unsaturations ($C_{38:2}$, $C_{38:3}$, respectively) (Figure 1). They are produced mainly by two species of unicellular algae: *Emiliania huxluji* and *Geophyrocpsa oceanica* (CASTAÑEDA *et al*., 2008; EGLINTON *et al*., 2008; SACHS *et al*., 2013; HEBERT *et al*., 2003.). These algae reside above the photic zone and require sunlight for photosynthesis (CASTAÑEDA *et al*., 2008; EGLINTON *et al*., 2008; SACHS *et al*., 2013).

Figure 1. Structure of methyl (Me) and ethyl (Et) long-chain alkenones. The position of the double bounds are indicated by red circles. Adapted from CASTAÑEDA et al., 2008.

By using the alkenones abundance it is possible to calculate the unsaturation index of ketones ( ) (Equation 1), a proxy developed by Brassel *et al.* in 1986 and considered one of the oldest and most applied proxies that use ratio of organic compounds (CASTAÑEDA *et al*., 2008; EGLINTON *et al*., 2008; SACHS *et al*., 2008; KIM *et al*., 2009; PRAHL *et al*., 2006).

A marine sediment core study showed that the index was sensitive to paleotemperature fluctuations in the late Pleistocene (BRASSEL *et al*., 1986), showing that when the temperature of the sea surface increases, the concentration of $C_{37:3}$ decreases relative to the concentration of $C_{37:2}$ (Figure 2) (CASTAÑEDA *et al*., 2008; EGLINTON *et al*., 2008).

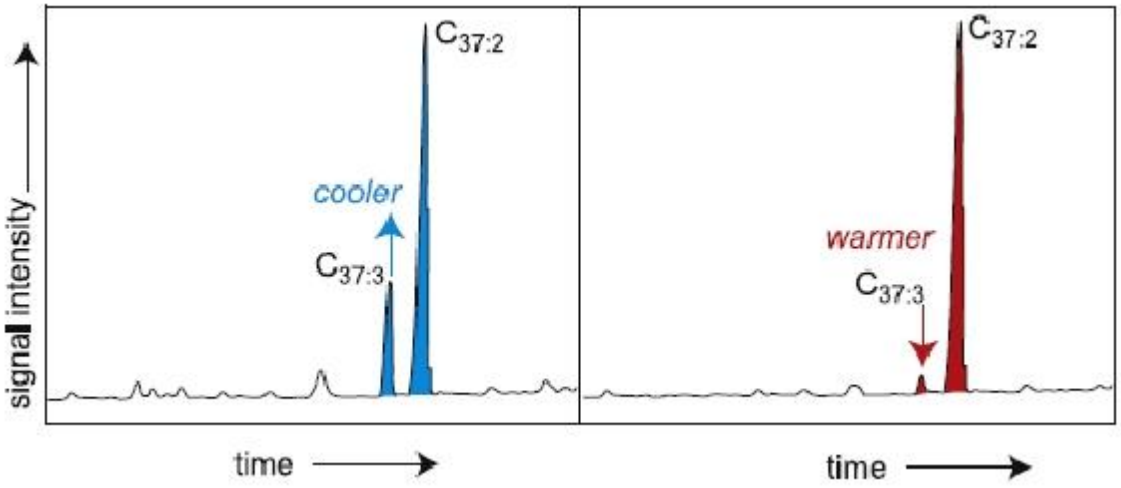

Figure 2. Illustration of the SST proxy. On the left, gas chromatogram of a sample with relatively cooler signal than the chromatogram on the right. Adapted from CASTAÑEDA et al., 2008.

Later studies by Prahl *et al.* (1987) showed that the concentration of $C_{37:4}$ in sediments was very low and did not produce significant differences in SST. Thus, the index developed by Brassel *et al.* was modified, generating (Equation 2), in which the concentration of $C_{37:4}$ is disregarded (CASTAÑEDA *et al*., 2008; SMITH *et al*., 2013; SACHS *et al*., 2013). The index relates to SST according to the Equation 3.

where is the proxy that relates the concentration of alkenones with 37 carbon atoms and two and three unsaturation, [$C_{37:2}$] and [$C_{37:3}$] respectively, and SST is the sea surface temperature (CASTAÑEDA *et al*., 2008; EGLINTON *et al*., 2008; SMITH *et al*., 2013; PRAHL *et al*., 2006).

This proxy presents an empirical relationship between and SST and the calculated values vary between zero and one. According to the literature, when assumes a value equal to one unit, it follows that the SST is equivalent to 29 °C, with some variations, because the constant calculation can take different values, which depend on the region where the calibration was performed (EGLINTON *et al*., 2008; FRITZSONS *et al*., 2008; TONEY *et al*., 2012).

2.3. PROXIES CARBON PREFERENCE INDEX AND AVERAGE CHAIN LENGTH AND SOURCE OF *N*-ALKANES

The *n*-alkanes (long-chain hydrocarbons) are biomarkers which provide important paleoenvironmental informations as well as alkenones. Through information on the size of the chains or distribution of the number of carbons it is possible to identify whether there is a predominance of terrigenous material taken to the sea or if these *n*-alkanes are produced in water bodies (CASTAÑEDA *et al*., 2008; DUAN *et al*., 2010).

Carbon preference index (CPI) measures the relative abundance of odd over even carbon chain lengths (CASTAÑEDA *et al.*, 2008; JENG *et al*., 2006). CPI is calculated according to equation 4.

$$CPI = -X \frac{\text{———————————}}{\text{———————————}} \quad (4)$$

where C25 and C26 are respectively the concentration of *n*-alkanes that have 25 to 26 carbons and so forth.

If the calculated value for the CPI is between 5 and 10, there is a predominance of chains with odd number of carbons, meaning that the source of *n*-alkanes is predominantly from terrigenous plants (JENG *et al*., 2006). Most of these *n*-alkanes with odd chains are derived from the wax layer that coats the leaves (EGLINTON *et al*., 1962). These waxes help protect the leaves, inhibiting insect attack, reducing water loss and protecting against excessive ultraviolet radiation (EGLINTON *et al*., 1967; EGLINTON *et al*., 2008; SPERA, 2012; CASTAÑEDA *et al*., 2008; DUAN *et al*., 2010).

CPI values near 1 indicate predominance of chains with even carbon number. In most cases, these alkanes are produced by marine microorganisms or introduced by petrogenic contamination (JENG *et al*., 2006).

The value obtained from the average chain length (ACL) has relation with the origin of *n*-alkanes and with the temperature. The ACL is based on the relationship between the average number of carbon atoms and the abundance of odd carbons, as shown in Equation 5. Low values of ACL indicate that the source of *n*-alkanes is predominantly from marine organisms or petrogenic hydrocarbons, similar to the CPI, presenting a linear relationship between these two proxies (JENG *et al*., 2006). On the other hand, low values of ACL also indicate the record of colder temperatures (JENG *et al*., 2006; MEYERS *et al*., 2003; CASTAÑEDA *et al*., 2008).

$$ACL = \frac{\qquad\qquad\qquad\qquad\qquad\qquad\qquad\qquad\qquad\qquad}{} \qquad (5)$$

2.4. STUDY AREA

Ceara Rise, a seismic ridge currently situated 2600-3200 meters below sea level, is located in the Atlantic Ocean (Figure 3) some 800 kilometers east of the Amazon River, surrounded on the north, west and south by distal deposits from Amazon Fan (HEINRICH *et al*., 2013).

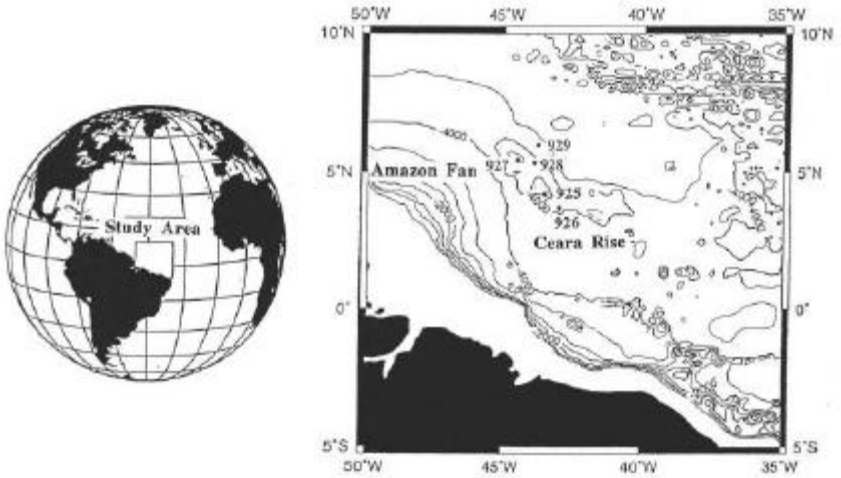

Figure 3. Location of Ceara Rise in the Atlantic Ocean. Adapted from CURRY *et al.,* 1994.

Some 80 million years ago, estimated time of origin of Ceara Rise according to studies by the age of igneous base ascension (SUPKO *et al*., 1977), the region was subjected to intense volcanic extrusion, generating fractures up to 2 km thick. This period was marked by fits of plates in the North and South Atlantic, generating an unusual volcanic activity (KUMAR *et al*., 1977).

After the cessation of extrusive activity, the volcanic pile resulting from such seismic activity was divided into two segments (Figure 4): the Ceara Rise, to the west, and the Sierra Leone Rise, to the east (KUMAR *et al*., 1977).

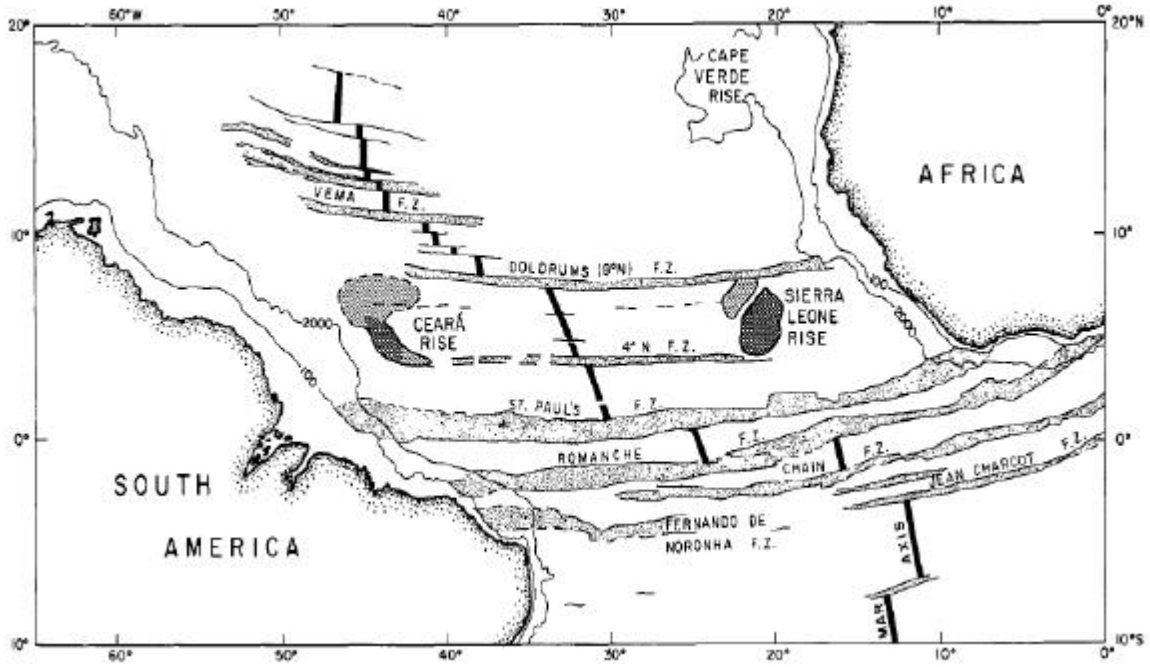

Figure 4. Structural map of the equatorial Atlantic and of the boundaries of the Ceara Rise and Sierra Leone Rise, from KUMAR *et al.,* 1977.

Since its formation, the deposition of limestone and siliceous material has decreased the elevation of the Ceara Rise. However, with the growth of Amazon Fan in the Early Miocene, there was also the intensification of influx of terrigenous material, which is greater during periods of low sea level and generated a very high sedimentation in the region (KUMAR *et al*., 1977; HEINRICH *et al*., 2013).

Amazon Fan is a body of sediments of deep submarine water located on the continental margins of Brazil and contains eroded material of the Amazon River basin. With sediments originated from this place it is possible to understand the effect of climate changes that occurred during the Quaternary, because the equatorial regions played an important role in transporting heat to high latitudes in this period (FLOOD *et al*., 1997). Thus, the main source of terrigenous material

present in Ceara Rise comes from Amazon (KUMAR *et al*., 1977), which makes it able to monitor the changes that have occurred over the years in the region (DOBSON *et al*., 2001).

This terrigenous material is usually deposited in the deepest parts of the rise, which has distinct stratigraphic sequence due to the deposition of clays and silts. In the higher parts of the Ceara Rise, where the sedimentation rate is low, the main constitution of sediments is pelagic material, in other words, it comes from the open sea (KUMAR *et al*., 1977).

There are also certain areas of hemipelagics sediments, consisting of both terrigenous and pelagic material. Thus, it is observed that the distribution of sediments has large influence of deepwater's movement (KUMAR *et al*., 1977). The depth of the sea that surrounds the Ceara Rise is approximately 4500 meters and surface waters show little seasonal variability (HEINRICH *et al*., 2013).

Therefore, the region is essential for understanding the dynamics of the climatic phenomena occurred near the Amazon Fan, one of the largest modern submarine fans (FLOOD *et al*., 1997).

2.4.1. PREVIOUS WORK

The present study is a continuation of the work developed by Dobson *et al*. (2001) and other researchers, as Curry *et al*. (1995) and Murayama *et al*. (1997), who also studied and analyzed different properties of the samples collected in Ceara Rise, site 925.

The work of Curry *et al*. (1995) presents a detailed description of sampling performed at site 925, specifying the drilling techniques, the division of the core into subparts and the relationship between depth and age of each sample, obtained through the study of calcareous nannofossils. Curry *et al*. (1995)

presented data of percentage of carbonates, magnetic susceptibility measurements, particle size and x-ray diffraction analyses, besides lithostratigraphic description of the samples (Appendix B).

Murayama et al. (1997) studied samples from site 925 Hole B, to evaluate the variation of ^{10}Be, based on the rate of accumulation of sediments, to explain the input of terrigenous material from the area of the Amazon drainage. They concluded that the ratio between ^{10}Be and ^{9}Be was nearly constant and decreases with depth. In addition, ^{10}Be is mainly associated with terrigenous fraction.

Subsequently, Dobson *et al.* (1997) performed chemical extractions to isolate components and calculate the terrigenous mass accumulation rates of 47 sediment samples from Ceara Rise. From the analysis of the elemental composition, they observed both terrigenous material source and the rate of accumulation of mass changed over the years, probably due to the influence of Andean uplift and the increase of the flow of the Amazon River.

In a following study, Dobson *et al*. (2001) evaluated the sources of river discharge in South America describing the rate of accumulation of mass in other 57 core sediment samples from Ceara Rise.

Recently, Heinrich et al. (2013) studied the content of calcareous dinoflagellate in sediment samples in Ceara Rise that corresponded to the Neogene. The fossils of these species that develop in the oceans are able to reflect the aquatic environment. They are also tools used for understanding the oceanographic changes, the development of the Amazon River and the conditions of the water surface in the Ceara Rise, site 926, where there were low acumulation rates of calcareous dinoflagellates under 12 Ma and the subsequent increase reflects differences in dissolution and preservation.

3. MATERIALS AND METHODS

3.1. SAMPLE COLLECTION AND PREPARATION

The sediments used in this study are originated from the exploration site 925, on the top of the Ceara Rise (Figure 5). The expedition took place in 1994 and the samples were collected by Curry *et al*. To ensure the completeness of information from core samples, three parallel holes (A, B and C) were made, and in this study two of them are analyzed, A and B. The samples originated from the site 925 A vary between 303 and 660 meters below seafloor (mbsf). However, the samples from site 925 B vary between zero and 312 mbsf. These intervals range from the early Oligocene (~30 million years ago) to the present day (CURRY *et al*., 1995). The depth and the corresponding age (Tables 1 and Table 2) for each sample were obtained through the study of nannofossil (CURRY *et al*., 1995). Information about holes A and B are shown in Table 3.

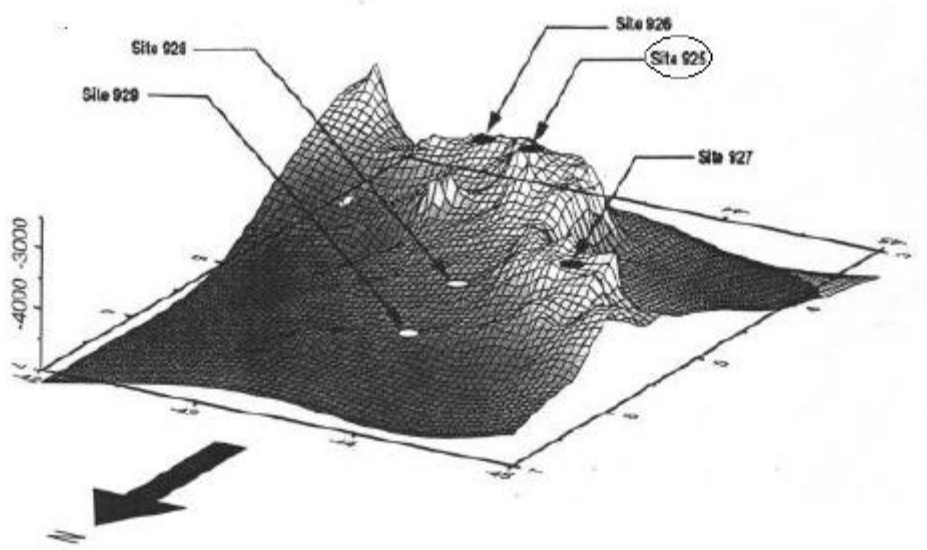

Figure 5. Pesperctive view of Ceara Rise, ODP 154, site 925. Adapted from CURRY *et al*., 1994.

Table 1. Information about the Core Recovery A (CRA): period, age, sample´s name and depth.

Expedition 154 Site 925 Hole A			
Period	Age (Ma)	Sample Name	Depth (mbsf)
Middle Miocene	12.88	CRA 3 R1	304.65
	13.42	CRA 4 R1	314.28
	13.96	CRA 5 R1	323.92
Early Miocene	14.21	CRA 5 R4	328.92
	14.51	CRA 6 R1	333.72
	14.71	CRA 6 R3	337.21
	15.19	CRA 7 R3	345.76
	16.05	CRA 8 R6	360.70
	16.45	CRA 9 R4	367.81
	16.75	CRA 10 R1	372.98
	17.25	CRA 11 R1	381.71
	17.66	CRA 11 R6	389.02
	17.78	CRA 12 R1	391.03
	18.33	CRA 13 R1	400.88
	18.85	CRA 14 R1	410.06
	19.19	CRA 14 R5	416.01
	19.45	CRA 15 R1	420.67
	20.21	CRA 16 R4	434.47
	20.70	CRA 17 R3	443.27
	21.15	CRA 18 R3	451.68
	22.04	CRA 20 R1	468.35
	22.29	CRA 20 R4	472.96
	23.18	CRA 22 R3	490.36
	23.49	CRA 22 R7	496.36
	23.72	CRA 23 R3	501.06
	24.02	CRA 24 R1	507.04
	24.92	CRA 26 R1	525.73
	25.35	CRA 26 R8	535.06
Late Oligocene	26.25	CRA 29 R1	555.02
	26.90	CRA 30 R5	570.35
	27.46	CRA 32 R1	583.88
Early Oligocene	28.13	CRA 33 R6	601.02
	29.25	CRA 36 R7	631.56
	30.10	CRA 39 R4	656.41

Table 2. Information about the Core Recovery B (CRB): period, age, sample´s name and depth.

Expedition 154 Site 925 Hole B			
Period	Age (Ma)	Sample Name	Depth (mbsf)
Pleistocene	0.02	CRB 1 H1	0.92
	0.26	CRB 2 H3	7.95
	0.65	CRB 3 H4	19.64
	0.91	CRB 4 H3	27.50
	1.58	CRB 6 H4	47.58
Late Pliocene	1.73	CRB 7 H1	52.15
	1.84	CRB 7 H3	55.53
	1.94	CRB 7 H5	58.40
	2.17	CRB 8 H3	65.36
Middle Pliocene	2.50	CRB 9 H3	74.86
	3.16	CRB 11 H3	93.87
	3.31	CRB 11 H6	97.93
Early Pliocene	3.94	CRB 13 H5	115.25
	4.22	CRB 14 H3	122.50
	4.50	CRB 15 H2	129.80
	4.92	CRB 16 H3	140.55
	5.23	CRB 17 H1	148.04
Late Miocene	5.43	CRB 17 H5	153.10
	5.75	CRB 18 H3	160.72
	6.31	CRB 19 H6	173.78
	6.75	CRB 20 H6	183.60
	6.95	CRB 21 H3	188.19
	7.24	CRB 21 H7	194.44
	8.34	CRB 24 H3	217.72
	9.06	CRB 25 H7	232.43
	9.26	CRB 26 H3	236.41
	9.49	CRB 26 H6	241.04
	9.79	CRB 27 H4	246.96
Middle Miocene	10.02	CRB 27 H7	251.29
	10.21	CRB 28 H3	255.09
	10.53	CRB 28 H7	261.18
	10.78	CRB 29 H4	265.94
	11.22	CRB 30 H3	274.27
	11.53	CRB 30 H7	279.93
	11.84	CRB 31 H4	285.69
	12.24	CRB 32 H3	293.00
	12.55	CRB 32 H7	298.60
	13.07	CRB 33 H7	308.10

Table 3. Basic information of the studied exploration core.

Core Code	ODP 154 SITE 925 A	ODP 154 SITE 925 B
Lat/long (°)	4°12.249 N, 43°29.334 W	4°12.248 N, 43°29.349 W
End depth (m)	930,4	318
Begin date	14th february 1994	8th february 1994
End date	19th february 1994	10th february 1994
Objective	Study the history of deep-water circulation	

In total, 72 sediment samples were analyzed in the present work. The samples were stored in bags at -18 °C until lab analyses.

3.2. ORGANIC GEOCHEMISTRY

3.2.1. CLEANING GLASSWARE

Initially, all glassware were washed with detergent and tap water. Then, the materials were washed with deionized water and maintained for at least one night in a solution 2-5 % of Extran MA 02 in deionized water. Removed from the detergent solution, the materials were washed with deionized water and dried in an oven at 100 °C for 2 hours. Finally, the openings of the recipients were sealed with aluminum foil. During laboratory work, each material was washed twice with methanol (MeOH) and twice with dichloromethane (DCM) before use.

3.2.2. LIPID EXTRACTION AND PURIFICATION

3.2.2.1. EXTRACTION OF ALKENONES AND *N*-ALKANES

For biomarker analysis, about 15 g of each sample was wrapped in aluminum foil and freeze dried (Liotop L101) for 24 hours. After drying, the samples were homogenized using a mortar and pestle until it formed a fine powder.

3 g of the homogenized sample were placed in centrifuge tubes and 5 mL of DCM/MeOH (2/1) solution was added (Figure 6). The centrifuge tube was placed in an ultrasonic bath (Cole-Parmer 8893) for 5 min and subsequently centrifuged at 300 rpm for 5 min (Kindly KCS). The supernatant was collected and the extraction procedure was repeated four more times.

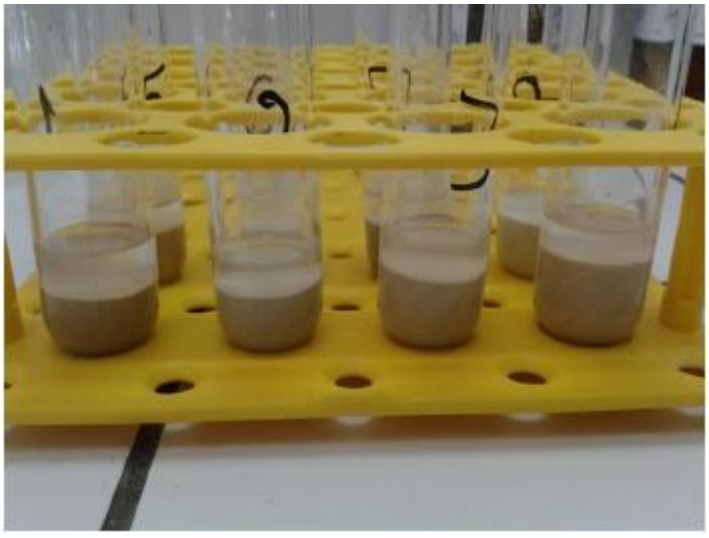

Figure 6. Extracts of sediment samples from Ceara Rise.

The resulting total lipid extract (TLE) was evaporated on a rotary evaporator (IKA RV 10 Basic) with heating bath at 30 °C. The final volume was transferred to a previously weighed vial of 4 mL through a column containing sodium sulfate (Na_2SO_4) and cotton at the bottom (Figure 7) and then completely dried by a stream of nitrogen (N_2). The vial was weighed to obtain the total mass of

TLE. 100 µL of each internal standard solution (scalene and ketone) were added to the TLE and the extract was dried again. The method used was adapted from the work of Kim *et al*. (2009), followed by validation.

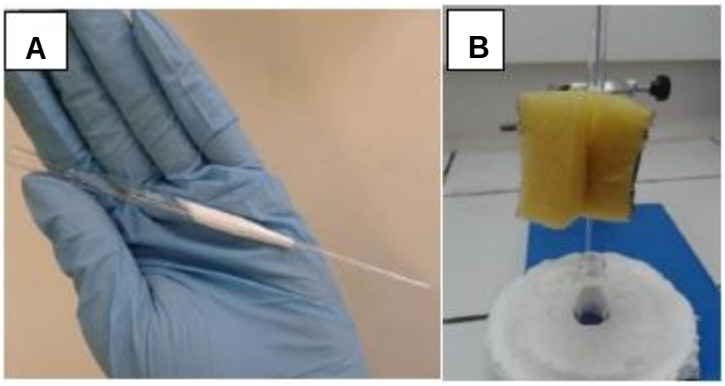

Figure 7. (A) Sodium sulfate column prepared in a Pasteur pipette and (B) system to transfer the extract to the vial through the column.

3.2.2.2. PREPARATION OF INTERNAL STANDARDS

The internal standard used for analysis of alkenones was prepared using a solution of 2-nonadecanone in hexane. To prepare the solution, 10 mg of 2-nonadecanone was weighed (Shimadzu Model AX200) in a vial and successive dilutions were made to obtain the concentration of 1 µg mL^{-1}. The process for the preparation of solution of squalene in hexane (1 µg mL^{-1}) used as internal standard in the nonpolar fraction was the same used for alkenones.

3.2.2.3. SEPARATION OF FRACTIONS OF ALKENONES AND *N*-ALKANES

To separate the TLE in fractions containing *n*-alkanes, alkenones and the polar compounds, a column containing aluminum oxide was prepared. To activate,

the aluminum oxide was kept in an oven at 150 °C for 2 hours and placed in a desiccator for 1 hour with desiccant agent. To prepare the column, it was used a small pipette with cotton at the bottom and approximately 4 cm of aluminum oxide.

First, the TLE was diluted in 2.5 mL of hexane/DCM (9/1) and transferred to the column. The column was then washed twice with 2.5 mL of hexane/DCM (9/1) solution to elute the nonpolar fraction of TLE.

For separating the fraction corresponding to alkenones, the vial that contained the extract was washed with a 2.5 mL of hexane/DCM (1/1) solution three times and transferred to a previously weighed vial of 1 mL using the same column used for the nonpolar fraction.

To separate the fraction corresponding to polar compounds, the procedure described above was repeated using 2.5 mL of DCM/MeOH (1/1) solution.

Finally, the solvent of each fraction was completed evaporated using nitrogen flow and the mass of each fraction was determined. The scheme of the analytical work is illustrated on Figure 8.

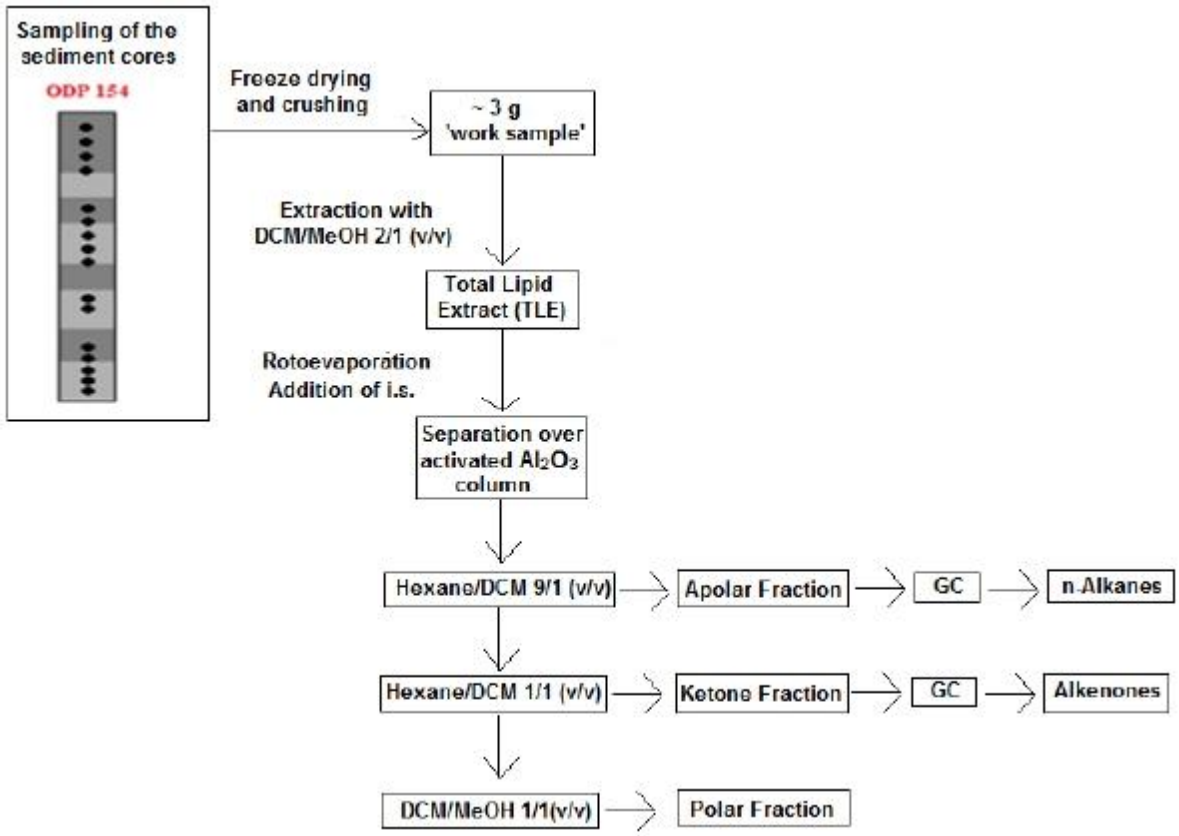

Figure 8. General scheme of the analytical work flow.

3.2.3. DETERMINATION AND QUANTIFICATION OF ALKENONES

The fraction corresponding to the alkenones was analyzed using a model 7890A Gas Chromatograph coupled to a Flame Ionization Detector (GC-FID from Agilent Technologies). All samples were dissolved in 50 µL of hexane and injected using an Agilent 7650A autosampler. The column used was a silica capillary (phase DB-5, 25 m x 0.32 mm, film thickness 0.25 µm). The injected sample volume was 1 µL and the column flow was 2.4 mL min^{-1}, at constant pressure.

The quantification of alkenones was taken in relation to the integration of the area under the peak. The area under the peak of alkenones was obtained and compared to the area under the peak of the internal standard. Each component was identified based on retention time.

3.2.4. DETERMINATION AND QUANTIFICATION OF *N*-ALKANES

The fraction corresponding to the *n*-alkanes was analyzed by GC-FID (same equipment used for alkenones quantification, Figure 9) and quantification of *n*-alkanes was taken in relation to the integration of the area under the peak. The area under the peak of *n*-alkanes was obtained and compared to the area under the peak of the internal standard.

Additionally, an analytical curve was made. This curve served as a tool for assessment the internal standard quantification method.

For building the analytical curve, 1.1 mL of *n*-alkanes standard solution (Supelco Analytical C8-C40 Alkanes Calibration Std, 500-5000 µg mL^{-1} in CH_2Cl_2) was diluted to 10 mL of hexane. The eight points of the analytical curve was constructed (0.055, 0.165, 0.33, 0.66, 1.1, 2.2, 4.4 and 5.5 µg mL^{-1}) with successive dilutions of the standard.

The standards used to construct the analytical curve are listed in Table 4.

Table 4. Information about the standard used to make the analytical curve.

Register number	Number of carbon	Name	Concentration (µg mL^{-1})
629-97-0	22	*N*-Docosane	499.0
638-67-5	23	*N*-Tricosane	500.5
646-31-1	24	*N*-Tetracosane	501.0
629-99-2	25	*N*-Pentacosane	501.0
630-01-3	26	*N*-Hexacosane	500.5
593-49-7	27	*N*-Heptacosane	501.0
630-02-4	28	*N*-Octacosane	501.0
630-03-5	29	*N*-Nonacosane	500.0

638-68-6	30	*N*-Triacontane	500.5
630-03-8	31	*N*-Hentriacontane	500.0
544-85-4	32	*N*-Dotriacontane	500.5
630-05-7	33	*N*-Tritriacontane	501.1
14167-59-0	34	*N*-Tetratriacontane	500.0
630-07-9	35	*N*-Pentatriancontane	500.1

Figure 9. Gas chromatography with flame ionization detector (GC-FID) Agilent 7650A.

The parameters used in the determination of alkenones and *n*-alkanes are summarized in the Table 5.

Table 5. Chromatographic parameters of the GC-FID used in the determination of alkenones and *n*-alkanes.

	Parameters	Alkenones method	*N*-alkanes method
Injector	Temperature (°C)	300	300
	Injection mode	Splitless	Splitless
	Purge flow to split vent	40 mL min^{-1} at 0.5 min	40 mL min^{-1} at 0.5 min
	Carrier gas	Helium	Helium
Column	Temperature programming	70 °C (hold time 0 min); 20 °C min^{-1} until 200 °C; 3 °C min^{-1} until 320 °C; 320 °C during 25 min	70 °C (hold time 0 min); 20 °C min^{-1} until 130 °C; 4 °C min^{-1} until 320 °C; 320 °C during 30 min
	Pressure	Constant	Constant
	Total run time (min)	71	71
Detector	Temperature (°C)	330	330
	Make up gas	Nitrogen	Nitrogen
	Flow (mL min^{-1})	24	24

3.3. VALIDATION

3.3.1. DETERMINATION OF OUTLIERS IN ANALYTICAL CURVES

Grubb's test, known as G test, was used to verify the possible presence of outliers in the analytical curves. In this test, the sample standard deviation is compared with the deviation of the suspected measured in relation to the media, according to equation 6:

$$G = \frac{\quad}{\quad} \qquad (6)$$

Where x is the value of the measure, is the average value and s is the standard deviation. If the calculated value of G is greater than the tabular value, the measure is an outlier and should be excluded from the line (MILLER *et al*., 2005).

3.3.2. LINEARITY

The analytical curves for quantification of n-alkanes were generated from 6 points in triplicate. The linearity of these curves was evaluated in relation to its coefficient correlation (R). According the National Institute of Metrology, Quality and Technology (Inmetro), a linear relationship is obtained for values of R greater than 0.90 (Aragão, 2009).

3.3.3. REPEATABILITY TEST

The precision of the analytical method was evaluated for repeatability. According to recommendations of the Guide to International Conference on Harmonisation (ICH) and the National Health Surveillance Agency (ANVISA) Resolution Number 899, the value of the numeric precision level of repeatability is estimated by the coefficient of variation (CV) of nine determinations covering the entire calibration range, with samples in triplicate (Equation 7) (RIBEIRO *et al*., 2008).

$$CV = \frac{\quad}{\quad} \qquad (7)$$

Solutions with external standards of 2-nonadecanone and squalene were used in the following concentration levels for this test: 0.11, 1.0 e 5 μg L^{-1}.

3.3.4.T TEST FOR COMPARISON OF CONCENTRATIONS

The t test for comparison of averages was used to assess whether the concentration obtained using the internal standard method are statistically equal to the values of concentration obtained from the external standard method.

In this test, the value of t-calculated is compared with the t-tabular value for a normal distribution with g degrees of freedom. If the calculated value of t is less than the tabular, it can be considered that the values are statistically equal. Otherwise, the values are statistically different. The calculated value of t and the number of g degrees of freedom are calculated, respectively, according to equations 8 and 9.

$$t = \frac{\quad}{\quad} \qquad (8)$$

$$g = \frac{\quad}{\quad} \qquad (9)$$

where and are, respectively, the average and the standard deviation of the concentration values calculated from the comparison with the area of the pattern, and are the average and standard deviation of the concentration values calculated from the analytical curves and and are the number of replicates for each case.

3.3.5. RECOVERY TESTS

Tests were performed to evaluate the recovery factor of the analytes in the following respects:

a) Rotoevaporation and concentration with a flow of nitrogen gas;

b) Complete method of extraction.

Sediment samples collected at Lake Paranoa (an artificial water reservoir located in the Distrito Federal, Brazil) were used to carry out the recovery tests.

For evaluation of the rotoevaporation step followed by concentration in nitrogen gas, 100 µL of squalene solution (1mg mL^{-1}) was added to 25 mL of DCM/MeOH (2:1 v/v) and it was subjected to concentration steps. This solution was analyzed by GC-FID and the results were compared with those obtained when the solution is not rotoevaporated and concentrated under nitrogen flow.

The same procedure described above was performed with respect to alkenones, using 100 µL of 2-nonadecanone solution (1mg mL^{-1}).

Finally, the recovery was compared when performing different numbers of extractions. For this step, the lake sediment was extracted five (in the same way as core samples), ten, fifteen and twenty times, and analyzed by GC-FID.

3.3.6. LIMITS OF DETECTION AND QUANTIFICATION

The limit of detection (LOD) is the lowest concentration of the analytical which can be detected by the technique and can be determined from the visual method. In this method, analysis of samples with low analyte concentrations were performed and the LOD is the lowest concentration that results in a peak that can be seen (RIBEIRO *et al*., 2008).

The quantification limit was taken as the lowest concentration point of the analytical curve.

4. RESULTS AND DISCUSSION

4.1. METHOD VALIDATION

4.1.1. VERIFICATION OF OUTLIERS

Grubb's test was performed to identify possible outliers in the analytical curves. The G values calculated were compared with the tabular value (P = 0.05 of significance and G critic equal to 1.155). Since none of the calculated values was greater than the critic value of G, it can be concluded that there were no outliers in the curves and no value has been rejected.

4.1.2. LINEARITY

The analytical curves were constructed from six points with different concentrations of *n*-alkanes, in triplicate. The values of the correlation coefficients obtained are shown in Table 6.

Table 6. Values of correlation coefficients obtained from the analytical curves.

***N*-alcane**	**R**
N-Docosane	0.9973
N-Tricosane	0.9977
N-Tetracosane	0.9974
N-Pentacosane	0.9979
N-Hexacosane	0.9973
N-Heptacosane	0.9977
N-Octacosane	0.9978
N-Nonacosane	0.9975

N-Triacontane	0.9982
N-Hentriacontane	0.9978
N-Dotriacontane	0.9975
N-Tritriacontane	0.9977
N-Tetratriacontane	0.9974
N-Pentatriacontane	0.9963

According to Inmetro all curves can be considered linear.

4.1.3. REPEATABILITY

The repeatability was evaluated taking into account the standard deviation (SD) and coefficient of variation (CV). Solutions of squalene and 2-nonadecanone standards were used in triplicate at three concentration levels: 0.11, 1.0 and 5.0 µg mL^{-1} (Table).

Table 7 Estimation of SD and CV to the standards of squalene and nonadecanone through the repeatability of areas (in picoampere (pA)).

	Concentration	Area 1	Area 2	Area 3	Average	SD	CV (%)
Squalene	0.11 µg mL^{-1}	1.21	1.03	1.22	1.15	0.10	9.08
	1.0 µg mL^{-1}	8.17	8.08	8.50	8.25	0.22	2.71
	5 µg mL^{-1}	52.97	46.09	48.09	49.05	3.54	7.22
2-Nonadecanone	0.11 µg mL^{-1}	1.01	1.01	1.06	1.03	0.03	2.75
	1.0 µg mL^{-1}	7.95	9.18	10.11	9.08	1.09	11.95
	5 µg mL^{-1}	55.23	36.66	49,.29	47.06	9.48	20.15

According Ribani *et al.* (2004) the maximum value for the coefficient of variation, when it takes into question analytes in low concentrations, is 20%. With

the exception of alkenones with concentration equal 5 µg mL^{-1}, the others coefficients of variation are smaller than 12%, validating the method of determination in trace level for *n*-alkanes and alkenones. None of the samples showed alkenones concentrations equal to or higher than 5 µg mL^{-1} and it is believed that the high coefficient for the most concentrated samples is due to loss of linearity the ends of a curve.

4.1.4. T TEST FOR COMPARISON OF CONCENTRATIONS

The test for comparison of values was used to validate the quantification performed from internal standard method. In this test, the values obtained from the internal standard method were compared with the concentrations obtained from the external standard method, taking in consideration the value of t calculated according to Equation 8.

This test was performed for the following Samples: CRB 4-3H, CRB 14H-3, CRB 24H-3, CRB 30H-7 , CRA-1 and CRA 14R-1 and CRA 18 R-3 injected in duplicate. The t values calculated for each is in Table 8.

Table 8. Values of t-calculated for the average comparison test.

	t-calculated													
Sample	**C-22**	**C-23**	**C-24**	**C-25**	**C-26**	**C-27**	**C-28**	**C-29**	**C-30**	**C-31**	**C-32**	**C-33**	**C-34**	**C-35**
CRB 3H-4	1.475	1.133	0.747	0.881	0.908	0.740	0.961	0.780	0.892	0.734	0.796	0.853	1.230	1.525
CRB 14H-3	4.758	7.415	2.909	1.756	1.068	0.212	0.625	0.402	2.653	0.148	1.013	1.092	2.035	1.379
CRB 24H-3	3.411	1.561	1.076	0.351	0.011	0.279	0.099	0.419	0.094	0.530	0.194	0.351	0.181	0.218
CRB 30H-7	9.408	5.873	4.264	7.784	1.160	0.859	0.563	2.245	1.314	0.066	0.684	0.797	8.795	0.396
CRA 14R-1	2.931	2.274	1.563	1.488	1.339	1.072	1.413	0.626	1.186	1.011	0.397	0.770	0.145	1.611
CRA 18R-3	0.275	1.818	1.908	3.548	3.783	1.100	1.501	1.908	6.920	1.922	0.299	0.229	0.344	3.398

The number of degrees of freedom for the samples, calculated according to Equation 7, was 2. Comparing the T-calculated and the respective degree of freedom with the t-tabulated value (9.925), it can be seen that for all samples used in this test, the value of the calculated concentration from the internal standard method is statistically equal to the concentrations calculated from the external standard method for 99.5% of reliability.

4.1.5. RECOVERY TESTS

The recovery method was evaluated in terms of the concentration step and for the complete method.

To evaluate the stage of rotoevaporation and concentration with flow of nitrogen gas, solutions with squalene (1mg mL^{-1}) and 2-nonadecanone (1mg mL^{-1}) standards were used. The recovery factor for alkenones and *n*-alkanes is shown in Figure 10.

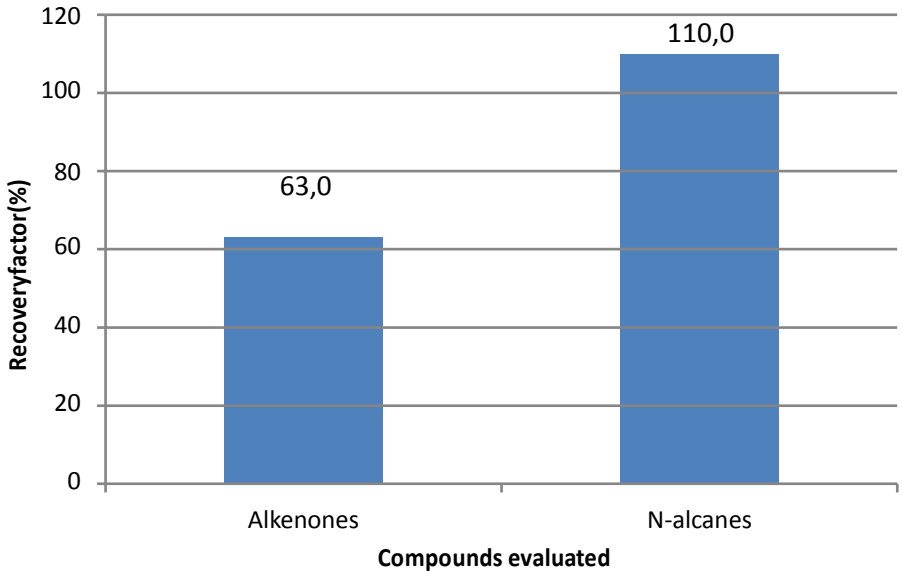

Figure 10. Recovery factors (%) of rotoevaporation and concentration steps of the solvent with a nitrogen flow.

To assess the recovery factor of the complete method, superficial sediment samples from Lake Paranoa were extracted in ultrasonic bath five times (as the method used for all the samples), ten, fifteen and twenty times. The results are show in Figure 11 and 12.

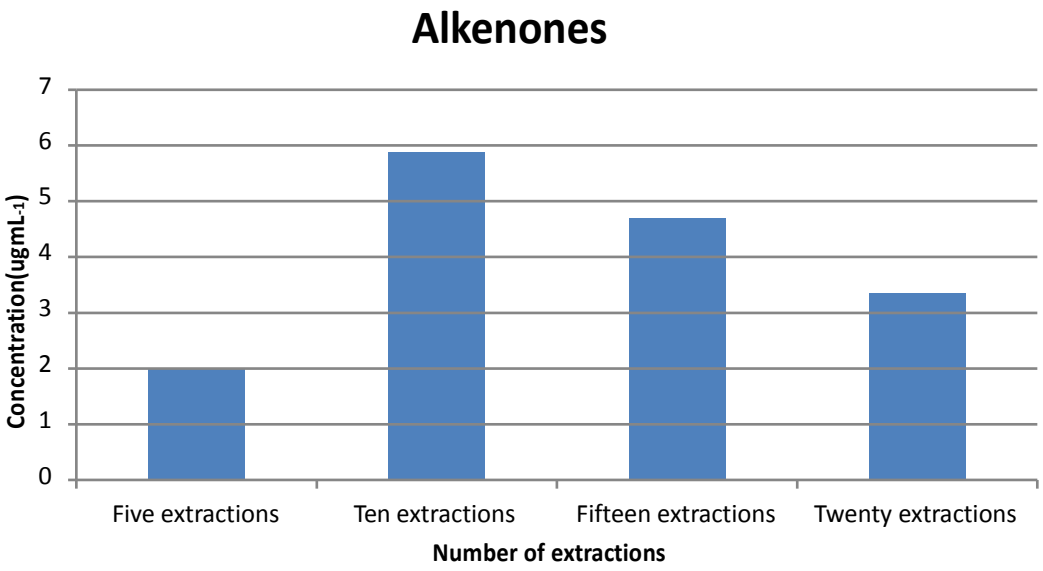

Figure 11. Comparing the concentrations obtained for different number of extractions of alkenones.

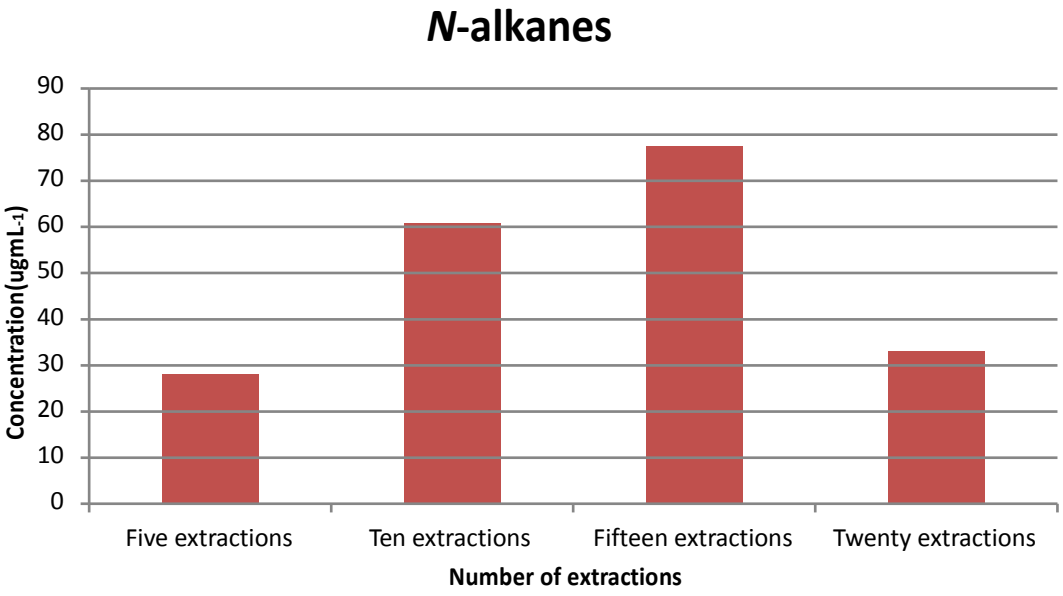

Figure 12. Comparing the concentrations obtained for different number of extractions of *n*-alkanes.

When five extractions were performed, the concentration of extracted alkenones and *n*-alkanes corresponded respectively to 34 and 36% of the

highest concentration extracted. For alkenones, the best result was obtained when the extraction was performed ten times and, for *n*-alkanes, fifteen times.

After reaching the maximum, the concentration of analyte in the extract decreases, probably due to the extensive time required of rotoevaporation to get the volume of 1 mL.

It can be seen by comparing Figure 11 and 12 that the concentrations of alkenones obtained in the recovery test are lower than those obtained for the *n*-alkanes. This can be explained by the fact that there was Unresolved Complex Mixture (UCM) in the chromatograms of fraction of ketones and also by the absence of alkenones objects of study in Paranoa Lake samples. This is because the sediments collected in the lake are shallow and probably there was not enough time for alkenones were deposited in the matrix.

4.1.6. LIMITS OF DETECTION AND QUANTIFICATION

The LOD, obtained by the visual method, and the LOQ obtained for the squalene and 2-nonadecanone standards are shown in Table 9.

Table 9. LOD and LOQ obtained for nonadecanone and squalene.

Parameter	**LOD (µg mL^{-1})**	**LOQ (µg mL^{-1})**
2-nonadecanone	0.0313	-
Squalene	0.0181	0.055

4.2. QUALITATIVE DETERMINATION OF *N*-ALKANES

The qualitative determination of *n*-alkanes was made from the correlation of retention time of aliphatic hydrocarbons present in the standard with peaks present in the nonpolar fraction.

The retention times (RT) of *n*-alkanes used for this comparison and to construct the analytical curves are shown in Table 10.

Table 2. Retention times (min) of *n*-alkanes used in the construction of analytical curves

***N*-alcane**	**Code**	**RT (in minutes)**
N-Docosane	C-22	34.1
N-Tricosane	C-23	36.4
N-Tetracosane	C-24	38.6
N-Pentacosane	C-25	40.7
N-Hexacosane	C-26	42.8
N-Heptacosane	C-27	44.8
N-Octacosane	C-28	46.7
N-Nonacosane	C-29	48.6
N-Triacontane	C-30	50.4
N-Hentriacontane	C-31	52.2
N-Dotriacontane	C-32	54.2
N-Tritriacontane	C-33	56.3
N-Tetratriacontane	C-34	58.6
N-Pentatriacontane	C-35	61.3

The samples show chromatographic profile similar to that obtained for the sample CRA 5 R4 (Figure 13).

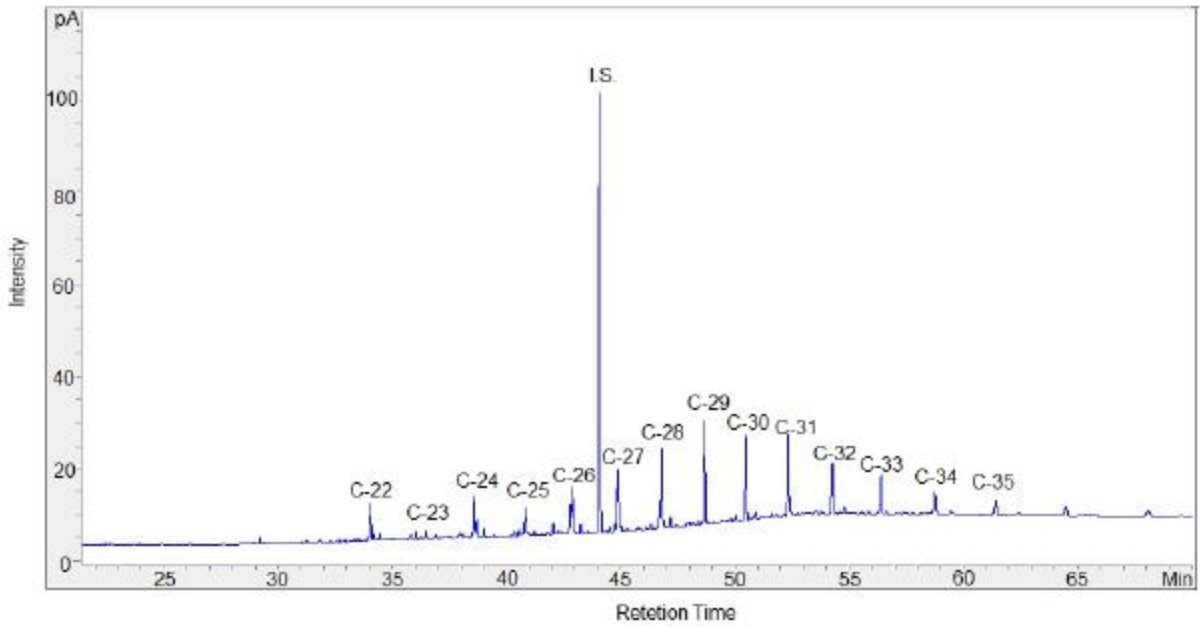

Figure 11. Typical chromatogram obtained for *n*-alkanes extracts (sample CRA 5 R4).

The other chromatograms obtained for the nonpolar fractions of the samples are in the Appendix C.

4.3. QUANTITATIVE DETERMINATION OF *N*-ALKANES

Analytical curves were constructed from *n*-alkanes present in the external standard. The curves (Figure 14 to 27) were plotted using the referent areas of each *n*-alkane (dependent variable) versus the known concentrations (independent variable) from 8 standard solutions prepared from diluting the stock solution (Table 11).

Table 11. Concentrations (µg mL $^{-1}$) and total areas of the external standard analytical curve of *n*-alkanes used.

	Average area (pA)													
Concentration (µg mL $^{-1}$)	**C-22**	**C-23**	**C-24**	**C-25**	**C-26**	**C-27**	**C-28**	**C-29**	**C-30**	**C-31**	**C-32**	**C-33**	**C-34**	**C-35**
0.055	1.2	1.2	1.2	2.0	1.2	1.1	1.5	1.1	1.5	1.1	1.2	1.0	1.1	1.2
0.165	3.1	3.1	2.9	4.5	3.1	2.7	3.2	2.9	3.1	2.6	2.9	2.7	2.7	2.4
0.33	5.8	5.9	5.8	6.7	6.0	5.6	6.1	5.6	5.9	5.4	5.9	5.5	5.6	5.9
0.66	11.5	11.6	11.4	12.2	12.3	11.0	12.2	11.7	12.6	10.9	11.6	11.4	11.6	13.2
1.1	23.3	23.5	23.5	24.8	24.5	22.7	23.7	23.4	23.4	22.7	23.0	23.1	23.3	23.3
2.2	34.2	34.9	34.8	37.2	35.4	34.6	35.3	35.1	37.2	34.0	34.6	34.9	34.8	38.7
4.4	65.0	66.5	66.5	70.1	67.7	65.8	67.7	66.9	69.2	65.5	66.1	67.4	67.2	66.9
5.5	81.5	83.3	83.1	88.9	84.2	81.7	84.5	83.1	87.8	82.6	81.3	82.8	82.4	82.8

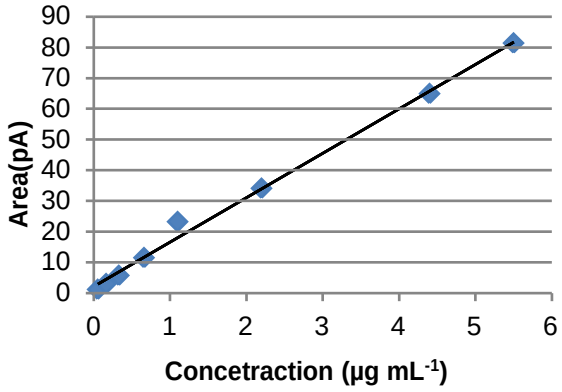

Figure 12. Analytical curve of C-22.

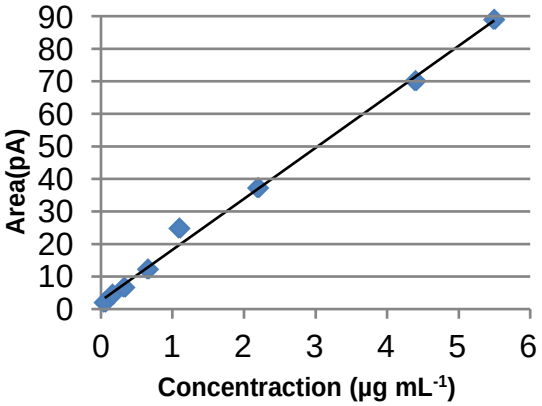

Figure 15. Analytical curve C-25.

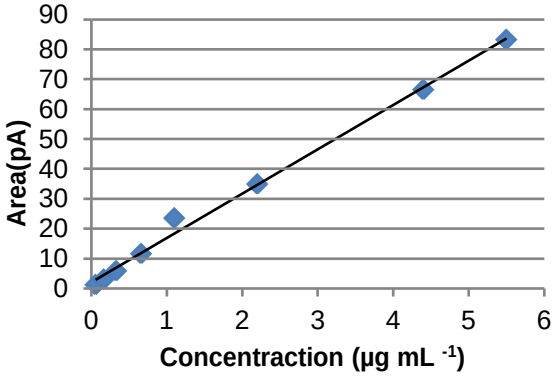

Figure 13. Analytical curve of C-23.

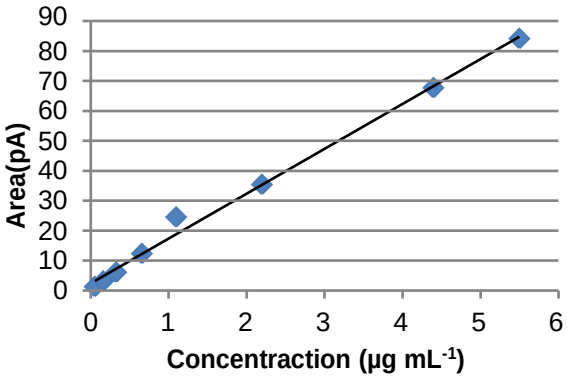

Figure 16. Analytical curve of C-26.

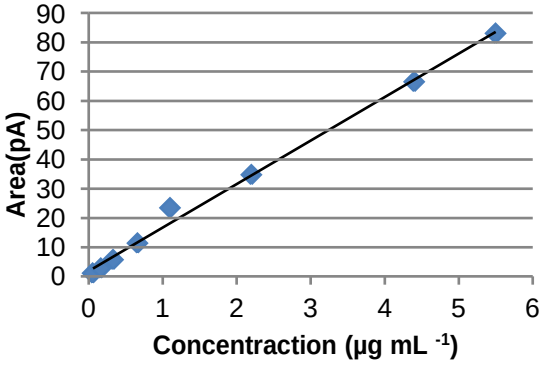

Figure 14. Analytical curve of C-24.

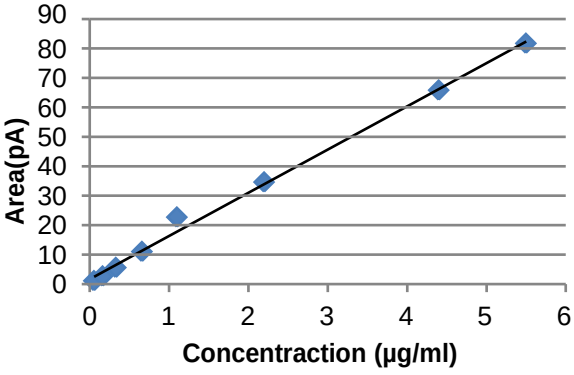

Figure 17. Analytical curve of C-27.

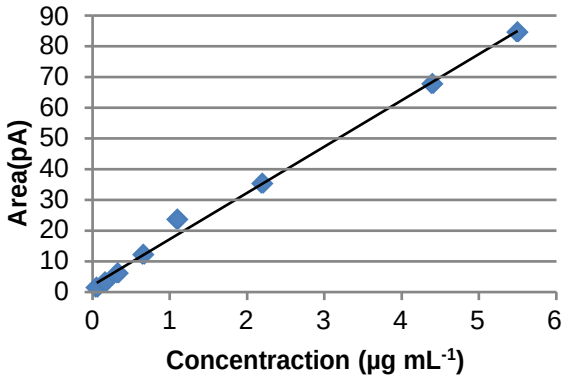

Figure 20. Analytical curve of C-28.

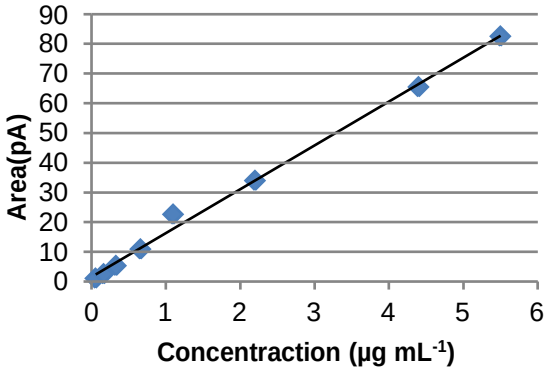

Figure23. Analytical curve of C-31.

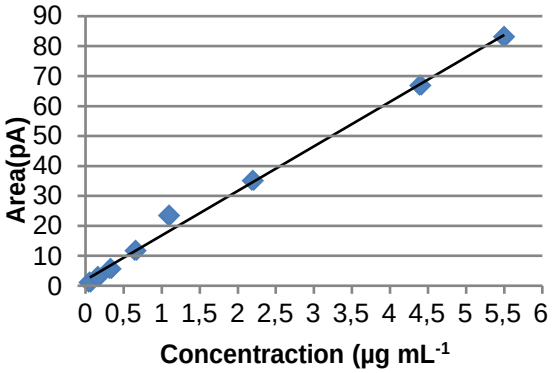

Figure 21. Analytical curve of C-29.

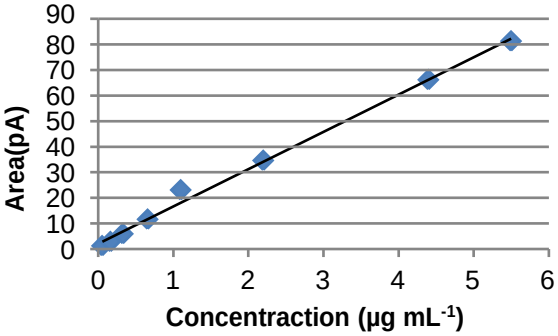

Figure 24. Analytical curve of C-32.

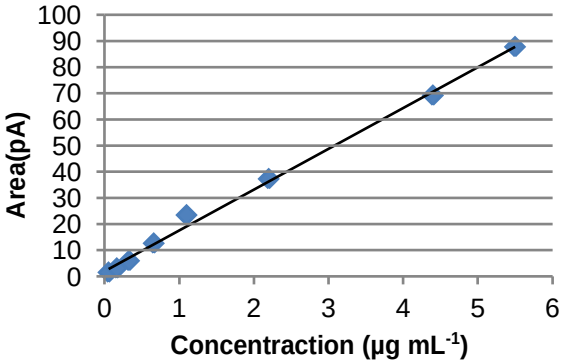

Figure 22. Analytical curve of C-30.

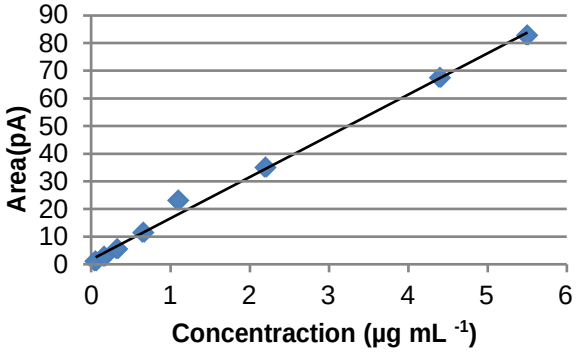

Figure 18. Analytical curve of C-33.

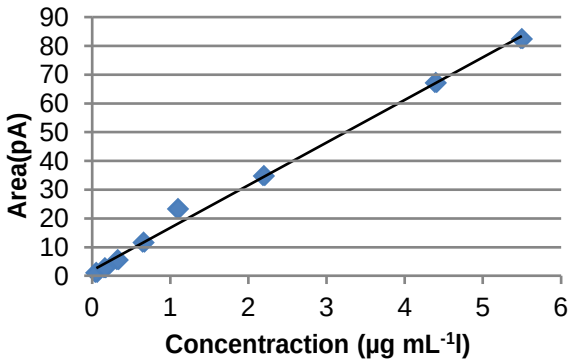

Figure 19. Analytical curve of C-34.

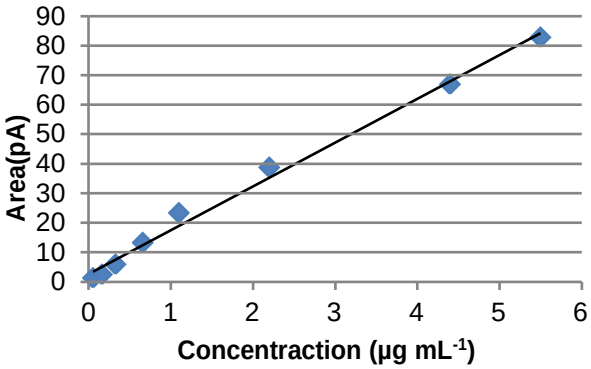

Figure 20. Analytical curve of C-35.

The equations of the lines of each respective *n*-alkane and R are shown in Table 12.

Table 12. Equations lines and R^2 for each *n*-alkane.

	Equation line	R
C-22	y=14.485 + 2.1032	0.9973
C-23	y=14.836 + 2.0247	0.9977
C-24	y=14.836 + 1.9342	0.9974
C-25	y=15.653 + 2.6065	0.9979
C-26	y=14.992 + 2.320	0.9973
C-27	y=14.67 + 1.7372	0.9977
C-28	y=15.039 + 2.1947	0.9978
C-29	y=14.875 + 1.9223	0.9975
C-30	y=15.597 + 1.9706	0.9982
C-31	y=14.752 + 1.5503	0.9978
C-32	y=14.578 + 2.0623	0.9975
C-33	y=14.914 + 1.7686	0.9977
C-34	y=14.836 + 1.8637	0.9974
C-35	y=14.834 + 2.5965	0.9963

The areas were obtained from the integration of the peaks and interpolated in the equations of the lines for the external standard method. The resulting concentration (in µg mL^{-1}) was divided by the mass of each sample multiplied by the volume present in each vial (50 µL) extract to give a final concentration in µg g^{-1} of sediment (Table 13).

For the internal standard method, the concentrations were obtained by the comparison with the area of the standard squalene. In this quantification method, the area of squalene, whose concentration in the sample is known, is compared with the area of the analyte (Table 14).

Table 3. Weight and sediment concentrations (μg g^{-1}) of 14 *n*-alkanes in the sediment samples of the cores CRA and CRB of Ceara Rise obtained by interpolation in the analytical curves.

		Concentration (in μg g^{-1})													
Sample	**Weight (in g)**	**C-22**	**C-23**	**C-24**	**C-25**	**C-26**	**C-27**	**C-28**	**C-29**	**C-30**	**C-31**	**C-32**	**C-33**	**C-34**	**C-35**
CRB-1H-1	2.02	<O	0.0385	0.0230	0.0415	0.0218	0.0524	0.0164	0.1119	0.0240	0.1173	0.0194	0.0575	<O	0.0159
CRB-2H-3	3.09	0.0562	0.0784	0.0581	<O	<O	0.0801	OLR	OLR	OLR	OLR	OLR	0.0792	OLR	OLR
CRB-3H-4	3.11	0.0111	0.0177	0.0259	0.0566	0.0752	OLR	OLR	OLR	OLR	OLR	0.0644	OLR	0.0279	0.0261
CRB-4H-3	3.13	0.0013	0.0039	0.0050	0.0115	0.0188	0.0355	0.0394	0.0708	0.0418	0.0746	0.0256	0.0376	0.0093	0.0103
CRB-6H-4	3.17	OLR	<O	OLR	<O	OLR	<O	OLR	OLR	OLR	OLR	OLR	OLR	OLR	OLR
CRB-7H-1	3.12	0.0237	0.0161	0.0160	0.0325	0.0293	0.0330	OLR	OLR	0.0257	OLR	0.0123	OLR	0.0123	0.0322
CRB-7H-3	3.20	0.0042	0.0080	0.0099	0.0196	0.0235	0.0540	0.0346	OLR	0.0424	OLR	0.0311	OLR	0.0114	0.0255
CRB-7H-5	3.07	0.0033	0.0063	0.0074	0.0166	0.0220	0.0373	0.0343	0.0830	0.0378	0.0836	0.0265	0.0530	0.0100	0.0176
CRB-8H-3	3.17	0.0024	0.0065	0.0082	0.0186	0.0208	0.0452	0.0264	0.0808	0.0296	OLR	0.0190	0.0779	0.0078	0.0193
CRB-9H-3	3.16	0.0010	0.0039	0.0039	0.0094	0.0141	0.0225	0.0196	0.0458	0.0244	0.0526	0.0169	0.0316	0.0075	0.0091
CRB-11H-3	3.02	0.0053	0.0081	0.0125	0.0209	0.0317	0.0393	0.0407	0.0691	0.0674	0.0736	0.0479	0.0429	0.0268	0.0185
CRB-11H-6	3.14	OLR	OLR	0.0717	OLR	OLR	<O	OLR	OLR	OLR	OLR	OLR	<O	OLR	OLR
CRB-13H-5	3.00	0.0086	0.0188	0.0232	0.0350	0.0492	0.0531	0.0568	0.0904	0.0606	0.0811	0.0479	0.0473	0.0274	0.0183
CRB-14H-3	3.06	0.0020	0.0053	0.0097	0.0174	0.0294	0.0383	0.0383	0.0611	0.0387	0.0613	0.0254	0.0324	0.0113	0.0103
CRB-15H-2	2.92	<O	<O	<O	OLR	0.0021	0.0054	0.0062	0.0113	0.0084	0.0134	0.0049	0.0066	0.0008	0.0015
CRB-16H-3	3.15	<O	OLR	0.0018	0.0049	0.0118	0.0194	0.0216	0.0440	0.0223	0.0721	0.0139	0.0345	0.0046	0.0083

CRB-17H-1	3.00	OLR	OLR	0.0013	0.0049	0.0162	0.0362	0.0498	0.0776	0.0552	0.0704	0.0322	0.0352	0.0142	0.0073
CRB-17H-5	2.04	0.0034	0.0081	0.0097	0.0131	0.0156	0.0302	0.0207	0.0776	0.0262	0.1297	0.0186	0.0913	0.0066	0.0231
CRB -18H-3	3.19	OLR	OLR	OLR	<0	OLR	OLR	OLR	OLR	OLR	0.0608	OLR	<0	OLR	OLR
CRB-19H-6	3.10	OLR	OLR	OLR	<0	OLR	OLR	OLR	OLR	OLR	0.0383	OLR	<0	OLR	OLR
CRB-20H-6	2.93	OLR	OLR	OLR	<0	OLR	OLR	OLR	0.0859	OLR	0.0488	OLR	<0	0.0875	0.0703
CRB-21H-3	3.19	0.0051	0.0151	0.0110	0.0140	0.0210	0.0434	0.0303	OLR	0.0371	OLR	0.0240	0.0601	0.0095	0.0184
CRB-21H-7	3.19	0.0014	0.0036	0.0091	0.0170	0.0315	0.0367	0.0393	0.0508	0.0425	0.0551	0.0333	0.0306	0.0179	0.0138
CRB-24H-3	3.04	<0	0.0018	0.0023	0.0062	0.0105	0.0133	0.0138	0.0302	0.0166	0.0423	0.0115	0.0224	0.0157	0.0062
CRB-25H-7	3.09	0.0011	0.0030	0.0038	0.0079	0.0169	0.0177	0.0178	0.0337	0.0277	0.0383	0.0194	0.0190	0.0102	0.0060
CRB-26H-3	3.14	OLR	<0	OLR	<0	OLR	OLR	OLR	OLR	OLR	<0	OLR	<0	OLR	OLR
CRB-26H-6	3.06	OLR	<0	OLR	<0	OLR	<0	OLR	OLR	OLR	OLR	OLR	OLR	OLR	OLR
CRB-27H-4	2.90	0.0011	0.0093	0.0077	0.0145	0.0224	0.0220	0.0250	0.0530	0.0352	0.0718	0.0303	0.0507	0.0178	0.0175
CRB-27H-7	3.03	<0	OLR	0.0019	0.0045	0.0080	0.0098	0.0108	0.0155	0.0094	0.0140	0.0054	0.0071	0.0015	<0
CRB-28H-3	3.05	0.0448	<0	0.0436	<0	0.0146	0.0246	0.0218	0.0396	0.0554	0.0456	0.0330	0.0236	0.0210	<0
CRB-28H-7	3.10	0.0123	<0	<0	0.0060	0.0038	0.0173	0.0181	0.0309	0.0315	0.0367	0.0163	0.0178	<0	<0
CRB-29H-4	3.15	0.0239	0.0025	0.0258	0.0096	0.0209	0.0185	0.0185	0.0341	0.0332	0.0283	0.0192	0.0150	0.0086	<0
CRB-30H-3	3.10	0.0019	0.0046	0.0067	0.0100	0.0156	0.0220	0.0166	0.0481	0.0384	<0	0.0209	0.0212	0.0110	0.0178
CRB-30H-7	3.04	0.0010	0.0077	0.0197	0.0362	0.0590	0.0689	0.0737	OLR	0.0762	0.0845	0.0559	0.0474	0.0277	0.0245
CRB-31H-4	3.00	OLR	0.0032	0.0044	0.0100	0.0155	0.0183	0.0192	0.0307	0.0234	0.0305	0.0169	0.0152	0.0059	0.0039
CRB-32H-3	2.96	0.0015	0.0051	0.0079	0.0168	<0	0.0694	0.0350	OLR	0.0429	OLR	0.0349	OLR	0.0113	0.0200

CRB-32H-7	3.00	OLR	0.0051	0.0113	0.0221	0.0356	0.0427	0.0451	0.0636	0.0434	0.0642	0.0327	0.0391	0.0147	0.0141
CRB-33H-7	2.07	<0	0.0176	0.0148	0.0262	0.0206	0.0275	0.0196	0.1003	0.0264	OLR	0.0221	0.1243	<0	0.0222
CRA-3R-1	3.09	OLR	0.0034	0.0044	0.0106	0.0162	0.0259	0.0269	0.0545	0.0303	0.0825	0.0235	0.0564	0.0090	0.0157
CRA-4R-1	3.12	0.0048	0.0100	0.0167	0.0343	0.0535	0.0765	0.0722	OLR	0.0707	OLR	0.0484	0.0559	0.0232	0.0216
CRA-5R-1	3.04	0.0039	0.0076	0.0085	0.0171	0.0230	0.0302	0.0285	0.0604	0.0670	0.0575	0.0444	0.0266	0.0208	0.0164
CRA-5R-4	3.05	0.0348	<0	<0	0.0229	0.0349	0.0469	0.0656	OLR	0.0693	OLR	0.0601	0.0500	0.0330	0.0246
CRA-6R-1	2.02	<0	0.0032	0.0026	0.0071	0.0140	0.0271	0.0342	0.0977	0.0519	OLR	0.0403	0.0877	0.0156	0.0197
CRA-6R-3	3.09	0.0063	0.0024	0.0029	0.0095	0.0152	0.0301	0.0391	0.0531	0.0442	0.0570	0.0328	0.0304	0.0181	0.0188
CRA-7R-3	2.00	0.0723	<0	OLR	<0	0.0372	<0	0.0498	0.0784	0.0322	0.0741	0.0435	0.0401	<0	<0
CRA-8R-6	2.95	0.0051	0.0054	0.0116	0.0203	0.0402	0.0611	0.0713	OLR	0.0818	OLR	0.0572	0.0842	0.0260	0.0371
CRA-9R-4	3.09	OLR	0.0084	0.0102	0.0220	0.0542	0.0634	0.0762	OLR	OLR	OLR	0.0642	0.0465	0.0278	0.0193
CRA-10R-1	3.16	<0	OLR	0.0016	0.0051	0.0128	0.0198	0.0238	0.0363	0.0250	0.0343	0.0161	0.0177	0.0068	0.0057
CRA-11R-1	3.02	OLR	<0	OLR	<0	OLR	<0	OLR	0.0671	OLR	0.0705	0.0660	0.0392	<0	<0
CRA-11R-6	3.10	0.0010	0.0040	0.0098	0.0167	0.0360	0.0588	0.0792	OLR	0.0840	OLR	0.0553	0.0509	0.0253	0.0219
CRA-12R-1	3.10	0.0111	0.0052	0.0052	0.0123	0.0234	0.0390	0.0532	0.0680	0.0551	0.0658	0.0376	0.0329	0.0162	0.0116
CRA-13R-1	3.01	<0	<0	<0	0.0173	0.0619	OLR	OLR	OLR	OLR	OLR	OLR	OLR	0.0576	0.0348
CRA-14R-1	3.17	0.0009	0.0029	0.0031	0.0097	0.0175	0.0338	0.0404	0.0556	0.0447	0.0494	0.0284	0.0240	0.0115	0.0076
CRA-14R-5	3.11	0.0037	0.0089	0.0132	0.0315	0.0689	OLR	OLR	OLR	OLR	OLR	OLR	OLR	0.0488	0,0409
CRA-15R-1	3.17	0.0301	0.0101	0.0115	0.0208	0.0318	0.0492	0.0521	OLR	0.0581	OLR	0.0503	OLR	0.0191	0,0255
CRA-16R-4	3.00	0.0311	0.0371	0.0339	<0	<0	0.0464	OLR	OLR	OLR	0.0707	OLR	0.0418	OLR	0,0534

CRA-17R-3	3.11	0.0035	0.0130	0.0148	0.0318	0.0439	0.0699	0.0801	OLR	0.0879	OLR	0.0586	OLR	0.0236	0,0263
CRA-18R-3	3.17	0.0025	0.0056	0.0062	0.0117	0.0167	0.0225	0.0190	0.0354	0.0273	0.0361	0.0291	0.0355	0.0164	0.0065
CRA-20R-1	3.32	0.0016	0.0043	0.0066	0.0147	0.0232	0.0385	0.0454	OLR	0.0496	OLR	0.0345	0.0597	0.0124	0.0133
CRA-20R-4	3.04	0.0031	0.0057	0.0086	0.0151	0.0232	0.0296	0.0335	0.0485	0.0322	0.0599	0.0241	0.0358	0.0102	0.0116
CRA-22R-3	3.04	0.0305	0.0114	0.0261	0.0245	0.0411	0.0612	0.0873	OLR	OLR	OLR	OLR	OLR	OLR	OLR
CRA-22R-7	3.13	0.0036	0.0023	0.0042	0.0086	0.0156	0.0211	0.0230	0.0348	0.0248	0.0413	0.0171	0.0223	0.0064	0.0066
CRA-23R-3	3.18	OLR	<0	OLR	<0	OLR	<0	OLR	OLR	OLR	0.0694	0.0697	<0	<0	0.0249
CRA-24R-1	3.15	0.0047	0.0131	0.0145	0.0297	0.0434	0.0753	0.0827	OLR	OLR	OLR	0.0778	OLR	0.0278	0.0274
CRA-26R-1	2.99	0.0018	0.0054	0.0084	0.0195	0.0427	0.0797	OLR	OLR	OLR	OLR	0.0698	0.0551	0.0297	0.0211
CRA-26R-8	3.06	0.0026	0.0056	0.0061	0.0118	0.0205	0.0252	0.0284	0.0445	0.0379	0.0459	0.0280	0.0304	0.0131	0.0098
CRA-29R-1	2.07	0.0029	0.0033	0.0040	0.0046	0.0103	0.0222	0.0276	0.0472	0.0335	0.0427	0.0212	0.0259	0.0108	0.0076
CRA-30R-5	2.96	0.0081	0.0131	0.0081	0.0118	0.0198	OLR	OLR	OLR	OLR	OLR	OLR	OLR	0.0472	0.0470
CRA-32R-1	2.94	0.0924	<0	0.0904	<0	OLR	<0	OLR	OLR	OLR	OLR	OLR	0.0724	0.0922	0.0878
CRA-33R-6	3.15	0.0020	0.0040	0.0053	0.0089	0.0214	0.0360	0.0443	0.0650	0.0440	0.0610	0.0290	0.0328	0.0106	0.0097
CRA-36R-7	3.14	0.0016	0.0049	0.0051	0.0102	0.0170	0.0208	0.0338	0.0416	0.0363	0.0478	0.0292	0.0273	0.0142	0.0075
CRA-39R-4	3.18	OLR	<0	OLR	<0	OLR	OLR	OLR	OLR	OLR	OLR	OLR	OLR	OLR	OLR

OLR = Out of the linear range

Table 4. Concentrations (µg g^{-1}l) of *n*-alkanes in 14 samples of sediment cores CRA and CRB of Ceara Rise obtained by comparison with the area of the internal standard.

	Concentration (in µg g^{-1})													
Sample	**C-22**	**C-23**	**C-24**	**C-25**	**C-26**	**C-27**	**C-28**	**C-29**	**C-30**	**C-31**	**C-32**	**C-33**	**C-34**	**C-35**
CRB-1H-1	-	0.0476	0.0298	0.0547	0.0294	0.0622	0.0231	0.1311	0.0324	0.1354	0.0256	0.069	-	0.023
CRB-2H-3	0.0564	0.0795	0.0594	-	-	0.0801	0.4854	0.2746	0.4105	0.2093	0.2483	0.0805	0.1501	0.0998
CRB-3H-4	0.0123	0.0186	0.0261	0.0584	0.0733	0.0978	0.0909	0.1786	0.1017	0.1634	0.0612	0.0845	0.0279	0.027
CRB-4H-3	0.0037	0.0064	0.0075	0.0159	0.0228	0.0393	0.0449	0.0777	0.049	0.0806	0.0291	0.0423	0.012	0.0139
CRB-6H-4	0.8703	-	0.7016	-	0.5654	-	0.4506	0.2091	0.3254	0.1525	0.2207	0.1000	0.1502	0.098
CRB-7H-1	0.0233	0.0167	0.0166	0.0341	0.0294	0.0317	0.1168	0.1554	0.0268	0.1197	0.0132	0.0321	0.0132	0.0321
CRB-7H-3	0.0069	0.0111	0.0132	0.0258	0.0288	0.061	0.0412	0.1489	0.0515	0.1816	0.0361	0.1455	0.0148	0.0312
CRB-7H-5	0.0045	0.0068	0.0077	0.0165	0.02	0.0315	0.0301	0.0692	0.034	0.0687	0.0229	0.0448	0.0098	0.0166
CRB-8H-3	0.0059	0.0109	0.013	0.0285	0.0299	0.0593	0.0371	0.1058	0.0423	0.1408	0.0265	0.1021	0.0124	0.0281
CRB-9H-3	0.0034	0.0062	0.0062	0.0132	0.0173	0.0251	0.0231	0.0499	0.0288	0.0562	0.0196	0.035	0.0098	0.0124
CRB-11H-3	0.0073	0.0099	0.014	0.024	0.0332	0.0392	0.0419	0.0686	0.0702	0.0719	0.0474	0.0433	0.0278	0.0205
CRB-11H-6	0.0527	0.0766	0.0399	0.0663	0.573	-	0.5059	0.1836	0.34	0.1056	0.2371	-	0.1584	0.104
CRB-13H-5	0.0095	0.0186	0.0224	0.0352	0.046	0.048	0.0529	0.0818	0.0581	0.0726	0.0436	0.0436	0.026	0.0187
CRB-14H-3	0.0043	0.0075	0.0119	0.0214	0.0325	0.0401	0.0415	0.0638	0.0432	0.0631	0.0275	0.0347	0.0135	0.0132
CRB-15H-2	-	-	-	0.0114	0.015	0.0232	0.0277	0.0427	0.0348	0.0476	0.0226	0.0274	0.0092	0.0142
CRB-16H-3	0.0019	0.0025	0.0033	0.0069	0.0123	0.0181	0.0209	0.0397	0.0219	0.0631	0.0136	0.0314	0.0056	0.0096
CRB-17H-1	0.0024	0.0028	0.0033	0.0076	0.0177	0.0353	0.0496	0.0749	0.0564	0.0672	0.0318	0.035	0.0153	0.0096
CRB-17H-5	0.0057	0.0095	0.0107	0.0151	0.0161	0.0271	0.0204	0.0672	0.0256	0.1091	0.0179	0.0785	0.008	0.0227

CRB-18H-3	0.4820	0.0273	0.4215	-	0.3547	0.2504	0.0746	0.1978	0.0421	0.1197	-	0.0774	0.0686	0.0686
CRB-19H-6	0.0322	0.5467	-	0.4250	0.4250	0.0972	0.3801	0.1797	0.3489	0.0407	0.2287	-	0.1595	0.1018
CRB-20H-6	0.5525	0.0358	0.4716	-	0.3678	0.0911	0.2609	0.0778	0.1877	0.0443	0.1149	-	0.0790	0.0646
CRB-21H-3	0.0061	0.0145	0.011	0.0148	0.02	0.0379	0.028	0.0868	0.0348	0.0959	0.0218	0.0527	0.0097	0.0179
CRB-21H-7	0.0031	0.0049	0.0097	0.0179	0.0297	0.0331	0.0365	0.0459	0.0405	0.0489	0.0302	0.0283	0.0172	0.0144
CRB-24H-3	0.0022	0.0044	0.0049	0.0105	0.0146	0.0168	0.0183	0.0361	0.0219	0.0488	0.0151	0.0272	0.0198	0.0101
CRB-25H-7	0.0033	0.0051	0.0058	0.0111	0.0194	0.0193	0.0203	0.0357	0.0311	0.0396	0.0212	0.0209	0.0122	0.0088
CRB-26H-3	0.5859	-	0.4918	-	0.4395	0.0953	0.3141	0.0997	0.2464	-	0.1758	-	0.1092	0.0626
CRB-26H-6	0.492	-	0.7277	-	0.5864	-	0.4674	0.2169	0.3375	0.1582	0.2289	0.1037	0.1558	0.1017
CRB-27H-4	0.0038	0.0124	0.0106	0.0196	0.027	0.0255	0.0299	0.0593	0.042	0.0784	0.0345	0.0567	0.0213	0.022
CRB-27H-7	-	0.0053	0.0086	0.0164	0.0228	0.0248	0.0286	0.0378	0.0258	0.0335	0.0164	0.0194	0.0076	-
CRB-28H-3	0.0565	-	0.0561	-	0.0212	0.0321	0.0301	0.0513	0.0741	0.0577	0.0425	0.0315	0.0283	-
CRB-28H-7	0.015	-	-	0.0096	0.0066	0.0199	0.0218	0.0347	0.0371	0.0401	0.0191	0.0208	-	-
CRB-29H-4	0.0295	0.0053	0.0321	0.0149	0.0271	0.0233	0.0243	0.0417	0.0427	0.0343	0.0242	0.0196	0.0122	-
CRB-30H-3	0.0041	0.0067	0.0087	0.0132	0.018	0.0233	0.0189	0.0496	0.0419	-	0.0224	0.0229	0.0128	0.0203
CRB-30H-7	0.0036	0.0107	0.0236	0.0444	0.0672	0.0757	0.0833	0.0997	0.089	0.0926	0.0619	0.0536	0.0322	0.0296
CRB-31H-4	0.0028	0.0053	0.0064	0.0131	0.0177	0.0195	0.0213	0.0321	0.0261	0.0312	0.0184	0.1687	0.0078	0.0066
CRB-32H-3	0.0044	0.0084	0.0116	0.0237	-	0.0809	0.0435	0.1566	0.0543	0.2412	0.042	0.1261	0.0154	0.0263
CRB-32H-7	0.0034	0.008	0.0148	0.0287	0.0421	0.0483	0.0527	0.0721	0.0523	0.0717	0.0376	0.0452	0.0184	0.0186
CRA-3R-1	0.0027	0.0055	0.0064	0.0139	0.0187	0.0272	0.0294	0.0562	0.0337	0.083	0.0251	0.0581	0.011	0.0183

CRB-33H-7	-	0.0179	0.0154	0.0274	0.0211	0.0258	0.0201	0.0891	0.0266	0.1473	0.0216	0.1098	-	0.0227
CRA-4R-1	0.0034	0.006	0.0092	0.0192	0.0278	0.0382	0.0372	0.0524	0.0377	0.0536	0.0245	0.0286	0.0124	0.012
CRA-5R-1	0.0041	0.0065	0.0071	0.0139	0.017	0.0211	0.0208	0.0415	0.0481	0.039	0.0304	0.019	0.0151	0.0128
CRA-5R-4	0.0366	-	-	0.0272	0.038	0.0486	0.0694	0.096	0.0755	0.0939	0.0618	0.0526	0.0353	0.0276
CRA-6R-1	-	0.0067	0.006	0.0121	0.0183	0.0305	0.0393	0.1037	0.0593	0.1558	0.0441	0.0934	0.0192	0.0246
CRA-6R-3	0.0077	0.0042	0.0046	0.0116	0.0161	0.0287	0.0381	0.0502	0.0441	0.0529	0.0313	0.0295	0.0183	0.0196
CRA-7R-3	0.064	-	0.5365	-	0.0357	-	0.0467	0.0706	0.0321	0.0659	0.0399	0.0373	-	-
CRA-8R-6	0.0062	0.0064	0.0116	0.0205	0.0363	0.0524	0.0628	0.1135	0.0741	0.1348	0.0492	0.0728	0.0236	0.0336
CRA-9R-4	0.0025	0.0086	0.01	0.0213	0.0467	0.0527	0.0649	0.0818	0.0784	0.0766	0.0533	0.0397	0.0243	0.018
CRA-10R-1	0.0019	0.0035	0.0049	0.0109	0.0205	0.0285	0.0353	0.0512	0.0379	0.0477	0.024	0.0262	0.0117	0.0113
CRA-11R-1	0.2210	-	0.1979	-	0.1601	-	0.112	0.0743	0.1197	0.0768	0.0718	0.0443	0.0018	-
CRA-11R-6	0.003	0.0058	0.0113	0.0193	0.0367	0.0567	0.078	0.1065	0.0854	0.095	0.0534	0.0502	0.0258	0.0233
CRA-12R-1	0.0126	0.0071	0.007	0.0153	0.0251	0.039	0.0543	0.0677	0.058	0.0647	0.0377	0.0337	0.0176	0.0139
CRA-13R-1	-	-	-	0.0205	0.0628	0.169	0.2448	0.305	0.2389	0.2146	0.1355	0.1016	0.0575	0.0364
CRA-14R-1	0.0029	0.0047	0.0049	0.0121	0.0189	0.033	0.0406	0.0541	0.046	0.0475	0.0282	0.0244	0.0126	0.0097
CRA-14R-5	0.0051	0.0097	0.0134	0.0316	0.0633	0.1121	0.1554	0.2227	0.1604	0.2031	0.0992	0.1045	0.0446	0.0383
CRA-15R-1	0.027	0.0104	0.0116	0.0211	0.0295	0.0431	0.0471	0.1223	0.054	0.1965	0.0441	0.1153	0.018	0.0241
CRA-16R-4	0.0289	0.0347	0.0319	-	-	0.0422	0.2055	0.103	0.1906	0.0636	0.1003	0.0388	0.0846	0.0497
CRA-17R-3	0.0046	0.0123	0.0138	0.0296	0.0381	0.0578	0.068	0.1144	0.0769	0.1284	0.0486	0.0733	0.0208	0.0237
CRA-18R-3	0.0047	0.0077	0.0083	0.0152	0.0194	0.0243	0.0217	0.0378	0.031	0.0378	0.031	0.0379	0.0185	0.0093

CRA-20R-1	0.0048	0.0084	0.0113	0.024	0.034	0.0526	0.0637	0.119	0.0714	0.1514	0.0476	0.0816	0.0189	0.021
CRA-20R-4	0.0054	0.0079	0.0109	0.019	0.0262	0.0315	0.0368	0.0513	0.0364	0.0618	0.0262	0.0383	0.0124	0.0147
CRA-22R-3	0.0209	0.0088	0.0184	0.0187	0.0287	0.0406	0.0592	0.0788	0.0749	0.0944	0.0711	0.0787	0.0643	0.0706
CRA-22R-7	0.0055	0.0042	0.006	0.0114	0.0174	0.0217	0.0246	0.0354	0.027	0.0409	0.0182	0.0233	0.0081	0.009
CRA-23R-3	0.2052	-	0.1937	-	0.1303	-	0.1094	0.0893	0.0461	0.0614	0.0614	-	-	0.0241
CRA-24R-1	0.0059	0.0132	0.0143	0.0295	0.04	0.066	0.0745	0.1553	0.0889	0.2064	0.068	0.1176	0.0258	0.0261
CRA-26R-1	0.0035	0.0065	0.009	0.0201	0.0391	0.0692	0.0968	0.1248	0.1042	0.101	0.0608	0.0492	0.0272	0.0205
CRA-26R-8	0.0047	0.0075	0.0079	0.0147	0.0223	0.0258	0.0299	0.0448	0.0403	0.0454	0.0285	0.0312	0.0145	0.0121
CRA-29R-1	0.0058	0.0061	0.0066	0.0084	0.0131	0.0231	0.0294	0.0471	0.0358	0.042	0.0226	0.027	0.0129	0.011
CRA-30R-5	0.0047	0.007	0.0047	0.007	0.0102	0.0201	0.034	0.1454	0.0733	0.1997	0.0528	0.096	0.0224	0.0227
CRA-32R-1	0.0826	0.071	0.0826	-	0.0976	-	0.091	0.2326	0.0977	0.1558	0.1992	0.0668	0.0842	0.081
CRA-33R-6	0.0037	0.0053	0.0064	0.0106	0.021	0.0326	0.0411	0.0585	0.0421	0.0543	0.0267	0.0303	0.011	0.0109
CRA-36R-7	0.0038	0.0071	0.0072	0.0136	0.0196	0.0225	0.0366	0.0438	0.0403	0.0493	0.0309	0.0294	0.0162	0.0103
CRA-39R-4	0.4394	-	0.4148	-	0.349	0.0736	0.2584	0.1881	0.207	0.2252	0.1311	0.1094	0.0684	0.0658

-: Species not detected.

The values for concentrations calculated using external analytical curves ranged from 0.0009 to 0.1297 µg g^{-1}. Concentrations calculated from the area compared to standard squalene ranged from 0.0019 to 0.8703 µg g^{-1}.

Since the samples had a range of very high concentration of *n*-alkanes, it was not possible to quantify some analytes. Quantification by the internal standard method have no limitation of the linear range, making it possible to quantify analytes in a wider range of concentrations.

4.4. QUALITATIVE DETERMINATION OF ALKENONES

The alkenones were identified qualitatively by injection of samples in a gas chromatograph coupled to a mass spectrometry detector, performed at the Laboratory NIOZ, Netherlands. The typical chromatogram with identified peaks is shown in Figure 28.

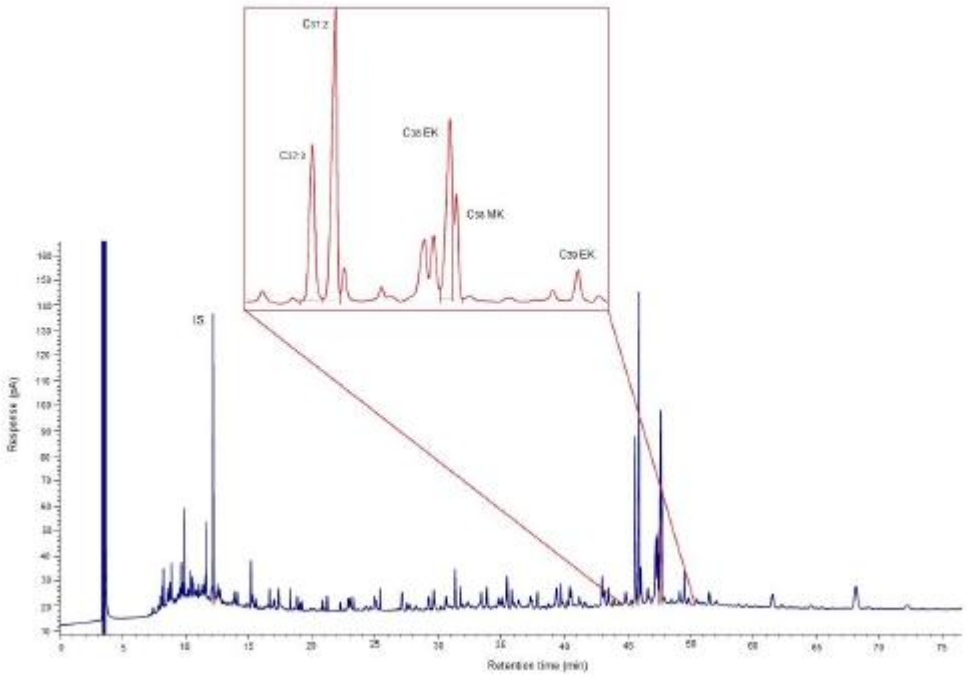

Figure 21. Representative chromatogram of sediment sample containing alkenones.

The chromatograms obtained for the alkenone fractions of the samples are in the Appendix D.

4.5. QUANTITATIVE DETERMINATION OF ALKENONES

As there are no standard available for construction of the analytical curve, the alkenones were quantified by comparing the peak area of the internal standard and the area of the analyte. The average concentrations in μg g^{-1}, for the samples are shown in Table 15.

Table 15. Concentrations (μg g^{-1}) of alkenones in sediment samples of cores CRA and CRB of Ceara Rise obtained by comparison with the area of the internal standard.

	Concentration (in μg g^{-1})				
Sample Name	**$C_{37:3}$**	**$C_{37:2}$**	**C_{38EK}**	**C_{38MK}**	**C_{39}**
925B-2H-3-(45-48)	0.006	0.108	0.071	0.036	0.011
925B-2H-6-(92-95)	0.020	0.331	0.232	0.102	0.041
925B-3H-4-(114-117)	0.017	0.301	0.155	0.071	0.011
925B-4H-3-(100-103)	0.001	0.050	0.029	0.014	0.002
925B-5H-3-(43-46)	0.003	0.094	0.043	0.025	0.006
925B-5H-6-(25-28)	0.008	0.192	0.093	0.047	0.012
925B-6H-4-(58-61)	0.005	0.151	0.082	0.048	0.013
925B-7H-1-(15-19)	-	0.132	0.084	0.040	0.015
925B-7H-3-(53-56)	0.015	0.386	0.130	0.112	0.035
925B-7H-5-(40-43)	0.001	0.102	0.057	0.026	0.004
925B-8H-3-(86-89)	0.015	0.239	0.140	0.069	0.022
925B-9H-3-(86-89)	0.001	0.084	0.043	0.019	0.005
925B-10H-3-(86-89)	0.006	0.152	0.081	0.036	0.011

925B-11H-3-(87-90)	-	0.033	0.018	0.006	0.001
925B-11H-6-(43-48)	0.007	0.205	0.116	0.040	0.015
925B-12H-4-(86-89)	0.002	0.064	0.036	0.017	0.004
925B-13H-5-(25-28)	-	-	-	-	-
925B-14H-3-(100-103)	-	0.032	0.016	0.006	-
925B-15H-2-(30-33)	-	0.032	0.019	0.012	-
925B-16H-3-(5-8)	-	0.032	0.016	0.004	-
925B-17H-1-(104-107)	-	0.020	0.013	0.007	-
925B-17H-5-(10-14)	-	0.021	0.016	0.004	-
925B-18H-3-(122-125)	-	0.006	0.006	-	-
925B-19H-3-(87-90)	-	-	-	-	-
925B-19H-6-(28-31)	0.004	0.044	0.032	0.012	0.005
925B-20H-6-(60-63)	-	0.017	-	-	-
925B-21H-3-(19-23)	-	0.009	0.009	0.004	-
925B-21H-7-(44-47)	-	0.008	0.008	0.001	-
925B-22H-7-(43-46)	0.004	0.022	0.017	0.012	0.021
925B-23H-5-(42-45)	-	0.017	0.011	0.005	0.001
925B-24H-3-(122-125)	-	0.008	0.006	0.003	-
925B-25H-2-(25-28)	-	0.007	0.005	-	-
925B-25H-7-(43-47)	-	-	-	-	-
925B-26H-3-(91-94)	-	-	-	-	-
925B-26H-6-(104-107)	-	-	-	-	-
925B-27H-4-(46-50)	-	-	-	-	-
925B-27H-7-(29-32)	-	0.002	0.001	-	-
925B-28H-3-(59-62)	-	0.006	0.006	0.005	-
925B-28H-7-(68-71)	-	-	-	-	-
925B-29H-4-(44-47)	-	0.013	0.009	0.003	-
925B-30H-3-(77-80)	-	0.030	0.018	0.007	0.001

925B-30H-7-(43-46)	0.001	0.057	0.015	0.012	0.002
925B-31H-4-(119-122)	0.003	0.109	0.058	0.021	0.006
925B-32H-3-(50-53)	0.004	0.140	0.081	0.019	0.009
925B-32H-7-(10-13)	0.002	0.026	0.014	0.015	-
925B-33H-7-(10-15)	-	0.043	0.065	0.010	0.008
925A-3R-1-(95-98)	0.002	0.117	0.076	0.024	0.006
925A-4R-1-(58-61)	-	0.013	0.008	0.003	-
925A-5R-1-(52-55)	-	0.014	0.008	0.001	-
925A-5R-4-(52-55)	-	0.014	0.011	0.037	-
925A-6R-1-(62-65)	0.008	0.516	0.307	0.055	0.029
925A-6R-3-(111-114)	0.003	0.017	0.010	0.002	-
925A-7R-3-(6-10)	-	0.010	0.007	0.008	-
925A-8R-2-(136-139)	-	0.030	0.018	0.009	0.002
925A-8R-6-(80-83)	0.002	0.093	0.056	0.011	0.005
925A-9R-4-(131-134)	-	-	-	-	-
925A-10R-1-(128-131)	-	-	-	-	-
925A-11R-1-(41-44)	-	-	-	-	-
925A-11R-6-(22-25)	-	-	-	-	-
925A-12R-1-(23-26)	0.003	0.042	0.021	0.007	-
925A-13R-1-(48-51)	-	0.017	0.007	0.004	-
925A-14R-1-(6-9)	-	0.008	0.005	0.002	-
925A-14R-5-(125-128)	0.002	0.053	0.029	0.012	0.003
925A-15R-1-(97-100)	0.006	0.235	0.142	0.058	0.017
925A-15R-7-(20-23)	0.003	0.061	0.031	0.011	0.003
925A-16R-4-(67-70)	0.004	0.334	0.184	0.069	0.019
925A-17R-3-(137-140)	0.004	0.234	0.151	0.057	0.018
925A-18R-3-(8-11)	0.002	0.093	0.054	0.020	0.006
925A-18R-7-(16-19)	0.006	0.237	0.134	0.074	0.021

925A-19R-3-(106-109)	0.014	0.174	0.108	0.038	0.012
925A-20R-1-(55-58)	0.001	0.062	0.041	0.014	0.006
925A-20R-4-(66-69)	0.017	0.033	0.025	0.009	0.004
925A-22R-3-(26-29)	0.002	0.091	0.053	0.021	0.004
925A-22R-7-(26-29)	0.004	0.018	0.011	0.004	-
925A-23R-3-(136-139)	-	0.050	0.035	0.012	0.006
925A-24R-1-(74-77)	0.015	0.156	0.112	0.044	0.017
925A-26R-1-(13-16)	-	0.021	0.016	0.006	0.001
925A-26R-8-(6-9)	-	0.040	0.033	0.033	0.005
925A-29R-1-(42-45)	-	0.094	0.073	0.022	0.011
925A-30R-5-(15-18)	0.001	0.059	0.045	0.014	0.006
925A-32R-1-(38-41)	-	0.060	0.046	0.014	0.003
925A-33R-6-(42-45)	-	0.048	0.039	0.011	0.003
925A-36R-7-(46-49)	-	0.037	0.031	0.009	0.005
925A-39R-4-(81-84)	0.001	0.154	0.128	0.047	0.020

-: Species not detected.

Values for concentrations calculated from the area compared with the 2-nonadecanone standard ranged from 0.001 to 0.516 µg g^{-1}. Except for samples CRB 33 H-7 and CRA 5 R-4, $C_{37:2}$ has the highest concentration among the other alkenones detected.

The predominant concentration of $C_{37:2}$ was also found by Boot *et al.* (2006) when evaluating the concentration of alkenones at site 942 (5°45'N, 49°6'W), located in the Amazon Fan. The dominance of $C_{37:2}$ alkenones in relation to the other suggests that their source is predominantly seaweed (ZINK *et al.,* 2001).

However, caution is needed with proxies results obtained from the quantification of lipids because of its degradation. As $C_{37:2}$ suffer less the effect

of degradation that $C_{37:3}$, the relative ratio between the compounds may be affected, resulting in a bias in the calculated temperatures (HOEFS *et al*., 2002).

4.6. PROXIES CARBON PREFERENCE INDEX AND AVERAGE CHAIN LENGTH

CPI values, which are calculated according to Equation 4, varied over the years and record, as can be seen in Figure 29. The minimum values are between 0.18 and 0.19 and are found in the portion of the core corresponding to the beginning of the Late Miocene. The maximum value is 4.1, corresponding to the end of the Middle Miocene.

In the intervals in which CPI values varies between ~1 and ~4, it is possible to suggest that the primary source of *n*-alkane was wax leaves of terrestrial plants (DUAN *et al*., 2010). At low degree, there is the influence of the activity of marine microorganisms as a source of aliphatic hydrocarbons the CPI values are less than 1(JENG *et al*., 2006; DUAN *et al*., 2010).

According to the proxy CPI, the main source of organic materials present in the studied cores comes from terrestrial source. This result is in agreement with the study by Boot *et al.* (2006) in the assessment of organic materials input to Amazon Fan, in which all sediments originating from site 942, were evaluated according to the CPI and indicated that the main source of organic matter of the area comes from terrigenous material.

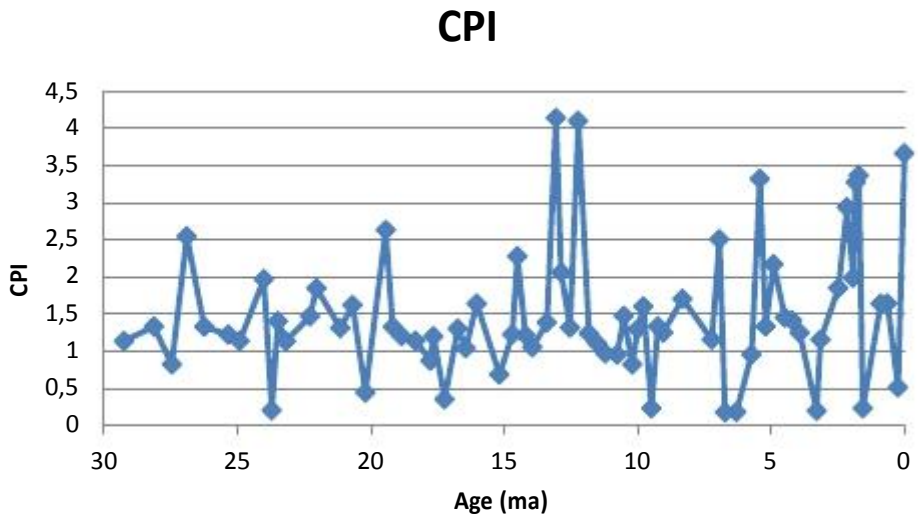

Figure 22. Calculated CPI values along the record at sites 925 A and 925 B, situated at Ceara Rise.

Throughout the record, the value of ACL varies between ~26.6 and ~30.7 (Figure 30), suggesting that the main source of *n*-alkanes also is derived from terrestrial sources, and meaning, in most cases, that the organic material was transported from the land to the sea due to the action of winds and the flow of rivers.

Boot *et al.* (2006) also evaluated the results of the ACL on site 942. In this work, the calculated values of ACL did not varied much, lying around ~29.8. This fact led researchers to conclude that small variations in ACL indicate consistency in the source of vegetation type, in which the primary source was also terrigenous.

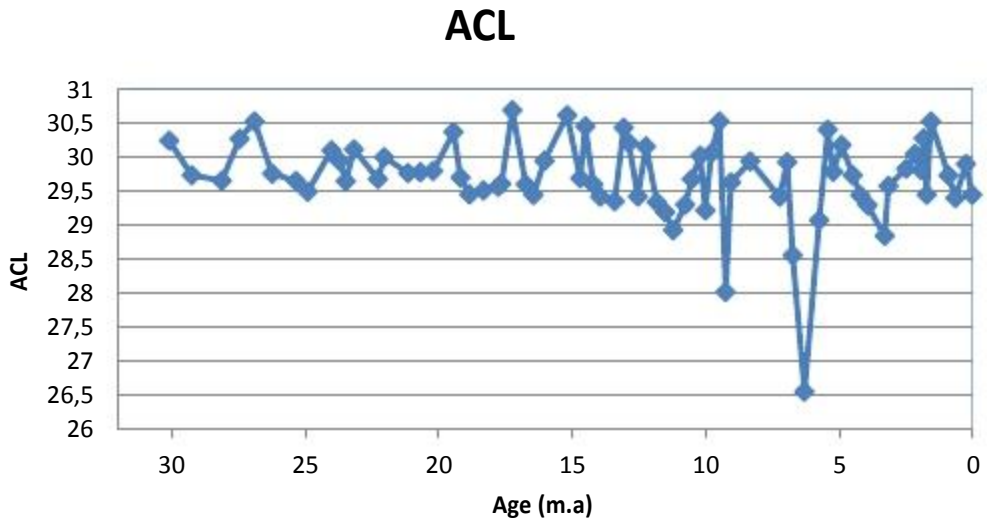

Figure 30. ACL values calculated over the record sites 925 A and 925 B, situated at Ceara Rise.

Dobson *et al.* (2001) also evaluated the terrigenous sediment on Ceara Rise and concluded that most of the terrigenous sediment deposited on Ceara Rise is product of weathering of rocks in the Andes, because terrigenous materials derived from other sources are hardly deposited in Ceara Rise due its location and the intense amount of sediment produced in Amazon, that forms a physical barrier.

In general, the concentration of *n*-alkanes is higher than alkenones because these are best preserved. This happens because the *n*-alkanes are tougher and its headquarters act as a protective barrier, which is why terrigenous lipids are better preserved than those present in marine sediments (HOEFS *et al*., 2002).

4.7. RECONSTRUCTION OF SST

The temperature profile obtained from the calculation of (Equation 1) for samples in which it was possible to quantify $C_{37:2}$ and $C_{37:3}$ is shown in Figure 31.

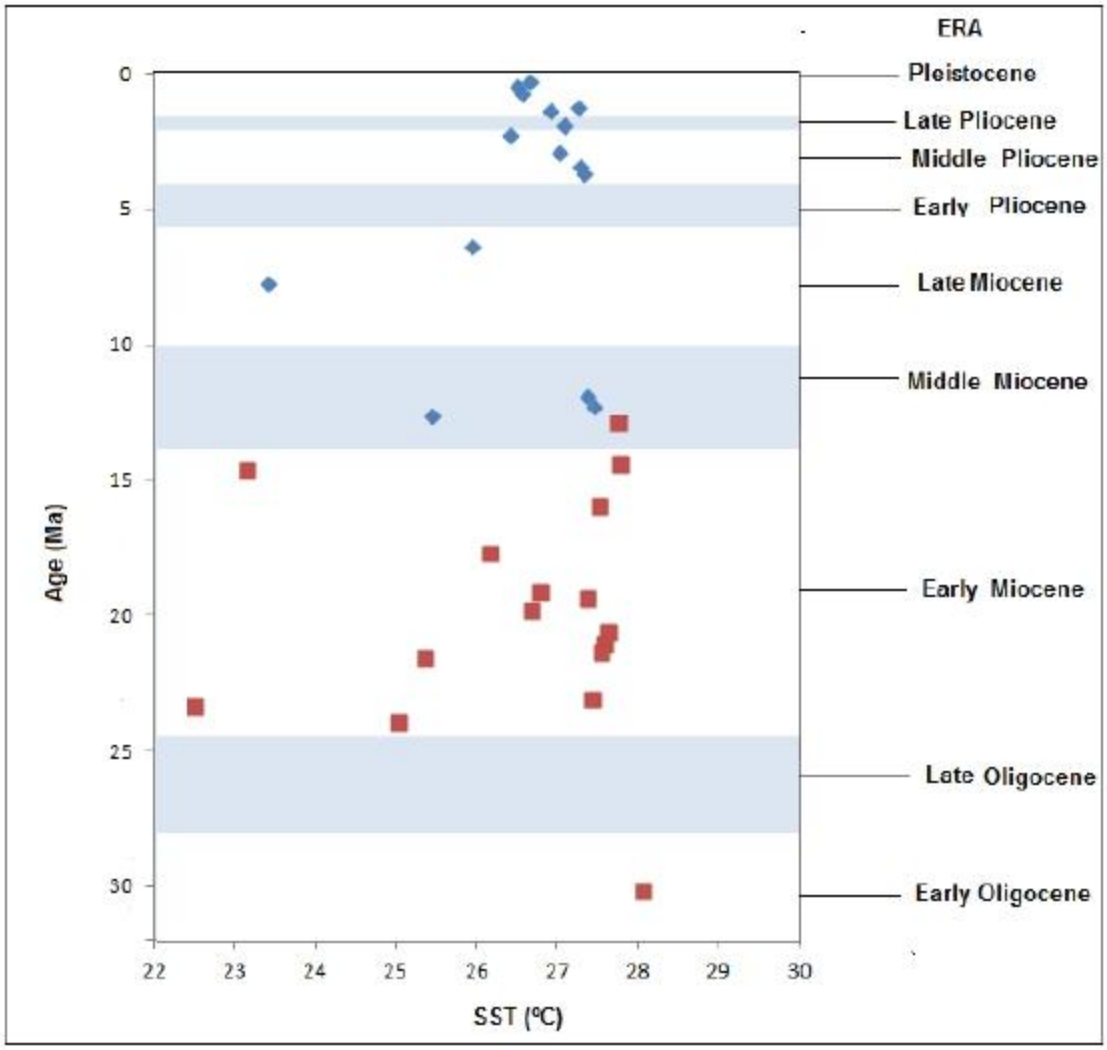

Figure 31. Alkenone derived sea surface temperature (°C) record at sites 925 A (represented in red) and 925 B (in blue), situated at Ceara Rise.

According to Figure 31, it can be observed that between Pleistocene and the Middle Pliocene there was little variation in the SST. From the Middle Pliocene to half of Late Miocene the tendency of the SST was reach coldest values, followed by heating until the beginning of the Early Miocene. At the end

of Early Miocene there was the lowest recorded SST (22.5 °C), which was followed again by a heating tendency until the registration of the highest temperature (28.5 °C) at half the Early Oligocene.

The work of Boot *et al.* (2006) were unable to estimate the SST for various samples of site 942. In this work, which included samples from 35 kyr, the estimated SST ranged from 23 to 26 °C in the glacial period, corresponding to the end of Pleistocene, and $C_{37:3}$ was not detected in the glacial periods. During the same period, the SST estimated for samples of Ceara Rise used in this work was ~26 °C.

Temperatures estimated in Ceara Rise are consistent with the global trend already observed by other researchers. Pearson *et al.* (2007) stated that the global trend during the Early Oligocene, period in which the planet was characterized as 'Greenhouse World' was heating. In samples analyzed in this work, the Early Oligocene was the period in which the highest SST was estimated (~ 28 °C).

In the studied cores, there was no sample covering the Late Oligocene, but estimates of SST from the beginning of the Early Miocene suggest that the trend was cooling, fact that is consistent with prediction made by Pearson *et al*. (2007) and coincides with the onset of glaciers.

During the Miocene until to the Early Pliocene, the world's propensity to cooling, but with intervals of higher temperatures, already observed by FEARY *et al*. (1990), ZACHOS *et al*. (2001) and LISIECKI *et al*. (2007). It was also observed in cores analyzed in this work. The interval when the highest temperatures were estimated happened in Middle Miocene. This period also coincides with the last interval of warmer temperatures than today. SSTs estimated in the Rio Grande Rise for this period are even 3 °C higher than the temperatures recorded today (DOWSETT *et al*., 1996).

Studies by Haywood *et al.* (2009) estimated an overall increase of SST from the Early Pliocene to the present day, which can also be observed for samples from site 925 at Ceara Rise (Figure 32).

The results obtained in the estimative of SST in Ceara Rise are consistent with other studies conducted, even when using different extraction methods or tool *proxies*. Therefore, this study may contribute to understanding global trends of variation of SST over the last 30 Ma.

5. CONCLUSIONS

The method for extraction of *n*-alkanes and alkenones in sediment samples, first used in AQQUA Group, generated satisfactory results in agreement with other studies conducted in what concerns the reconstruction of sea surface temperatures and main origin of organic materials present in these sediments.

The extraction with ultrasonic used little volume of solvent, resulted in small amount of residues and generated satisfactory results in relation to the recovery test of *n*-alkanes. For the recovery of alkenones the recovery factors were not so good due the presence of UCM in chromatograms and absence of alkenones used in this study at the sediment used for the recovery test.

Quantification of *n*-alkanes was performed from analytical curves and the concentrations obtained from the curves were compared with the measurement performed by the comparison of the area of the analyte to the area of standard added to the sample, quantification method commonly used in studies of paleotemperature. The results were concordant for both quantifying and statistically equal, which, by analogy, justified the quantification of alkenones only by the method of comparing areas, since there is no standard of alkenones commercially available.

The Carbon Preference Index and Average Chain Length proxies used to determine the main source of the organic material present in sediments were both consistent and showed that the main source of organic matter in sediments of the Ceara Rise is coming from terrigenous source, that is, the material present in the coastal region was sent to the place from transport of rivers and winds.

The concentration of the alkenones ranged from 0.001 to 0.516 μg g^{-1} and $C_{37:2}$ was the compound with the highest concentration among these

alkenones. The proxy brought estimated values of SST ranging between 22.5 and 28.5 °C. The results presented are in agreement with other studies that show the South Atlantic paleoclimatic reconstruction.

Despite the temporal distance of the estimated temperature records, it was possible to show the general trend of warming/cooling that occurred in Ceara Rise during the last 30 Ma, result that contributes to a better understanding of variations in temperature that occurred across the South Atlantic and collaborates with studies of others important world regions, as the Amazon Fan.

6.BIBLIOGRAPHIC REFERENCE

ANVISA, Resolução-RE n° 899 – Guia de validação de métodos analíticos e bioanalíticos, de 29 de maio de **2003**. Available at <http://portal.anvisa.gov.br/wps/wcm/connect/4983b0004745975da005f43fbc4c6735/RE_899_2003_Determina+a+publica%C3%A7%C3%A3o+do+Guia+para+valida%C3%A7%C3%A3o+de+m%C3%A9todos+anal%C3%ADticos+e+bioanal%C3%ADticos.pdf?MOD=AJP> Accessed July 29,2014.

Aragão N. M.; *Quim. Nova,* **2009**, 32, 2476.

Blyth A. J.; Baker A.; Collins M. J.; Penkman E. H.; Gilmour M. A.; Moss J. S.; Genty D.; Drysdale R. N.; *Quat. Sci. Rev.,* **2008**, 27, 905.

Boot C. S.; Ettwein V. J.; Maslin M. A.; Weyhenmeyer C.E.; Pancost R.D.; *Org. Geochem.* **2006**, 37, 208.

Brassel S. C.; Eglinton G.; Marlowe I. T.; Pflaumann U.; Sarnthein M.; *Nature,***1986**, 320, 129.

Castañeda I. S.; Schouten S.; *Quat. Sci. Rev.,* **2008**, 30, 2851.

Curry W. B.; Shackleton N. J.; Richter C.; *Sci Results,* **1995**, 154,1.

Dobson D. M.; Dickens G. R.; Rea D. K.; *Sci Results,* **1997**, 154, 465.

Dobson D. M.; Dickens G.; Palaegeogr*. Palaeclimatol. Palaeoclimatol.,* **2001**, 165, 215.

Duan F.; He K.; Liu X.; *J. Environ. Sci.,* **2010**, 22, 998.

Eglinton T. I.; Eglinton G.; *Earth Planet. Sci. Lett.,* **2008**, 275,1.

Eigenbrod F.; Armsworth P. R.; Anderson B. J.; Heinemeyer A.; Gillings S.; Roy D. R.; Thomas C. D.; Gaston K. J. J.; *Appl. Ecol.,* **2010**, 47, 377.

Feary D. A.; Davies P. J.; Pigram C. J.; Symonds P. A.; *Palaegeogr. Palaeclimatol. Palaeoclimatol.,* **1991**, 89, 341.

Figueiredo J.; Hoorn C.; Ven P.; Soares E.; *Geological Society of America,* **2009**, 37, 619.

Flood R. D.; Piper D. J. W.; *Sci Results,* **1997**, 155, 653.

Friztsons E.; Mantovan L. E.; Aguiar A. V.; *Rev. Est. Amb.,* **2008**, 10,49.

Haywood A. M. M.; Dowsett H. J., Valdes P. J., Lunt D. J., Francis J. E.; Sellwood B. W.; *Phil. Trans. R. Soc. A*, **2009**, 367, 3.

Hebert T. D.; *Treatise on Geochemistry,* **2003**, 6, 391.

Helmond N. A. G. M. **Palynological and organic geochemical characterization of marine and terrestrial Early Pleistocene climate in northwest Europe.** 2010. Dissertation (Master in Biogeology) – Utrecht University, Netherlands, 2010.

Heinrich S.; Zonnevel K. A. F.; Palaegeogr*. Palaeoclimatol. Palaeclimatol.,* **2013**, 386, 599.

Hoefs M. J. L.;Rupstrra W. I.C.; Damsté J. S. S.; *Geochim. Cosmochim. Ac.,* **2002**, 66, 2719.

Jeng W.; *Mar. Chem.,* **2006**, 102, 242.

Kim J. H.; Huguet C.; Zonneveld K. A. F.; Versteegh G. J. M.; Roeder W.; Damsté J. S. S.; Schouten S.; *Geochim. Cosmochim. Ac.,* **2009**, 73, 2888.

Kumar N.; Embley R. W.; Geological Society of America Bolletin, **1977**, 88, 683.

Lisiecki L. E.; Raymo M. E.; *Quartenary Sci. Reviews,* **2007**, 26, 56.

Mann M. E.; Zhang Z.; Hughes M. K.; Bradley R.S.; Miller S. K.; Rutherford S.; Ni F. P.; *Natl. Acad. Sci. USA,* **2008**, 105, 13252.

Meyers P. A.; *Org. Geochem.,* **2003**, 34, 261.

Miller J. M.; Miller J. C.; *Statistics and Chemometrics for Analytical Chemistry,* 5° ed.; Pearson Education Limited: England, 2005

Müller P.; Kirst G.; Ruhland G.; Storch I.; Rosell-Melé A.; *Geochim. Cosmochim. Acta*, **1998**, 62, 1757-1772.

Murayama M.; Nagai H.; Imamura M.; Hatori S.; Kobayashi K.; Taira A.; *Nucl. Instr. and Meth. In Phys. Res. B,* **1997**, 123, 302.

http://www.cpc.ncep.noaa.gov/data/indices/sstoi.atl.indices, accessed in November of 2014.

Ohkouchi N.; Wada E.; *Sci Results,* **1997**, 154, 501.

Pearson P. N.; Dongen B. E.; Nicholas C. J.; Pancost R. D.; Schouten S.; Singano J. M.; Wade B. S.; *Geology,* **2007**, 35, 211.

Peter B.; *Earth Planet. Sci. Lett.*, **2004**, 220, 3.

Prahl F .G.; Wakeham S. G.; *Nature,* **1987**, 330, 367.

Prahl F. G.; Mix A. C.; Sparrow M. A.; *Geochim. Cosmochim. Ac.,* **2006**, 70, 101.

Ribani M.; Bottoli C. B. G.; Collins C.H.; Jardim I. C. S. F.; Melo L. F. C.; .; *Quím. Nova,* **2004**, 27, 771.

Riberio F. A. L.; Ferreira M. M. C; Morano S. C.; Silva L. R.; Schneider R. P.; *Quím. Nova,* **2008**, 31, 164.

Rommerskirchen F.; Condon T.; Mollenhauer G.; Dupont L.; Schefuss E.; *Paleoceanography,* **2011**, 26, 1.

Sachs J. P.; Pahnke K.; Smittenberg R.; Zhang Z.; *Encyclop. Quat. Sci.,* **2013**, 2, 775.

Smith M.; Deckker P.; Rogers J.; Brocks J.; Hope J.; Schmidt S.; Santos R. L.; Shouten S.; *Org. Geochem.,* **2013**, 64, 94.

Spera A. M. **Registro de variações ambientais dos últimos 3000 anos da Região da Ria do Mamanguá, Rio de Janeiro, utilizando marcadores orgânicos moleculares.** 2012. Dissertation (Master in Science) – Oceanographic Institute, University of Sao Paulo, Sao Paulo, 2012.

Toney J. L.; Theroux S.; Andersen R. A.; Coleman A.; Amaral-Zettler L.; Huang Y.; *Geochim. Cosmochim. Ac.,* **2012**, 78, 51.

Villalba R.; Grosjean M.; Kiefer T.; *Palaeogeogr. Palaecocl.,***2009**, 281,175.

Zachos J.; Pagani M.; Sloan L.; Thomas E.; Billups K.; *Sci*., **2001**, 292, 686.

Zachos J. C.; Dickens G. R.; Zeebe R. E.; *Nature,* **2008**, 451, 279.

Zink K. G..; Leythaeuser D.; Melkonian M.; Schwark L.; *Geochim. Cosmochim. Ac, **2001**, 65, 253.*

APPENDIX

APPENDIX A: GEOLOGICAL TIME SCALE

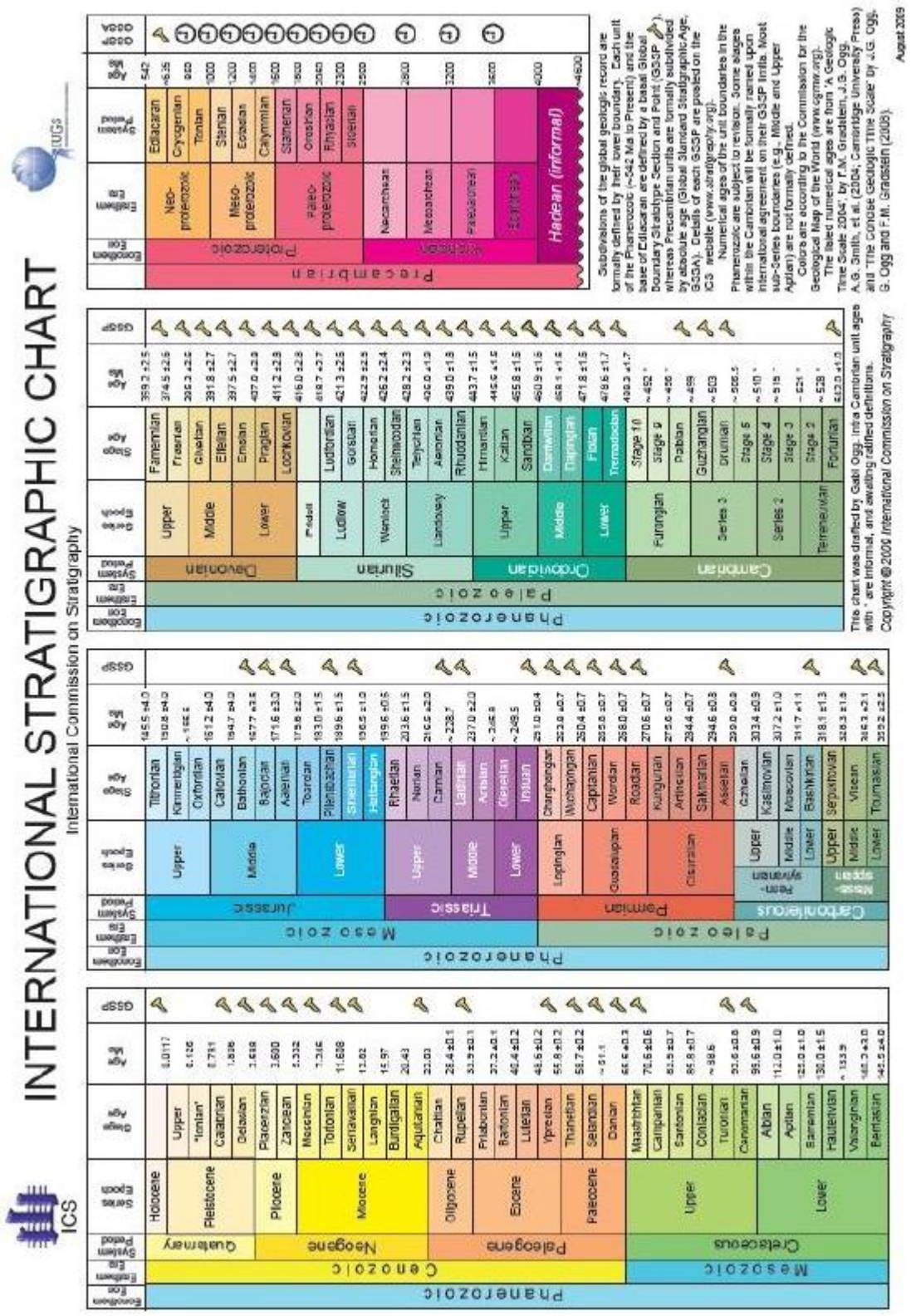

APPENDIX B. RESULTS OF THE WORK OF CURRY *ET AL.* (1995)

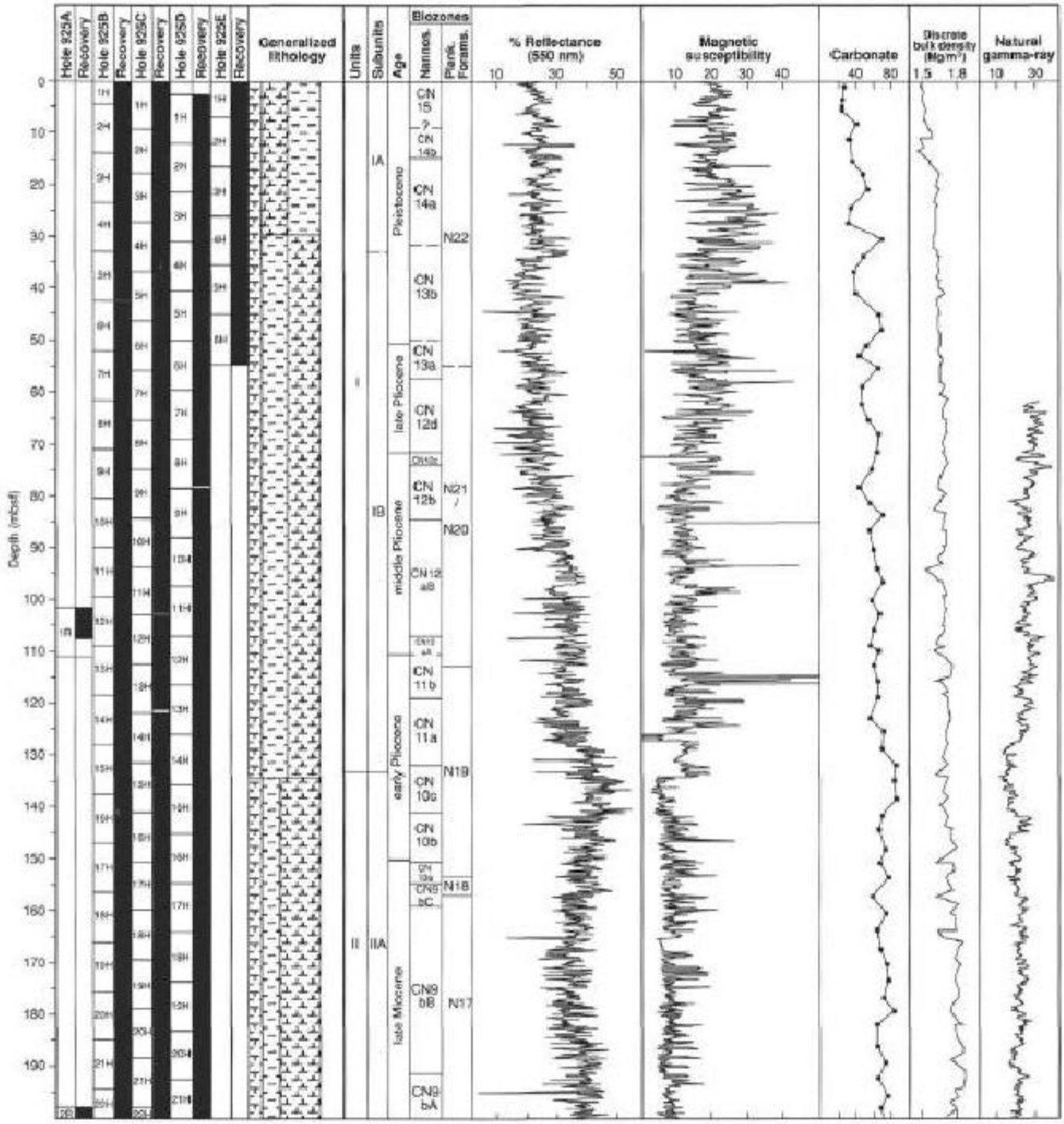

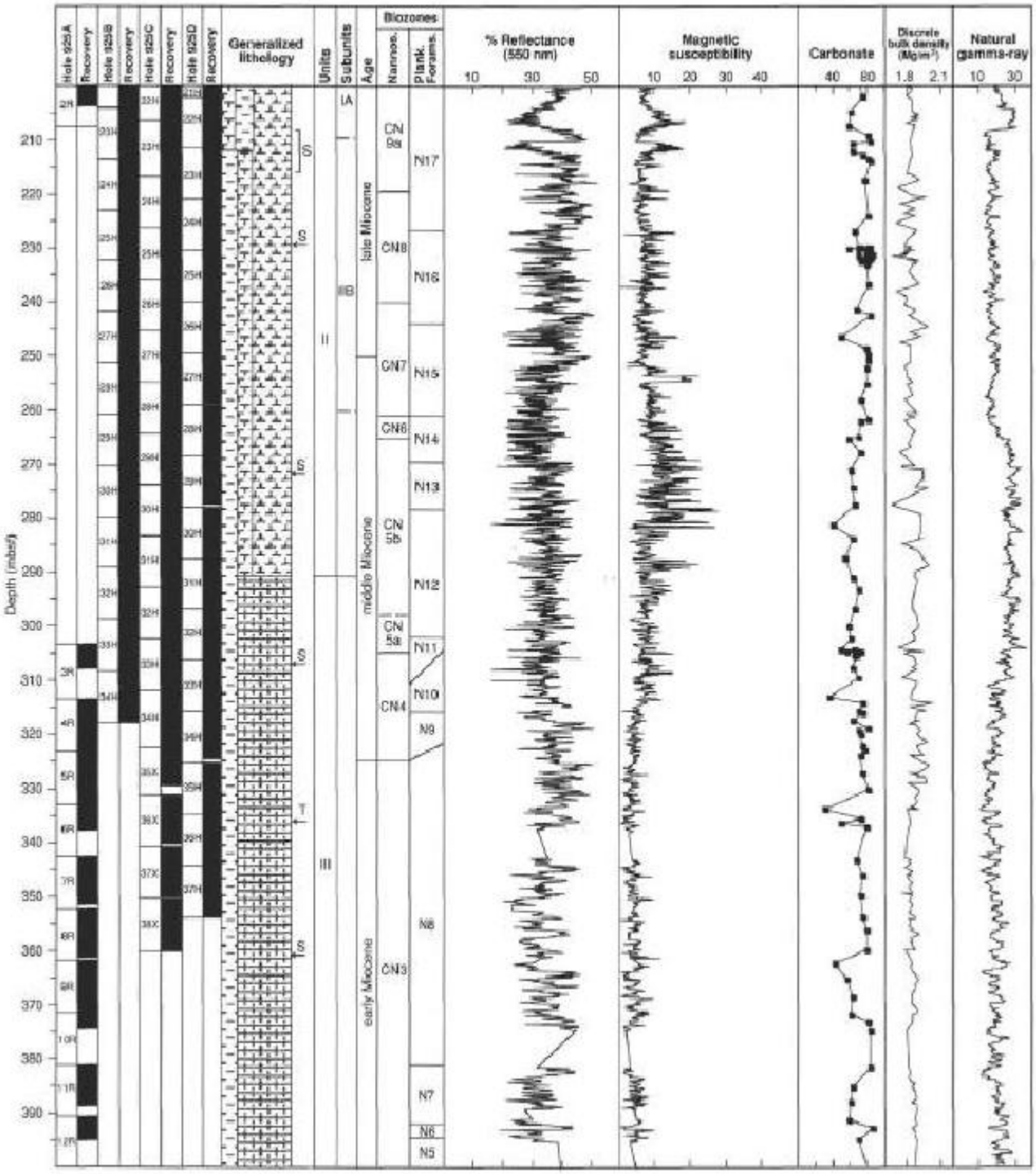
Hole 925A
Recovery
Hole 925B
Recovery
Hole 925C
Recovery
Hole 925D
Recovery
Generalized lithology
Units
Subunits
Age
Biozones:
Nannos.
Plank. Foramns.
% Reflectance (550 nm)
Magnetic susceptibility
Carbonate
Discrete bulk density (Mg/m³)
Natural gamma-ray
Depth (mbsf)
late Miocene
middle Miocene
early Miocene
CN 9a
CN 8
CN 7
CN 6
CN 5b
CN 5a
CN 4
CN 3
N17
N16
N15
N14
N13
N12
N11
N10
N9
N8
N7
N6
N5

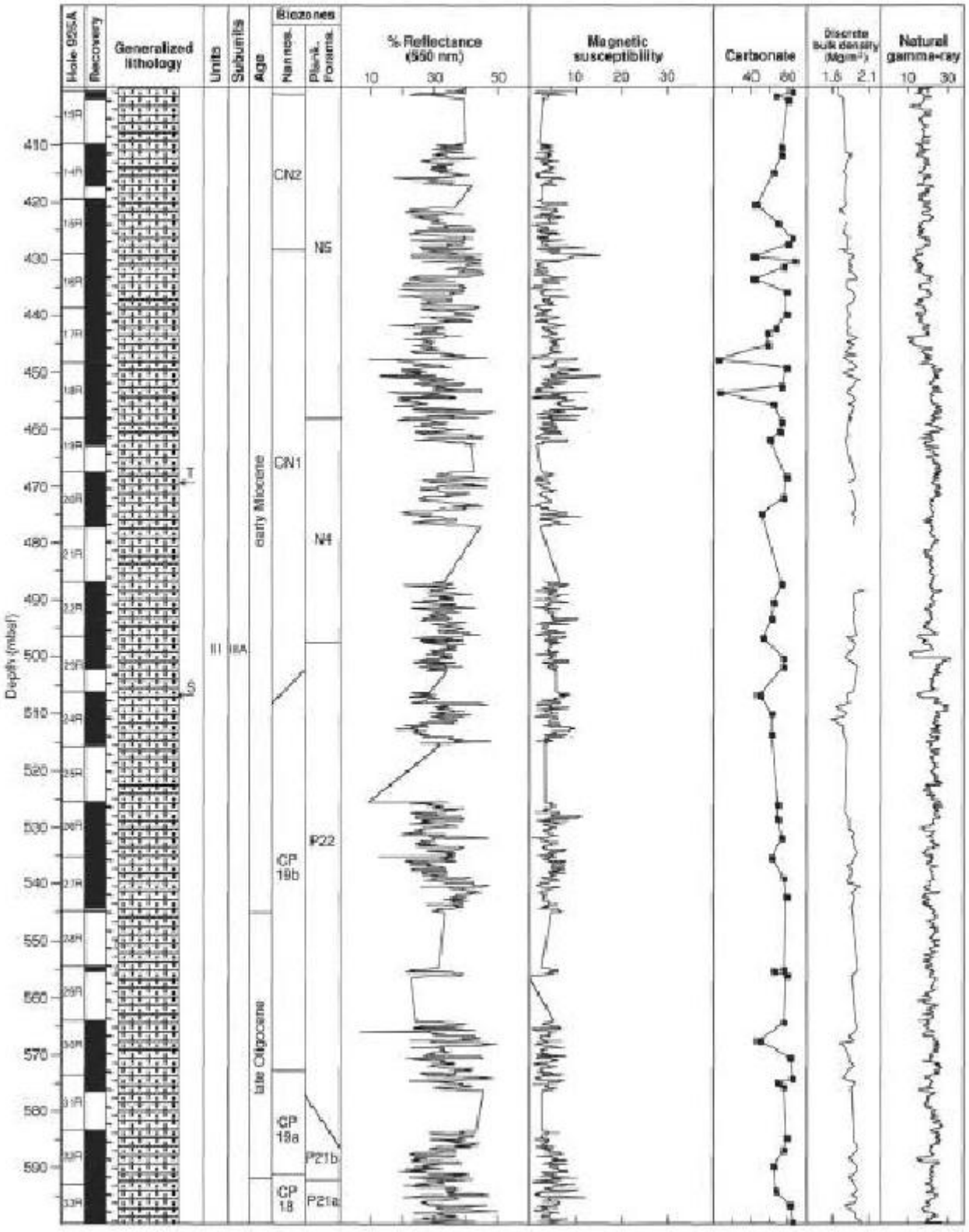
Hole 925A
Recovery
Generalized lithology
Units
Subunits
Age
Biozones
Nannos.
Plank. Foramns.
% Reflectance (550 nm)
Magnetic susceptibility
Carbonate
Discrete bulk density (Mg/m³)
Natural gamma-ray
Depth (mbsf)
410
420
430
440
450
460
470
480
490
500
510
520
530
540
550
560
570
580
590
14R
15R
16R
17R
18R
19R
20R
21R
22R
23R
24R
25R
26R
27R
28R
29R
30R
31R
32R
33R
T
S
III
IIIA
early Miocene
late Oligocene
CN2
CN1
CP 19b
CP 18a
CP 18
N5
N4
P22
P21b
P21a
10
30
50
10
20
30
40
60
1.8
2.1
10
30

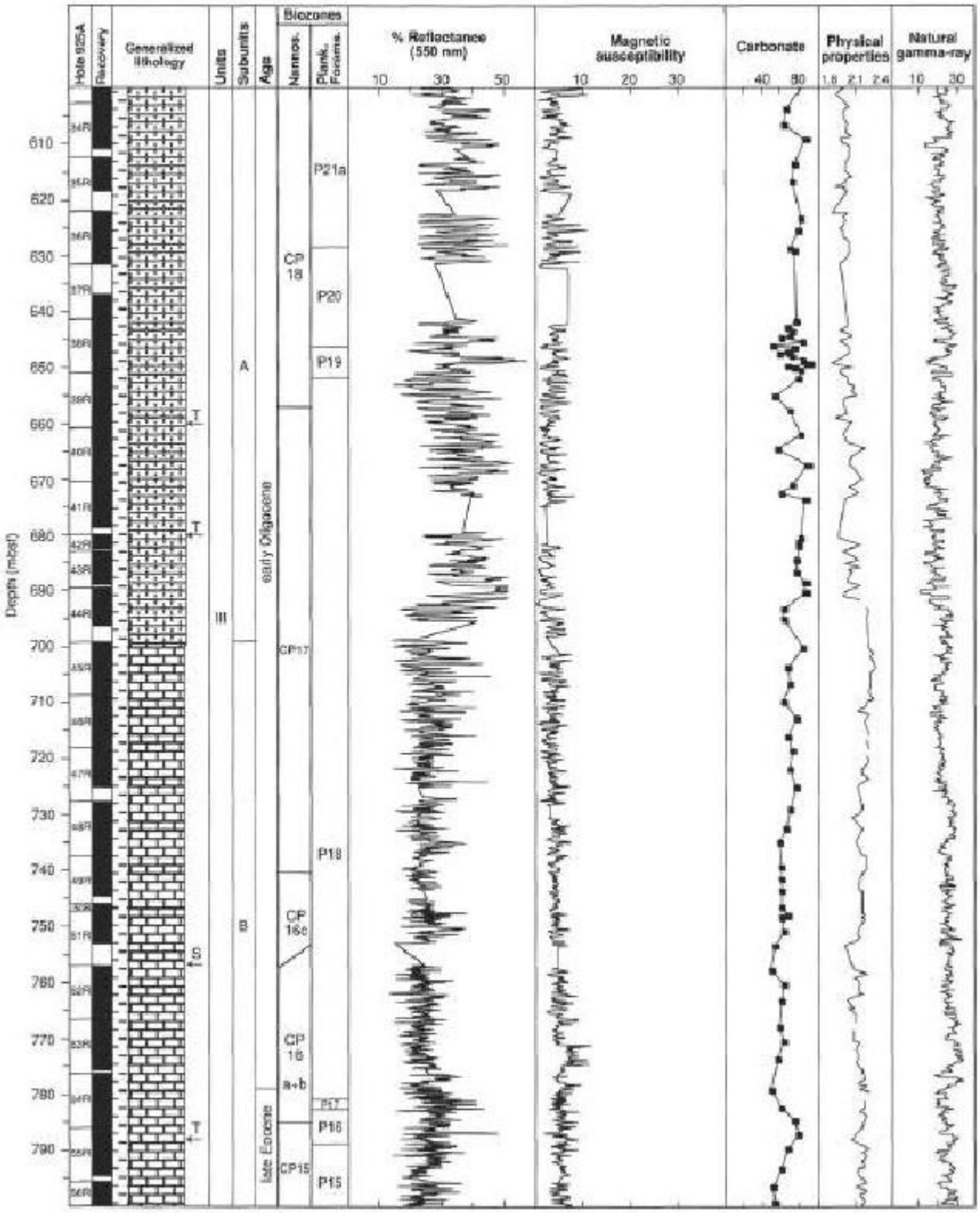
Hole 925A
Recovery
Generalized lithology
Units
Subunits
Age
Biozones
Nannos.
Plank. Foramns.
% Reflectance (550 nm)
Magnetic susceptibility
Carbonate
Physical properties
Natural gamma-ray
Depth (mbsf)
early Oligocene
late Eocene
P21a
P20
P19
P18
P16
P15
CP 18
CP 16c
CP 16
CP 16a+b
CP15
A
B
III

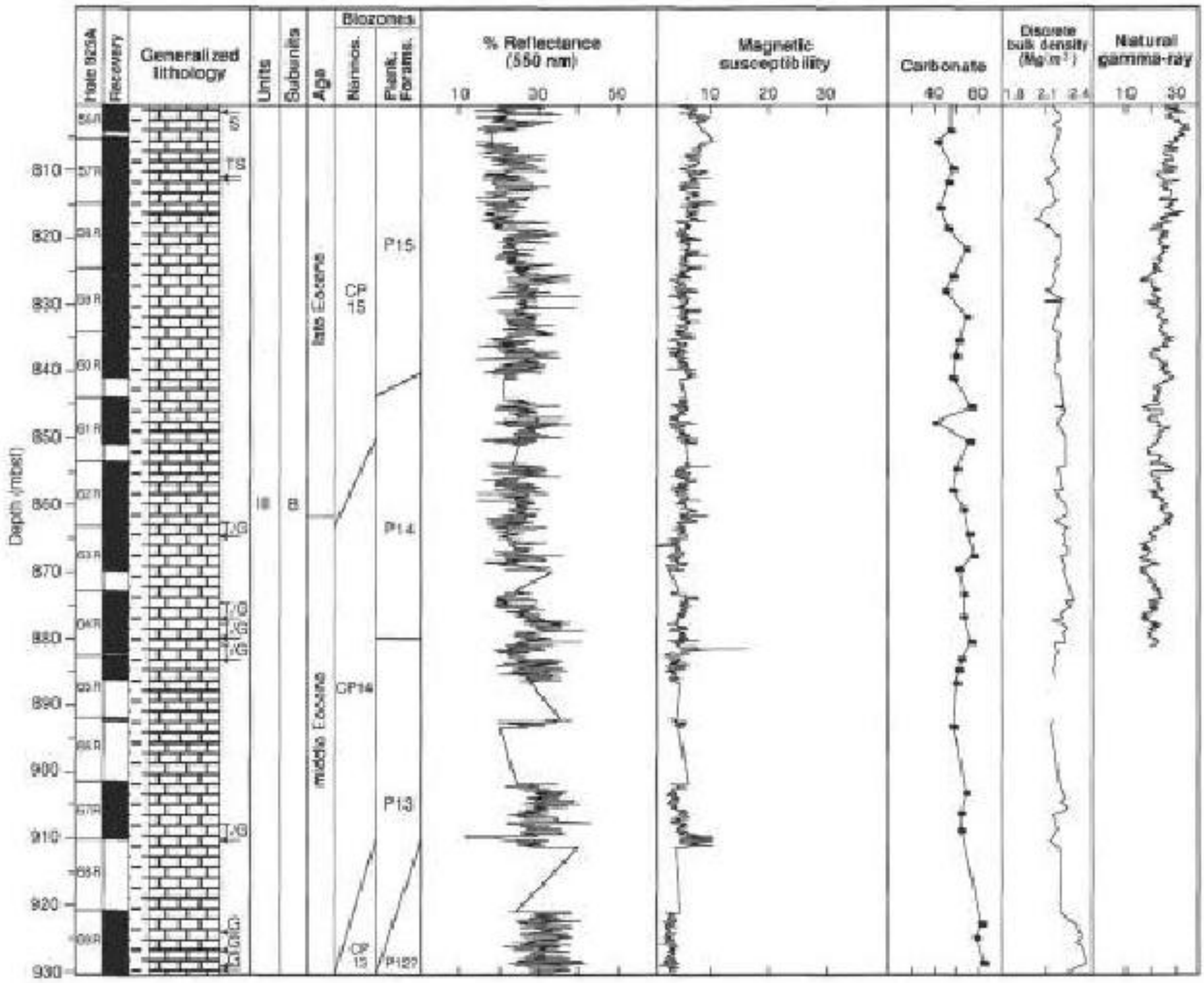
Hole 925A
Recovery
Generalized lithology
Units
Subunits
Age
Biozones
Nannos.
Plank. Forams.
% Reflectance (550 nm)
Magnetic susceptibility
Carbonate
Discrete bulk density (Mg/m³)
Natural gamma-ray
Depth (mbsf)
late Eocene
middle Eocene
CP 15
CP14
P15
P14
P13
III
B

APPENDIX C. CHORMATOGRAMS OF *N*-ALKANES' EXTRACTS

Sample CRA 3 R1

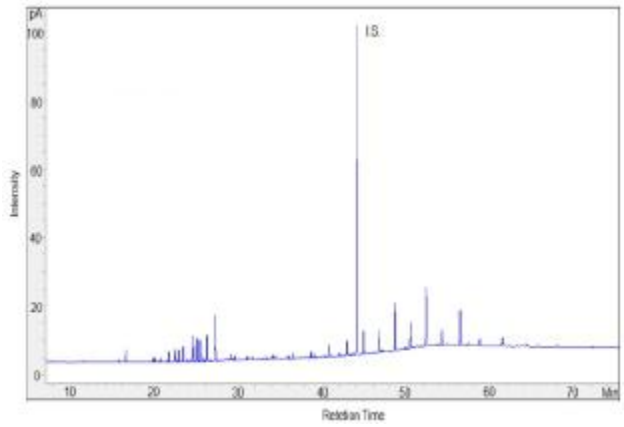

Sample CRA 5 R4

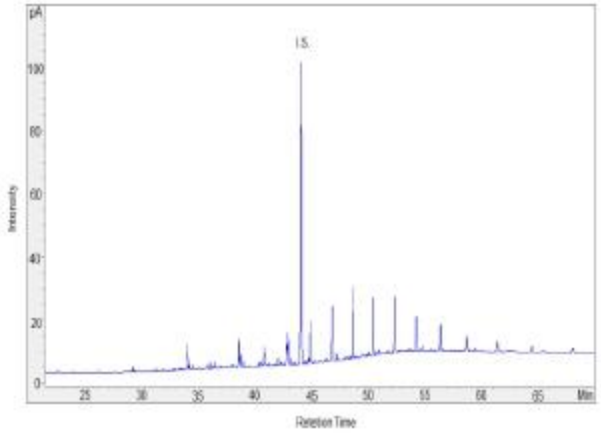

Sample CRA 4 R1

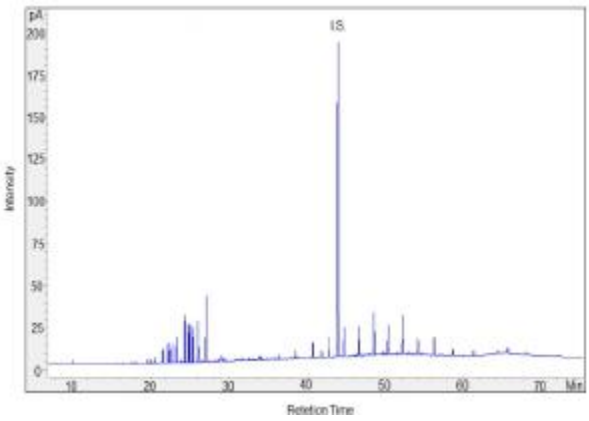

Sample CRA 6 R1

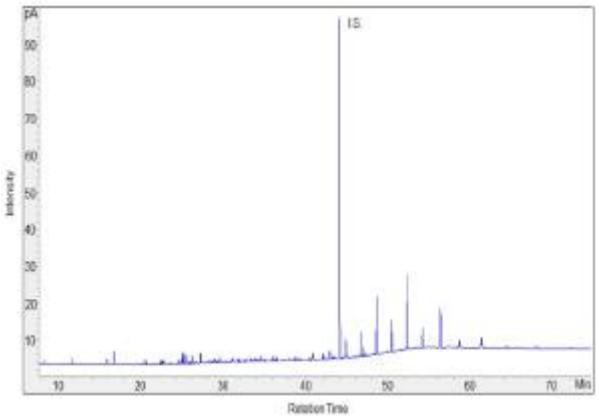

Sample CRA 5 R1

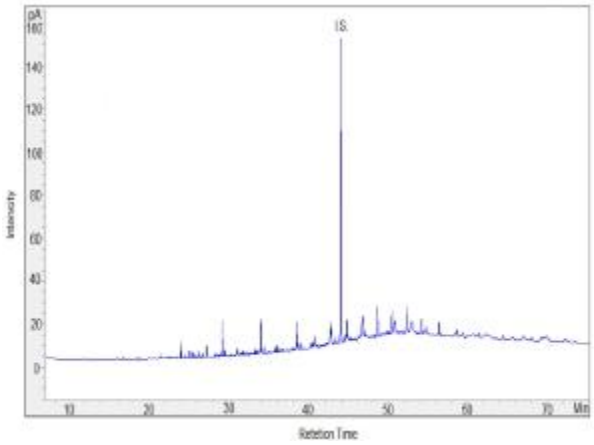

Sample CRA 6 R3

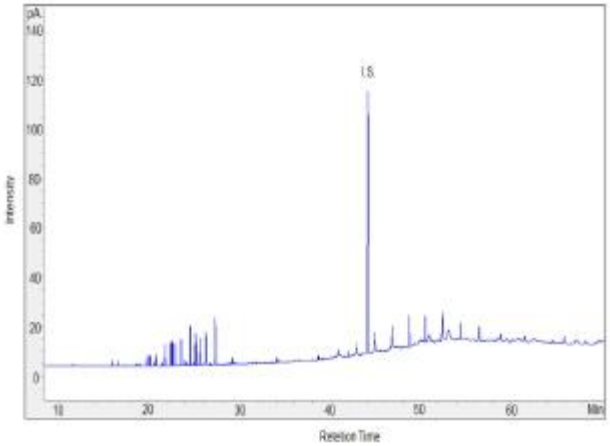

Sample CRA 7 R3

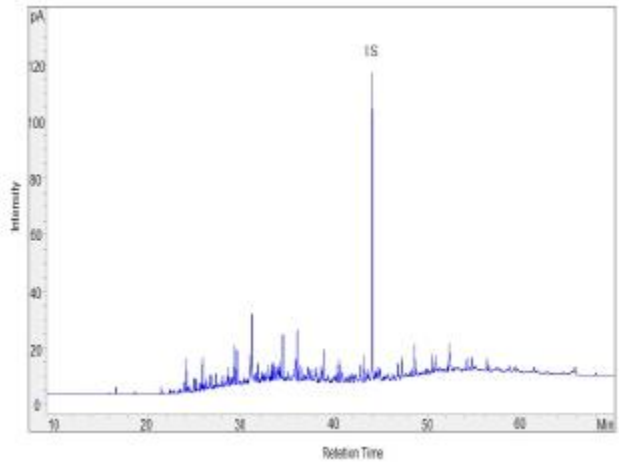

Sample CRA 10 R1

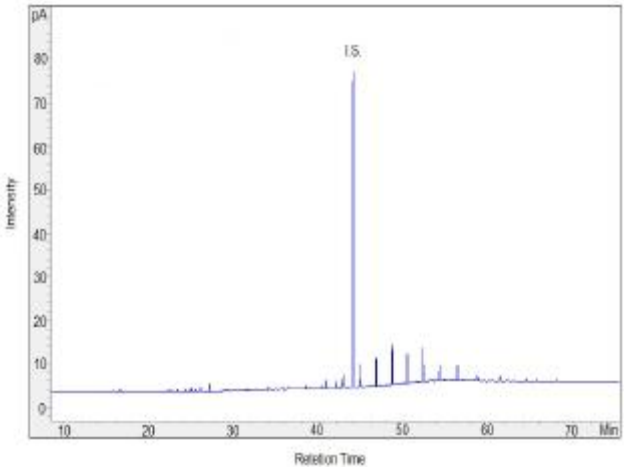

Sample CRA 8 R6

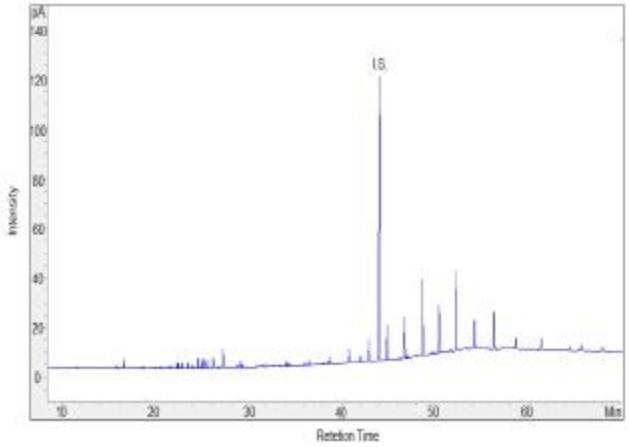

Sample CRA 11 R1

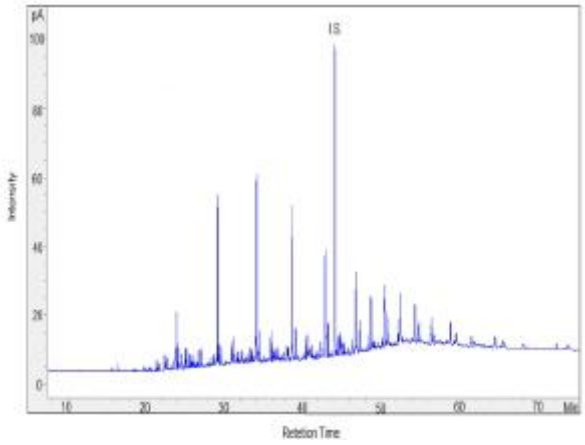

Sample CRA 9 R4

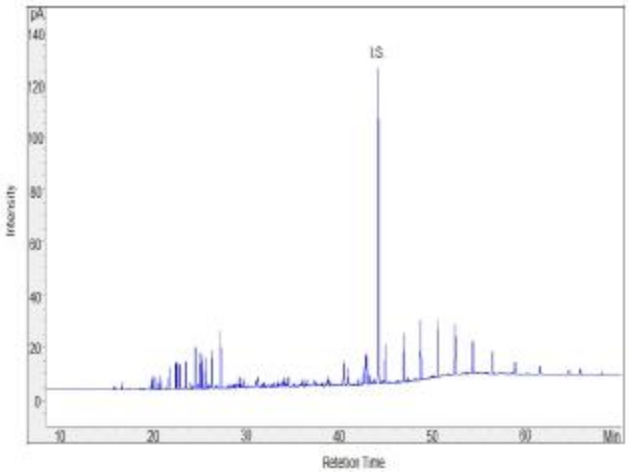

Sample CRA 11 R6

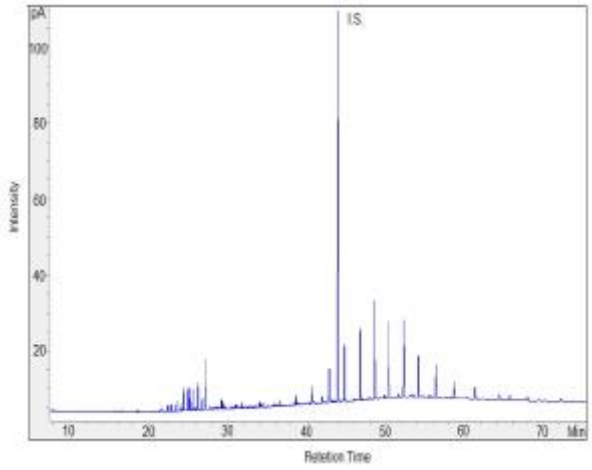

Sample CRA 12 R1

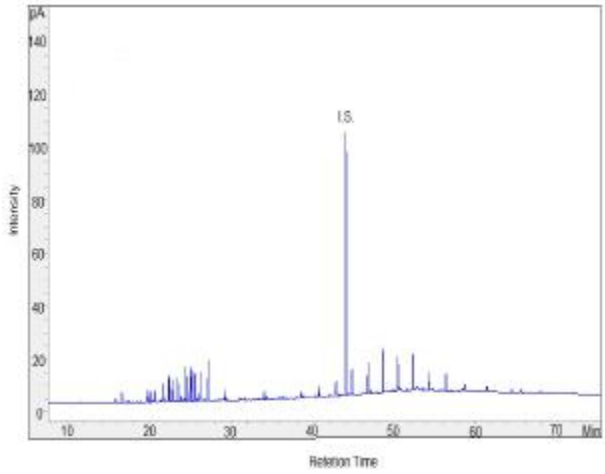

Sample CRA 14 R5

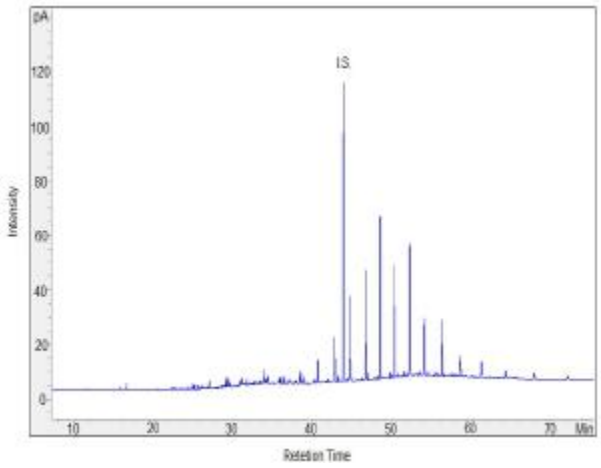

Sample CRA 13 R1

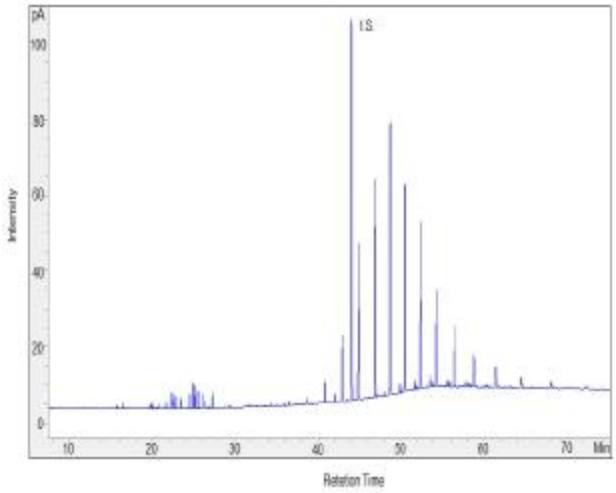

Sample CRA 15 R1

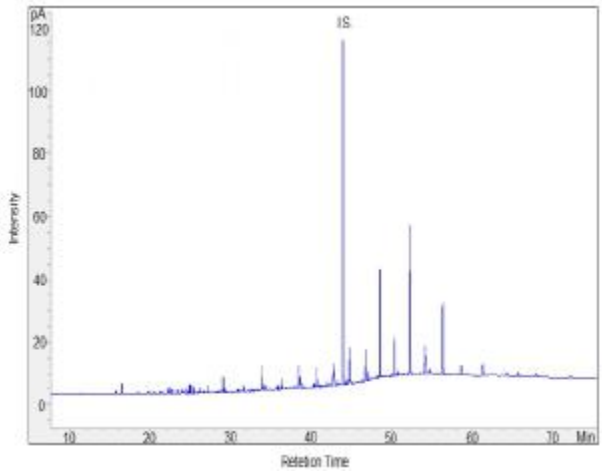

Sample CRA 14 R1

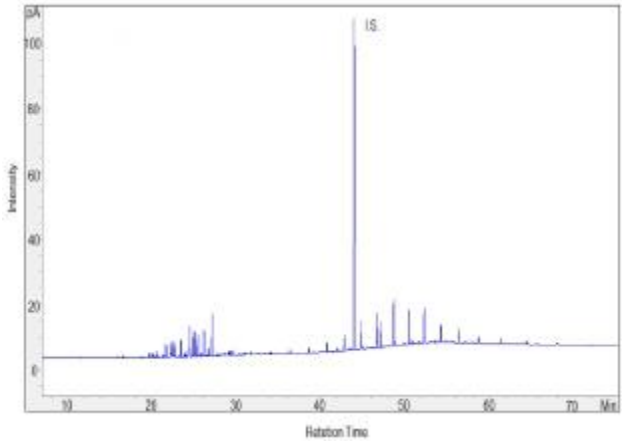

Sample CRA 16 R4

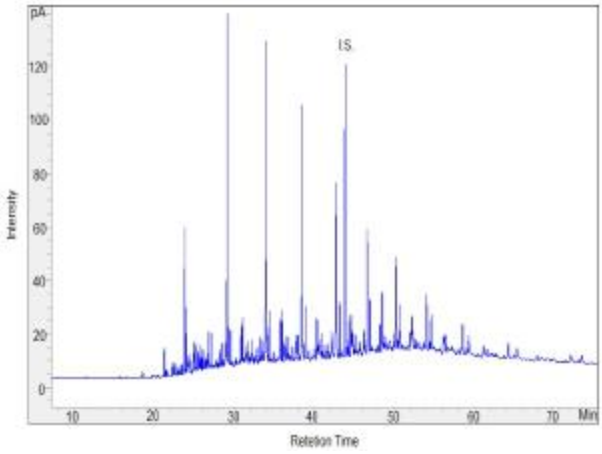

Sample CRA 17 R3

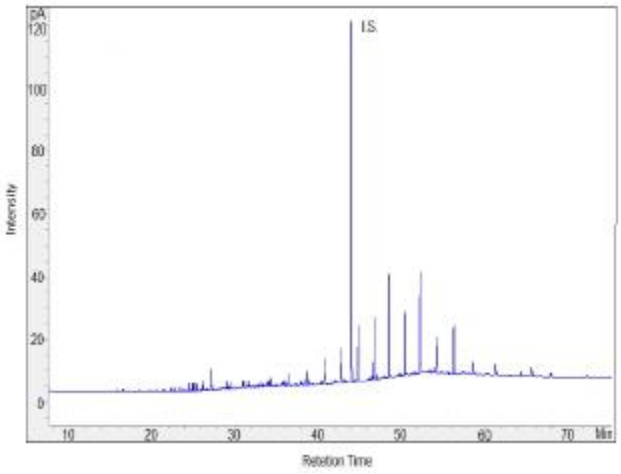

Sample CRA 20 R4

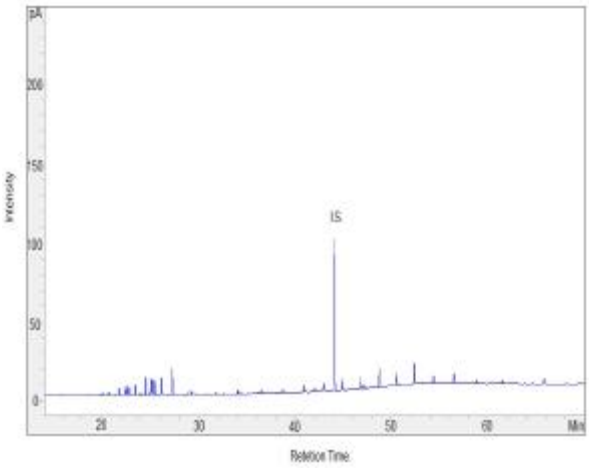

Sample CRA 18 R3

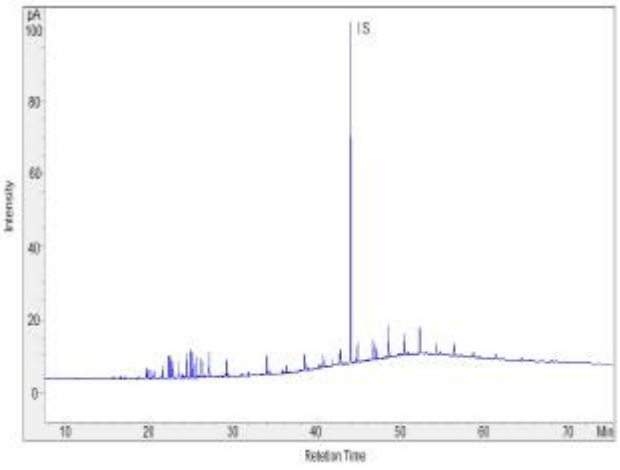

Sample CRA 22 R3

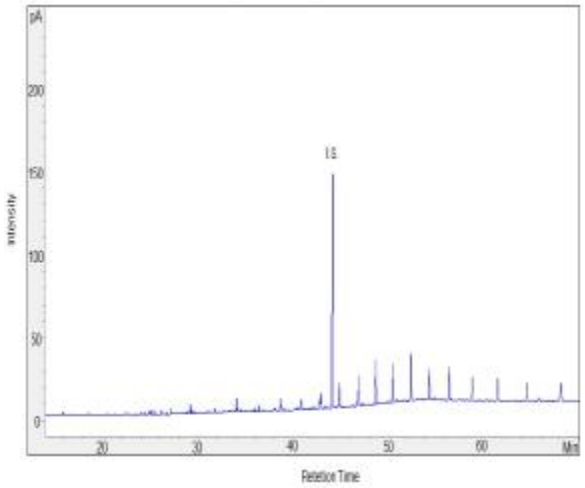

Sample CRA 20 R1

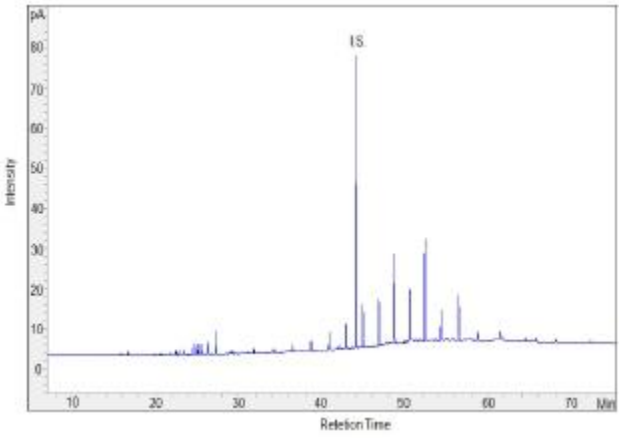

Sample CRA 22 R7

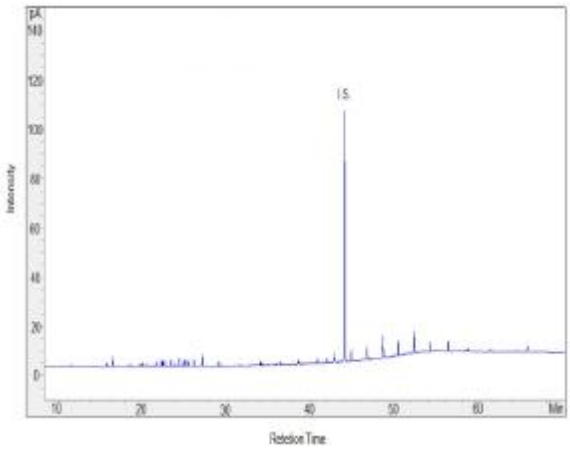

Sample CRA 23 R3

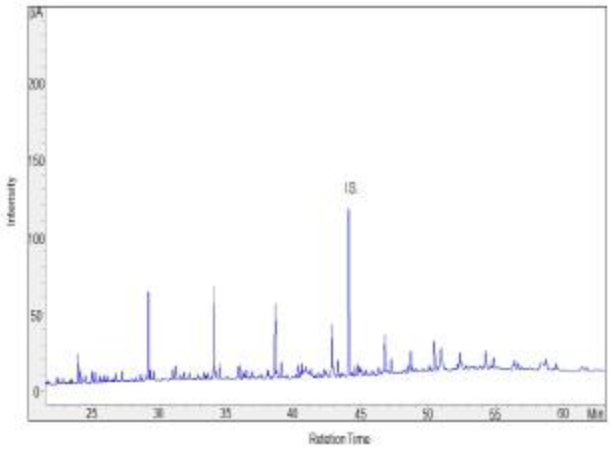

Sample RA 26 R8

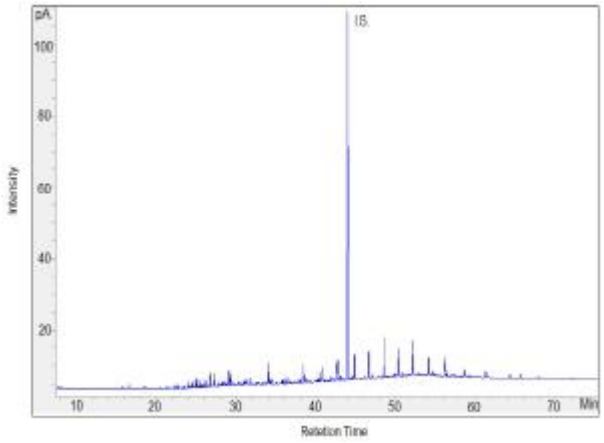

Sample CRA24 R1

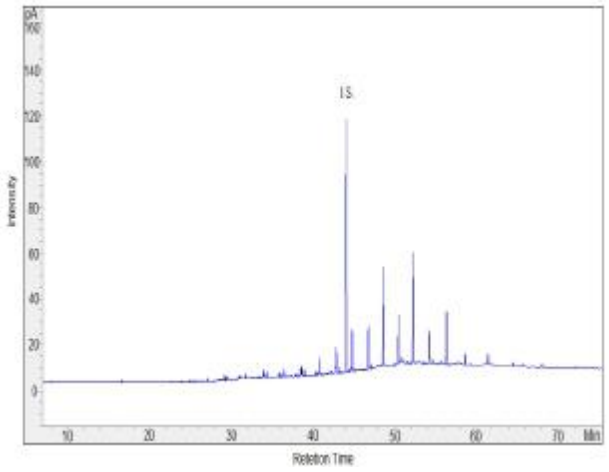

Sample CRA 29 R1

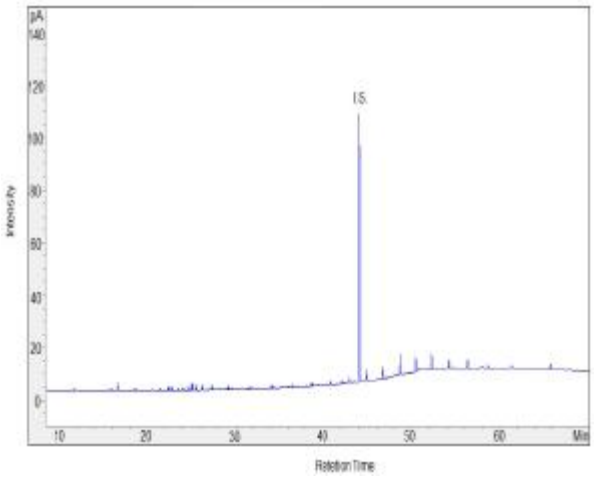

Sample CRA 26 R1

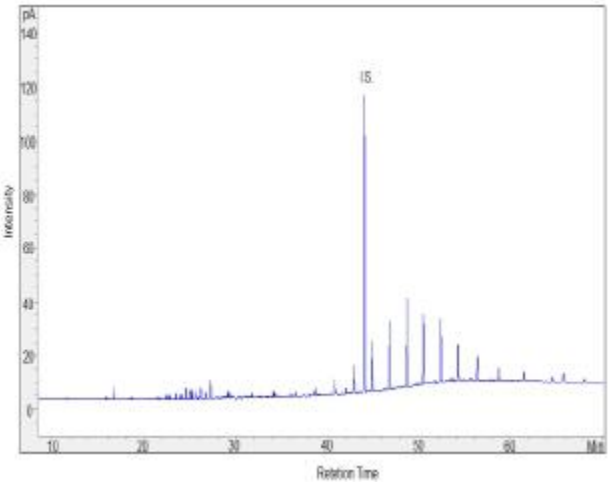

Sample CRA 30 R5

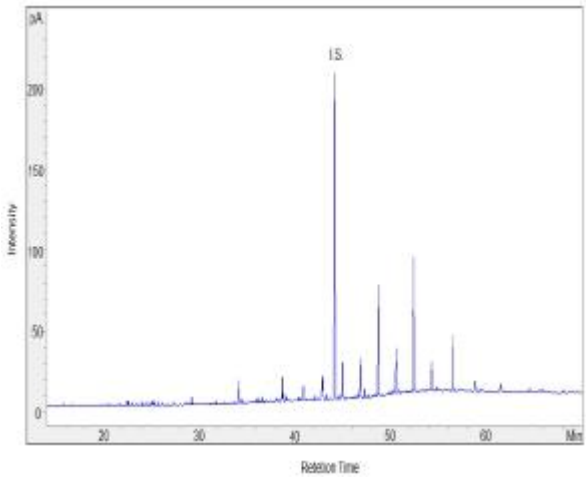

Sample CRA 32 R1

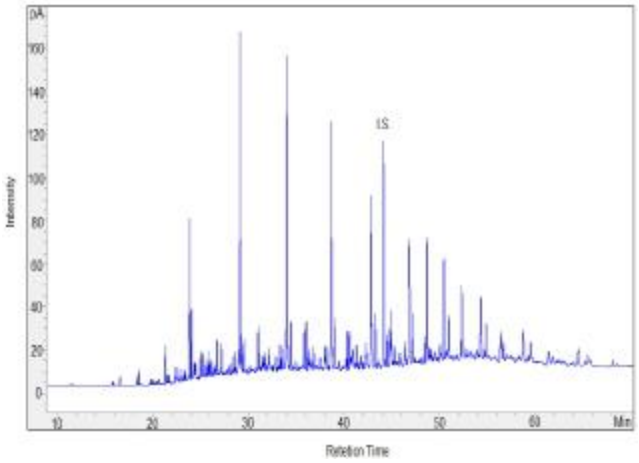

Sample CRA 39 R4

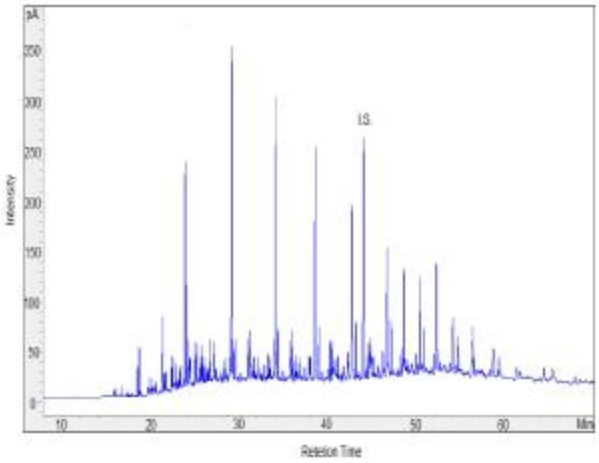

Sample CRA 33 R6

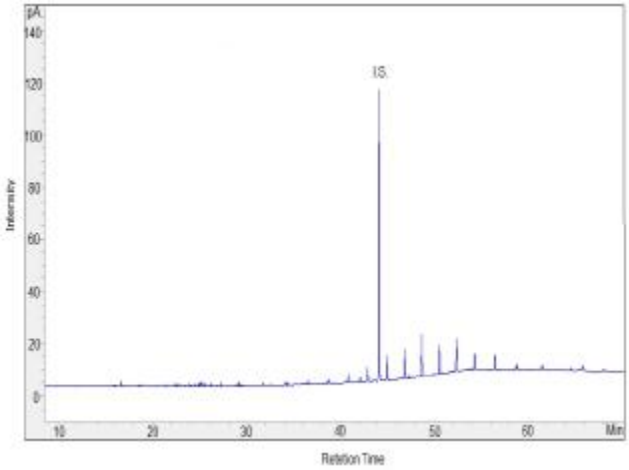

Sample CRB1 H1

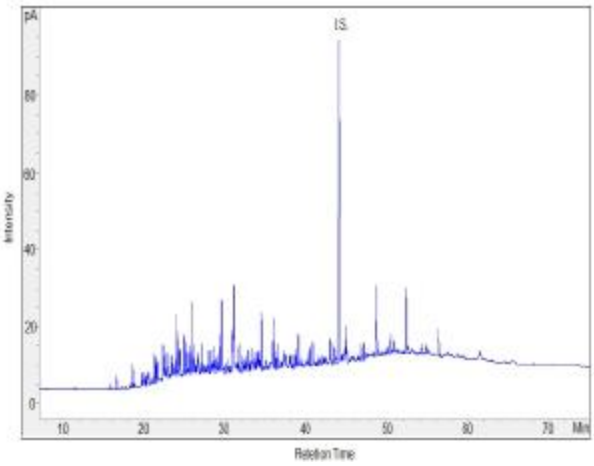

Sample CRA 36 R7

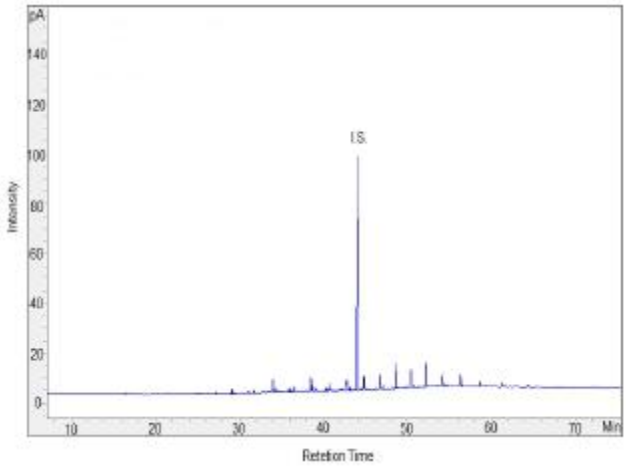

Sample CRB 2 H3

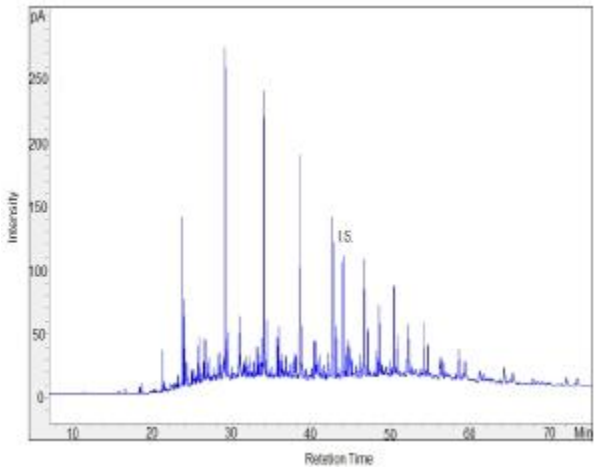

Sample CRB 3 H4

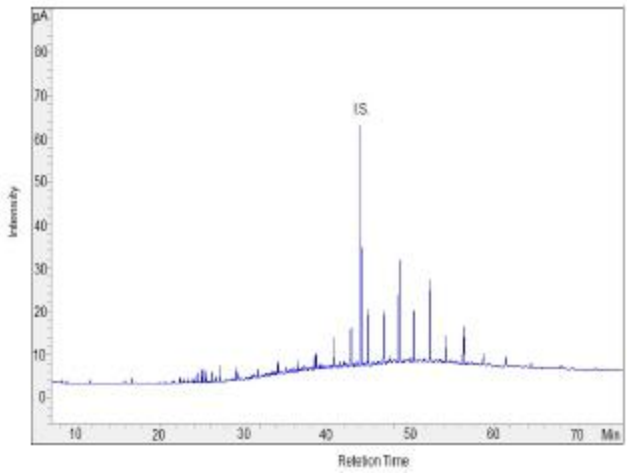

Sample CRB 7 H1

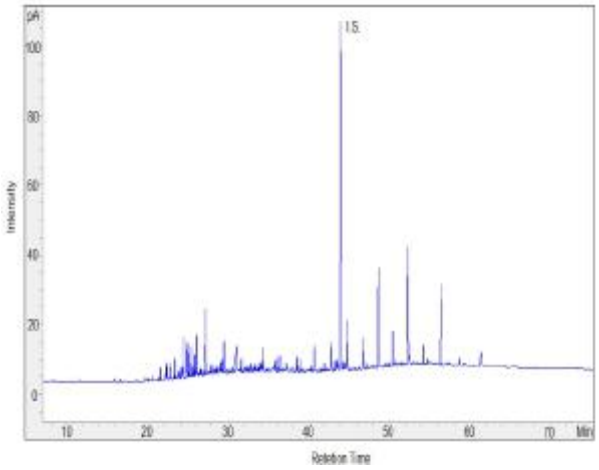

Sample CRB 4 H3

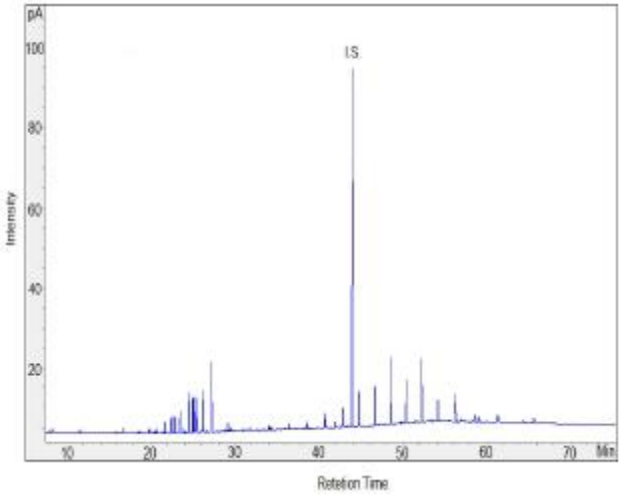

Sample CRB 7 H3

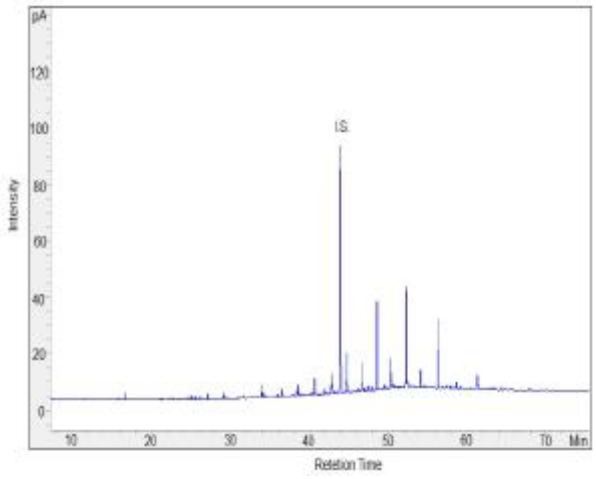

Sample CRB 6 H4

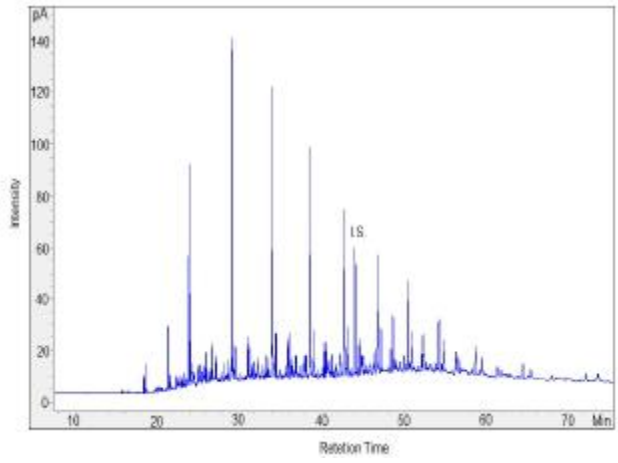

Sample CRB 7 H5

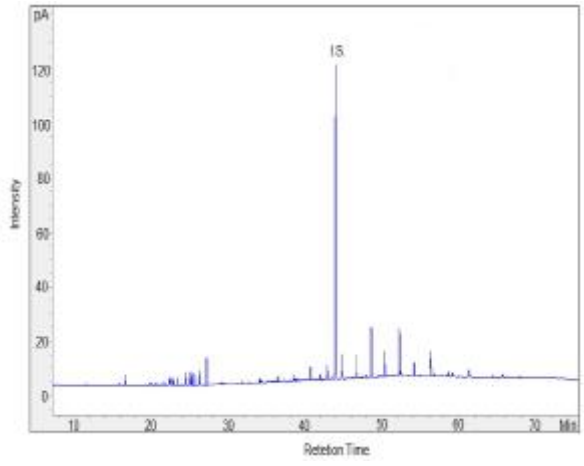

Sample CRB 8 H3

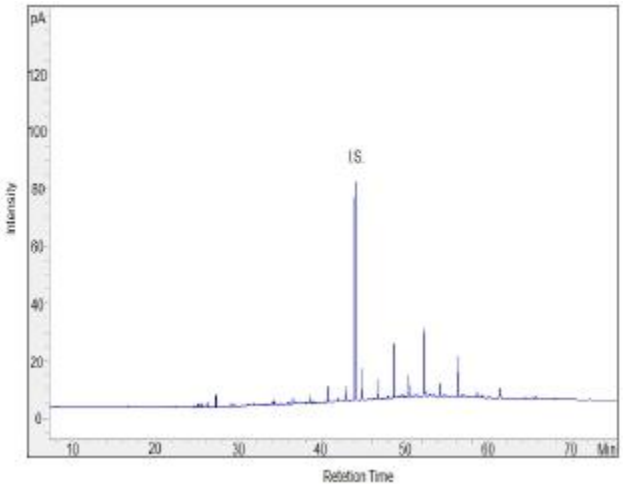

Sample CRB 11 H6

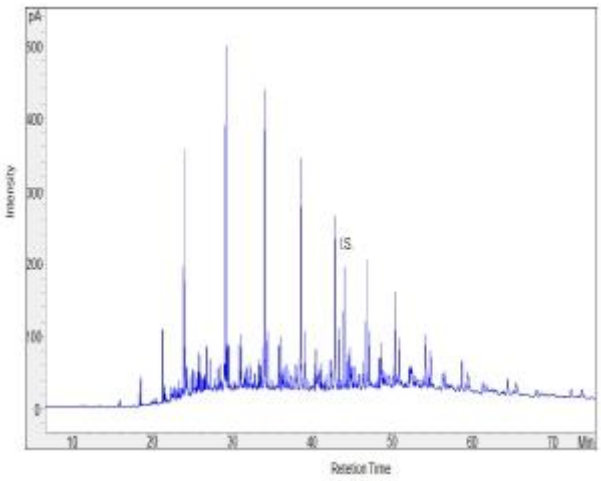

Sample CRB 9 H6

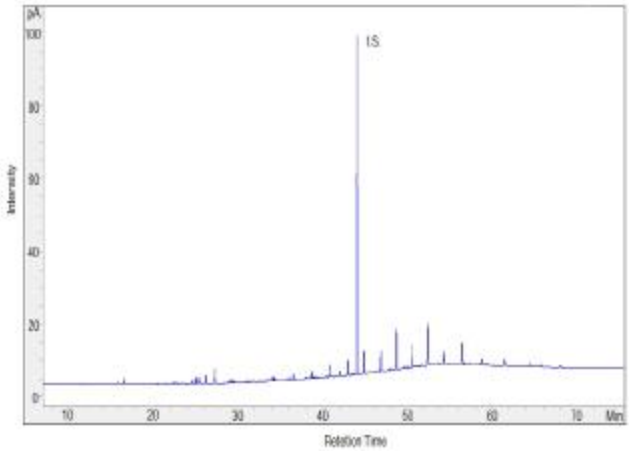

Sample CRB 13 H5

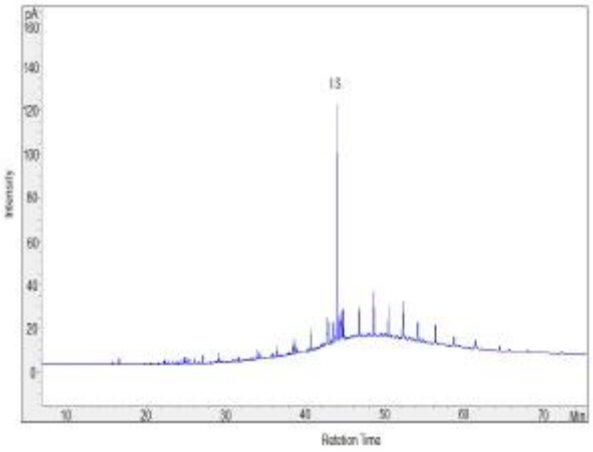

Sample CRB 11 H3

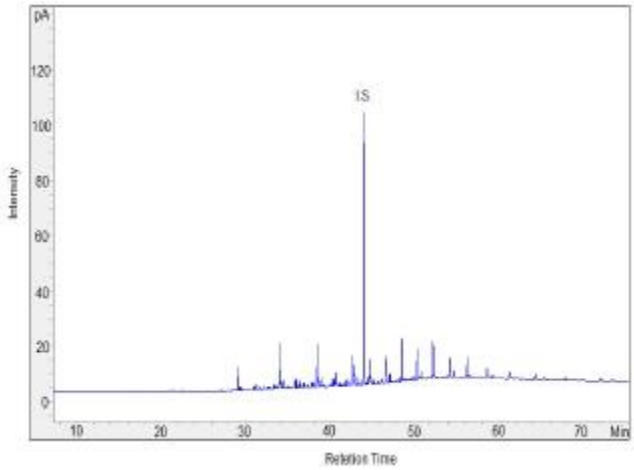

Sample CRB 14 H3

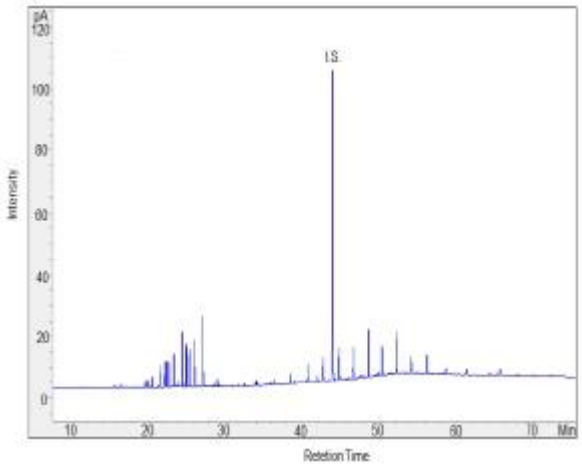

Sample CRB 15 H2

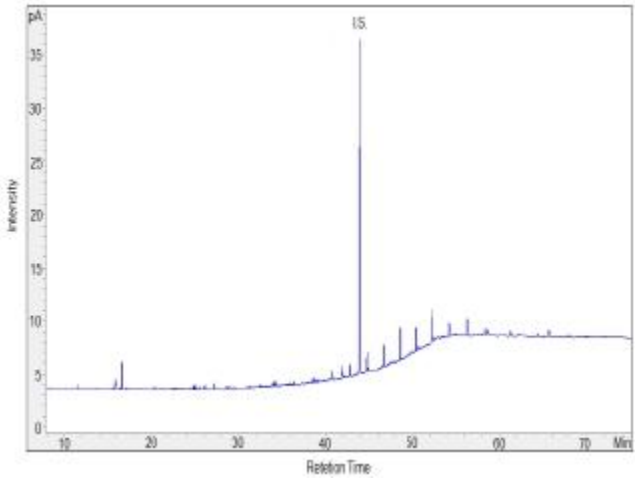

Sample CRB 18 H3

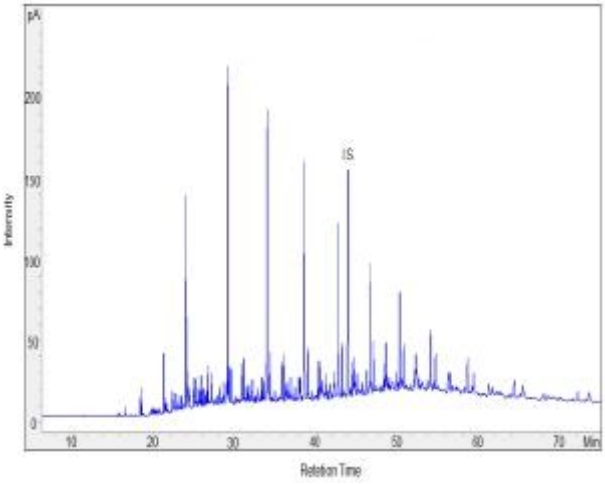

Sample CRB 16 H3

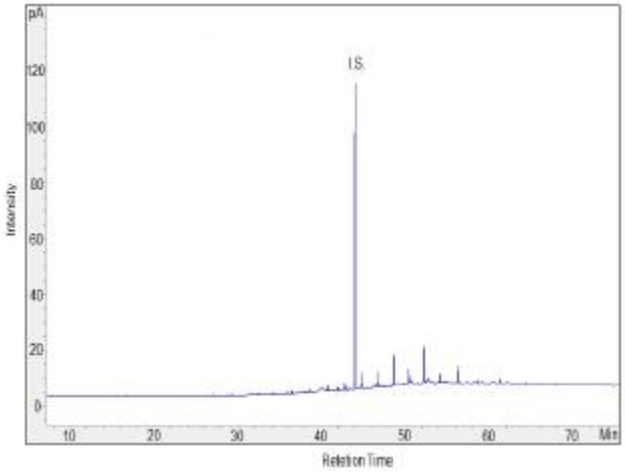

Sample CRB 19 H3

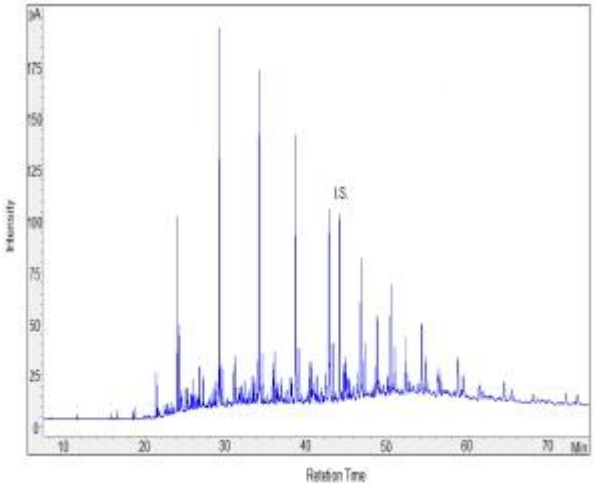

Sample CRB 17 H5

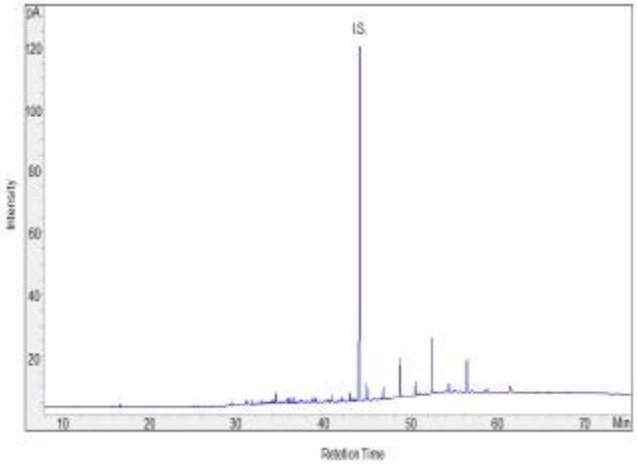

Sample CRB 20 H6

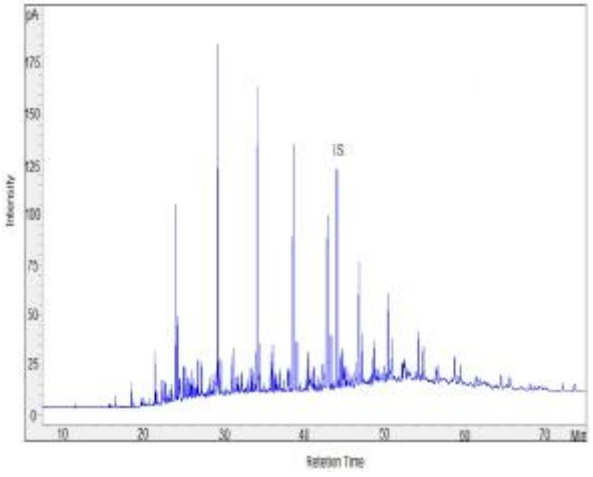

Sample CRB 21 H3

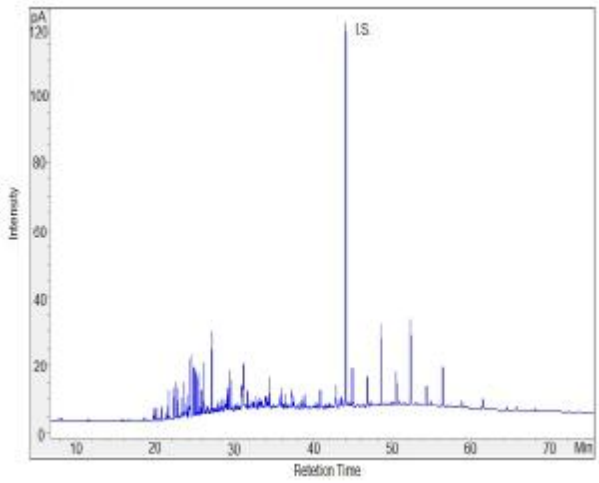

Sample CRB 25 H7

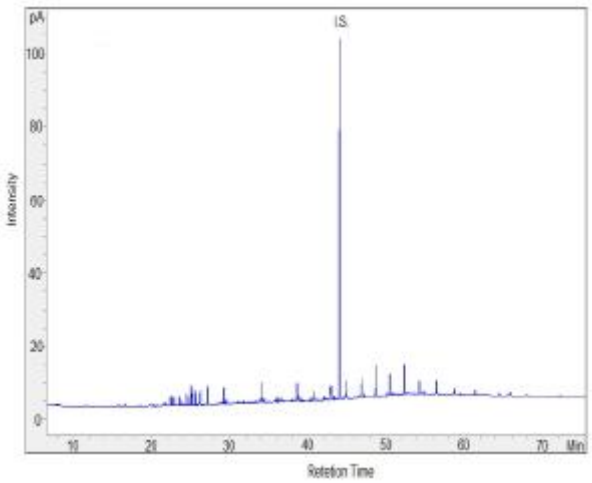

Sample CRB 21 H7

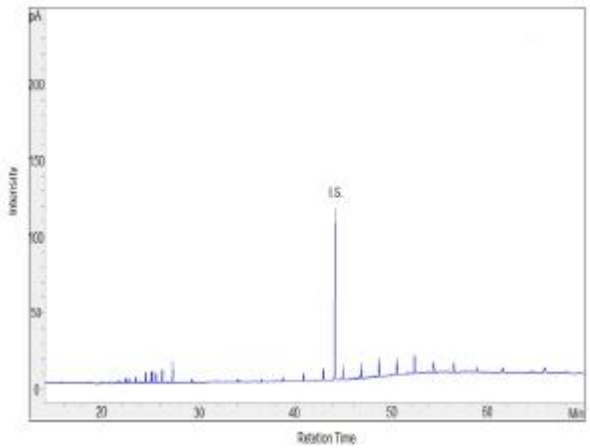

Sample CRB 26 H3

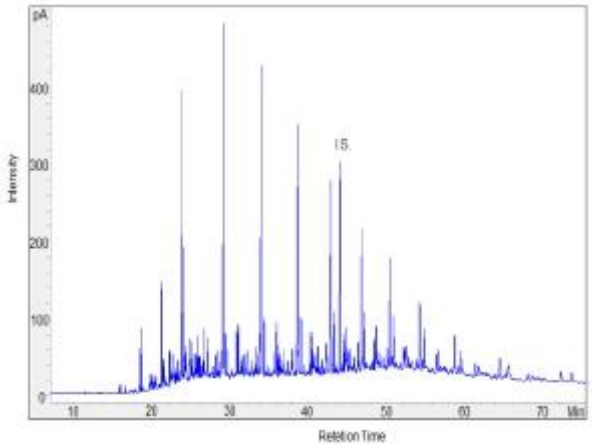

Sample CRB 24 H3

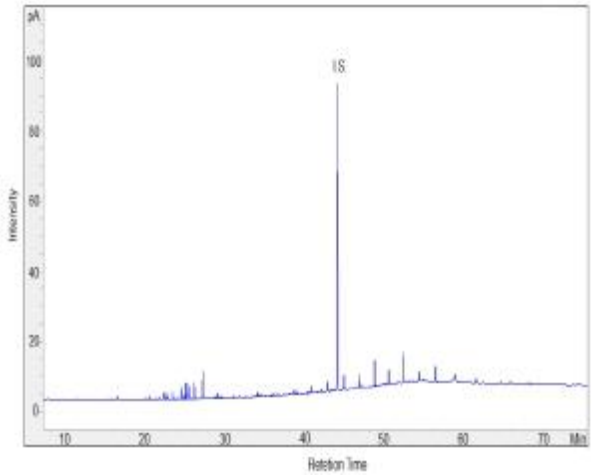

Sample CRB 26 H6

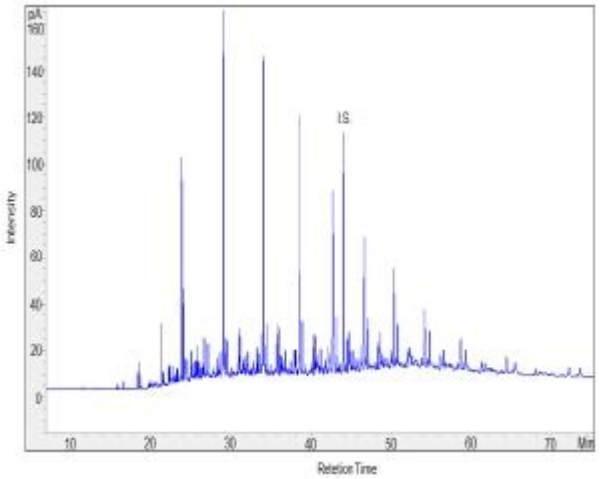

Sample CRB 27 H4

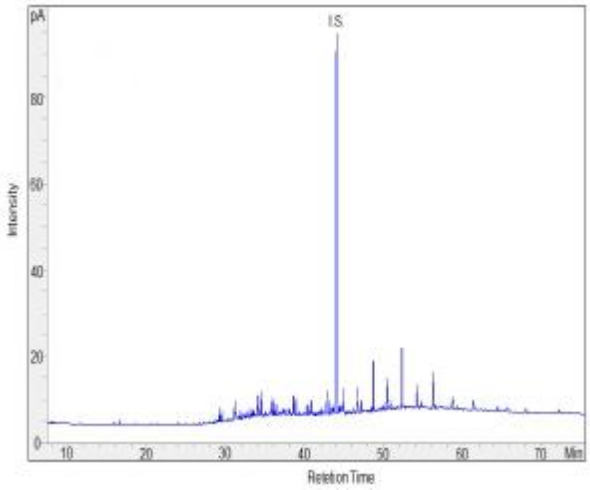

Sample CRB 28 H7

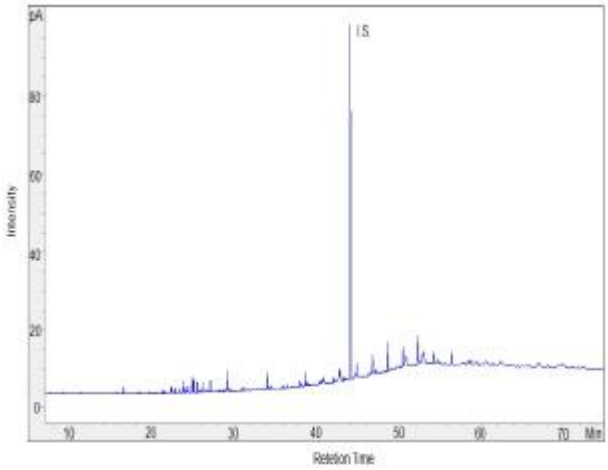

Sample CRB 27 H7

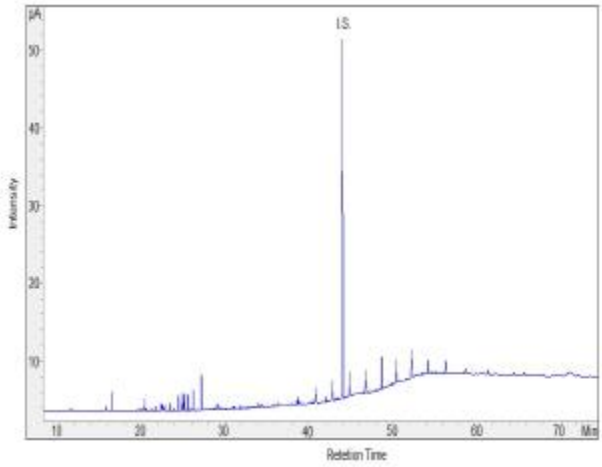

Sample CRB 29 H4

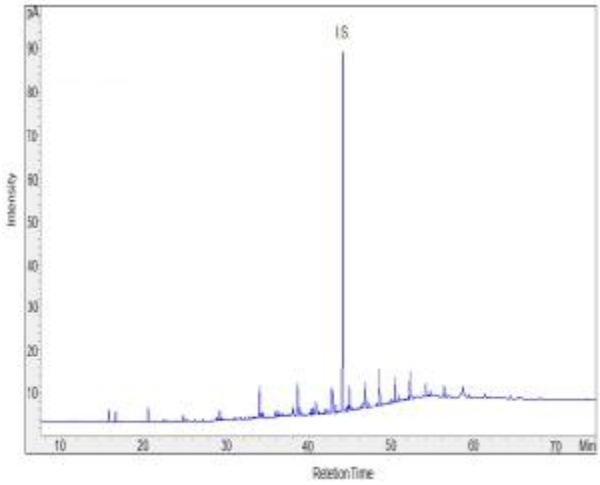

Sample CRB 28 H3

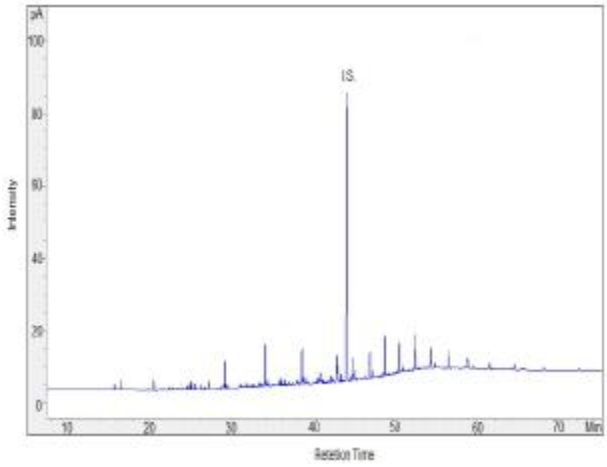

Sample CRB 30 H3

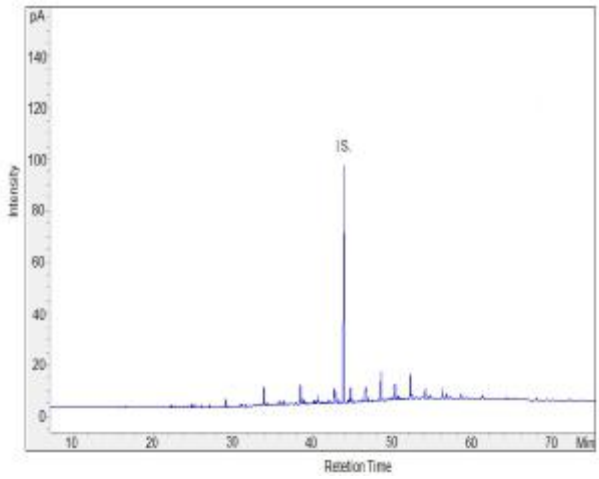

Sample CRB 30 H7

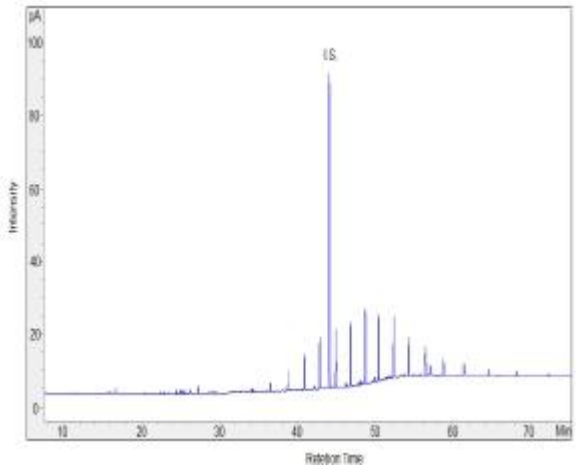

Sample CRB 32 H7

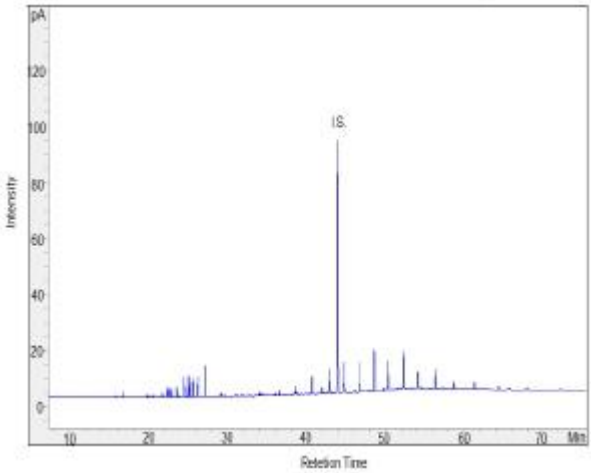

Sample CRB 31 H4

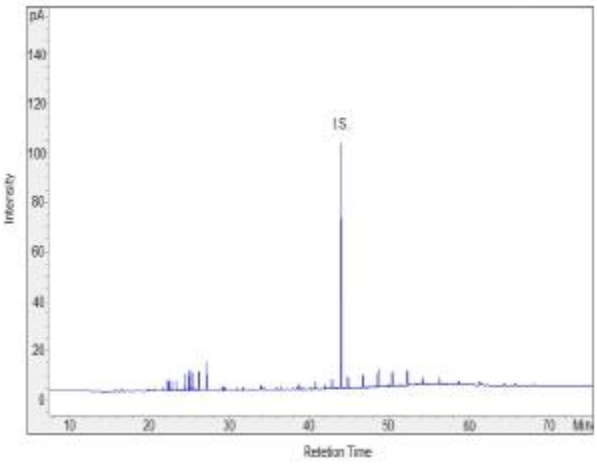

Sample CRB 33 H7

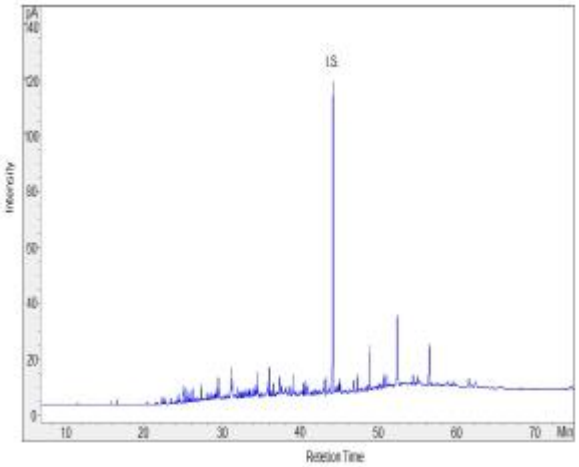

Sample CRB 32 H3

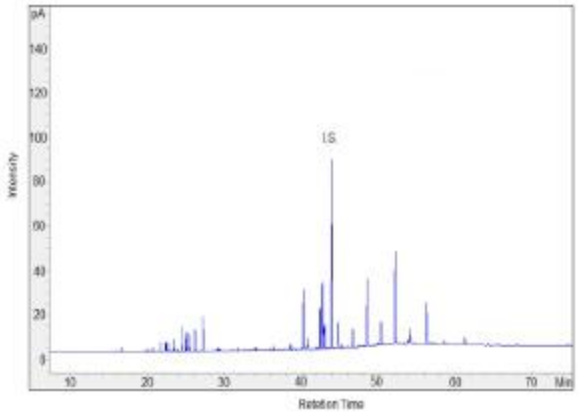

APPENDIX D. CHORMATOGRAMS OF ALKENONES' EXTRACTS

Sample CRA 3 R1

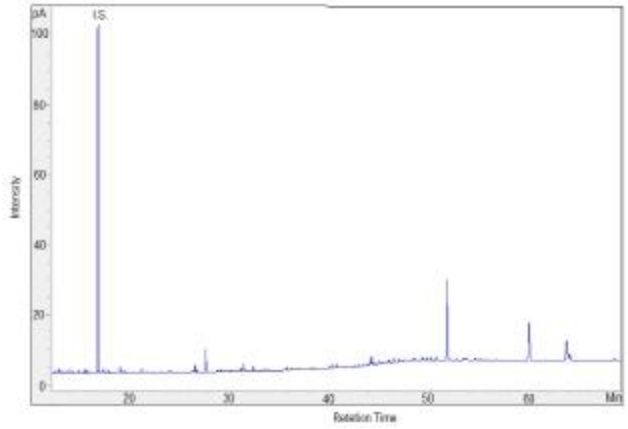

Sample CRA 6 R1

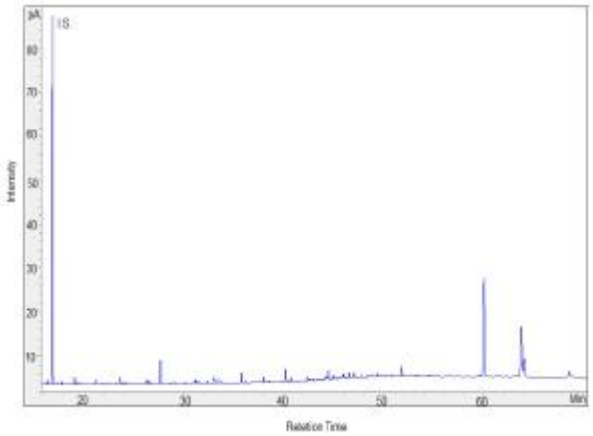

Sample CRA 4 R1

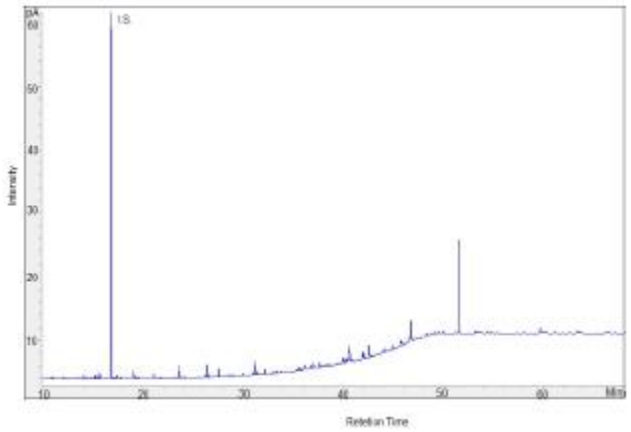

Sample CRA 6 R3

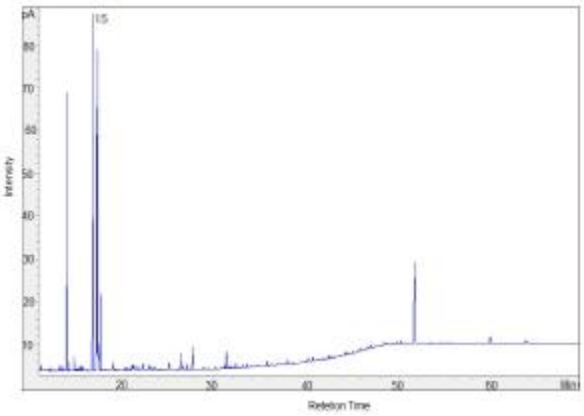

Sample CRA 5 R1

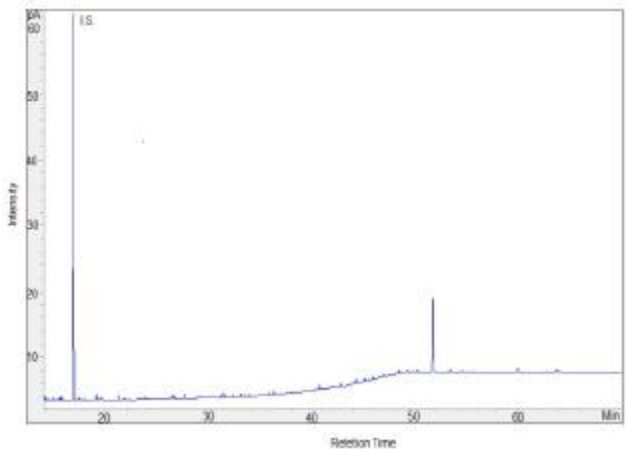

Sample CRA 8 R2

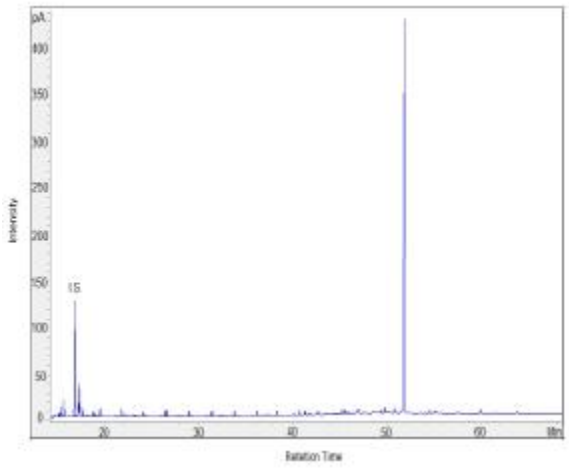

Sample CRA 8 R6

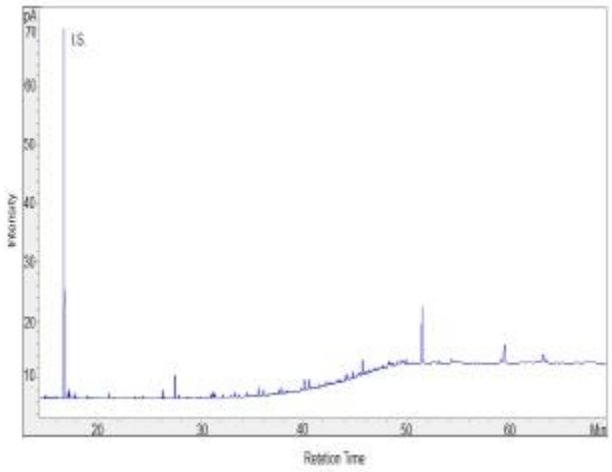

Sample CRA 11 R1

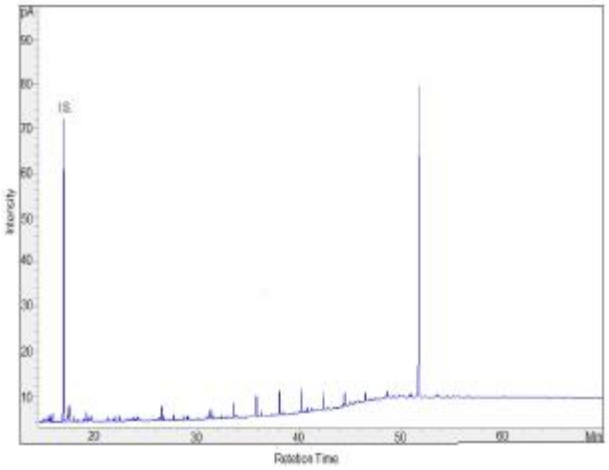

Sample CRA 9 R4

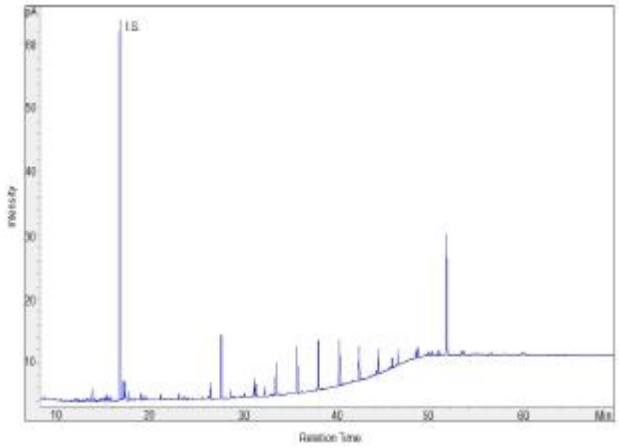

Sample CRA 12 R1

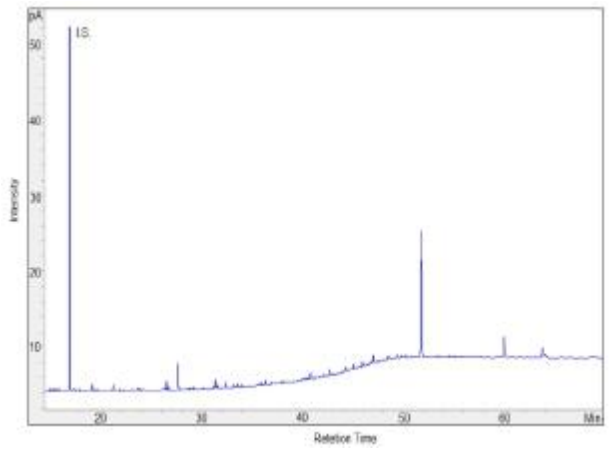

Sample CRA 10 R1

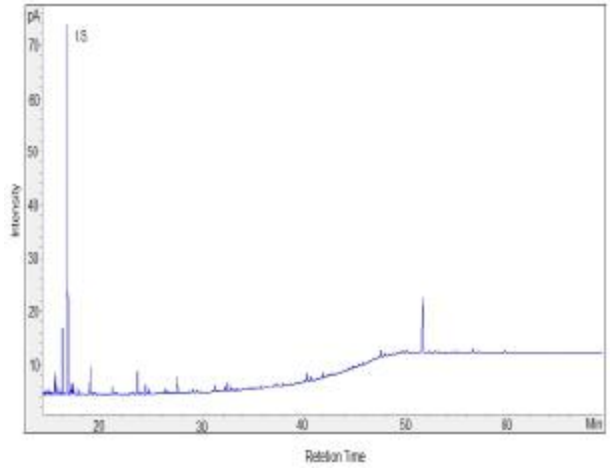

Sample CRA 13 R1

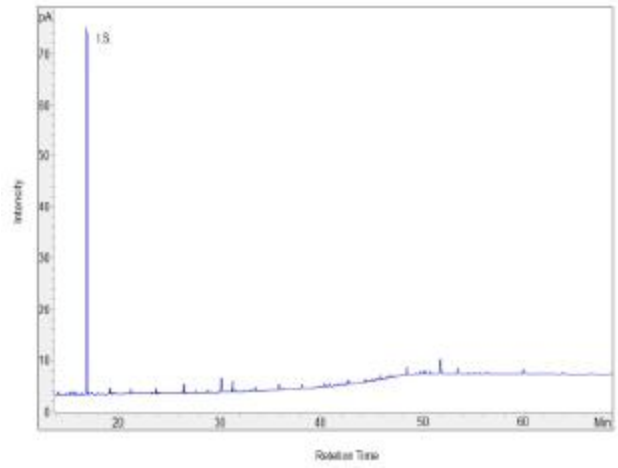

Sample CRA 14 R1

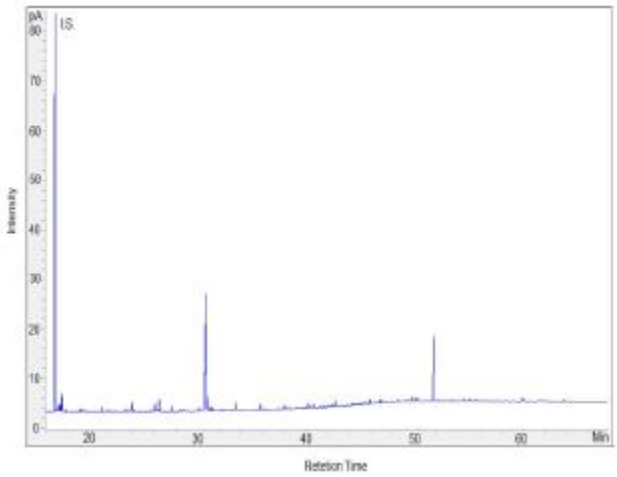

Sample CRA 15 R7

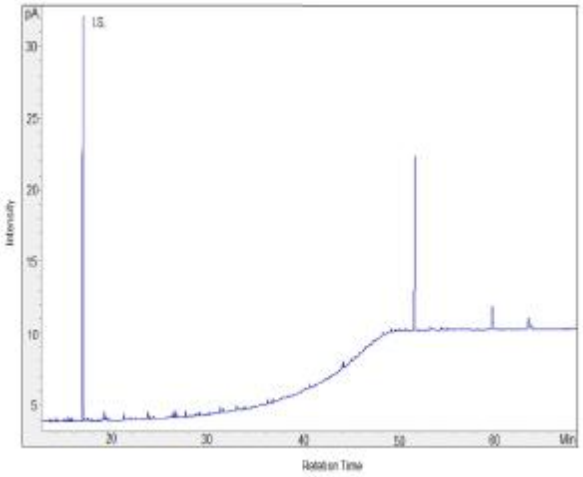

Sample CRA 14 R5

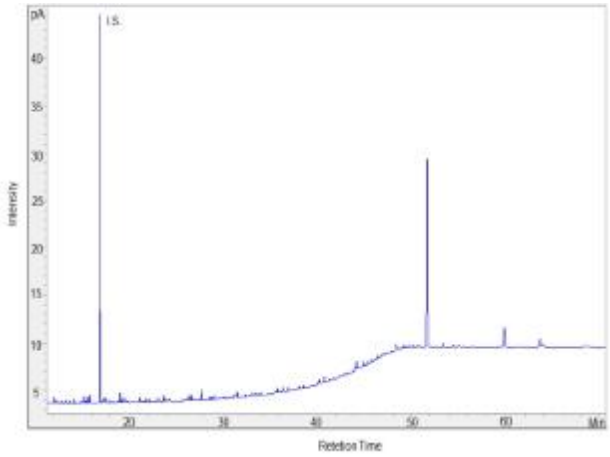

Sample CRA 16 R4

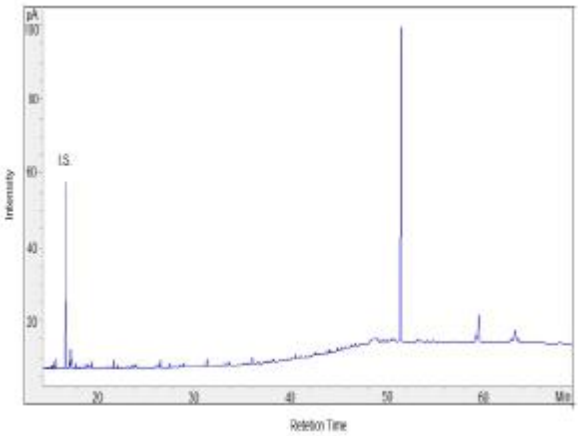

Sample CRA 15 R1

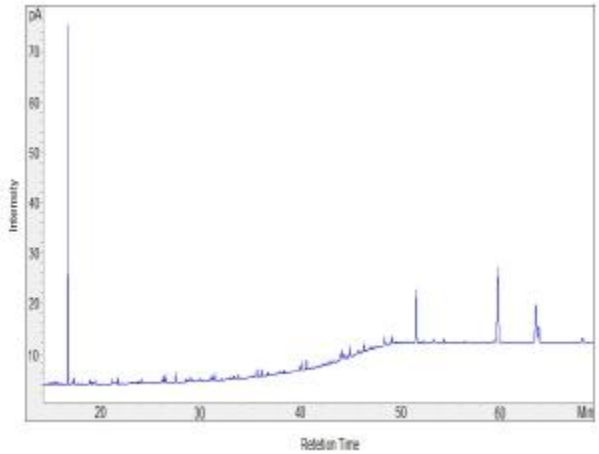

Sample CRA 17 R3

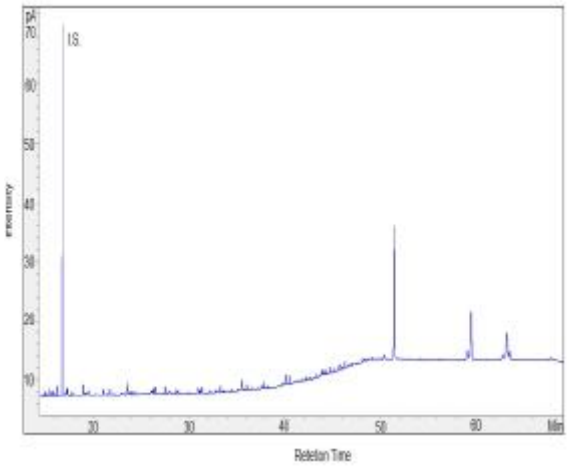

Sample CRA 18 R3

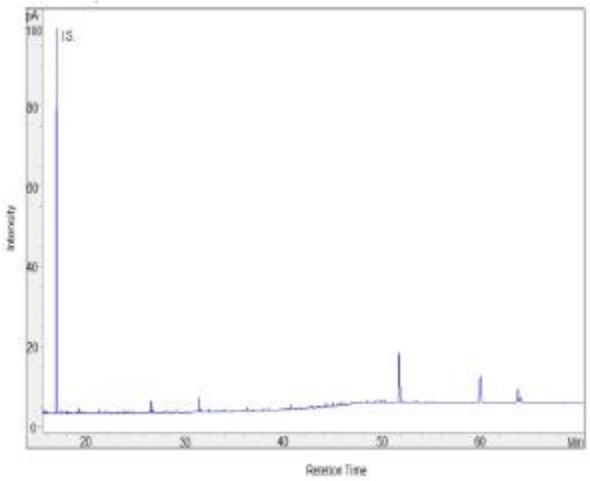

Sample CRA 20 R1

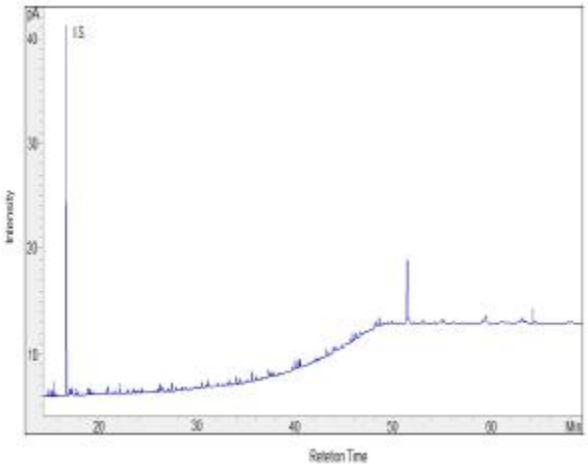

Sample CRA 18 R7

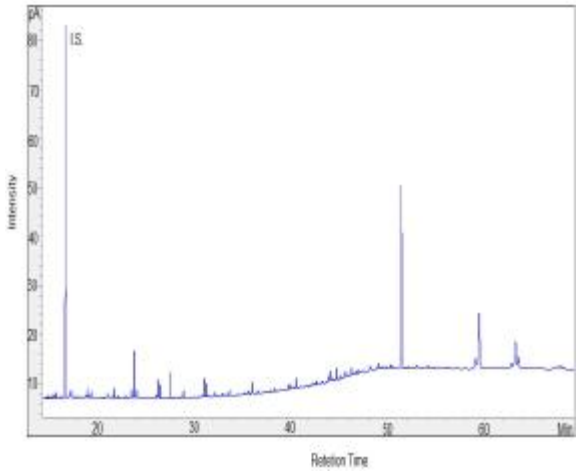

Sample CRA 20 R4

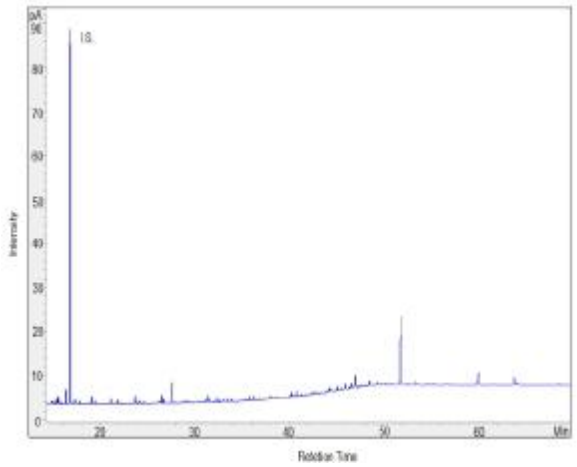

Sample CRA 19 R3

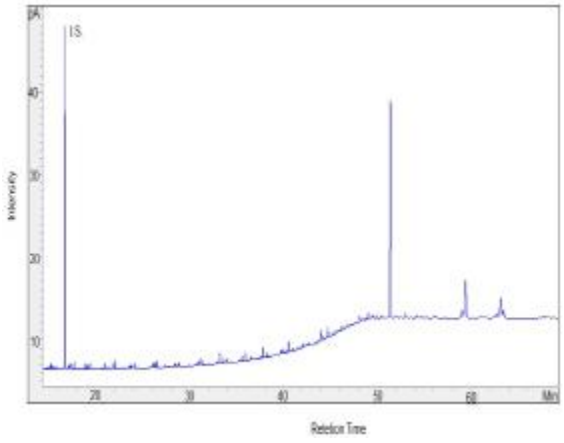

Sample CRA 22 R3

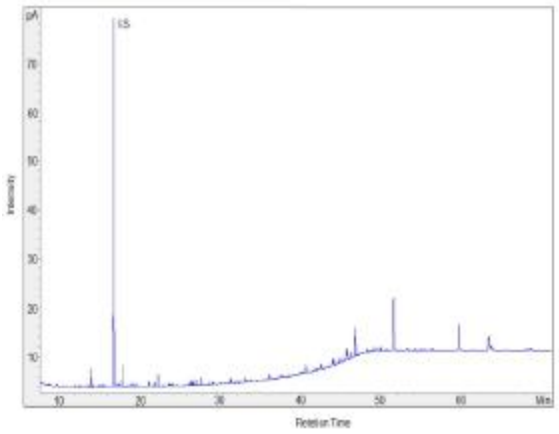

Sample CRA 22 R7

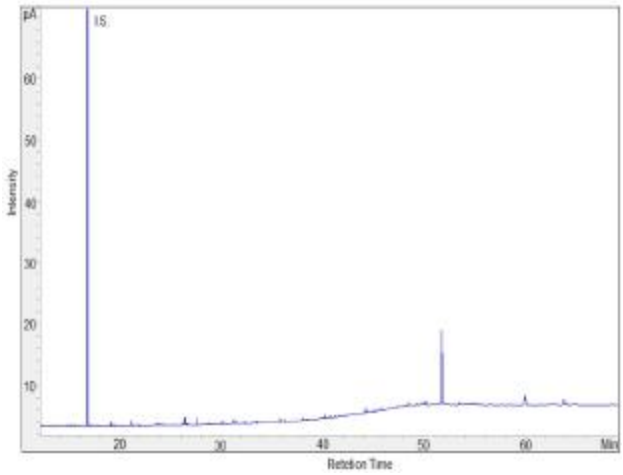

Sample CRA 26 R1

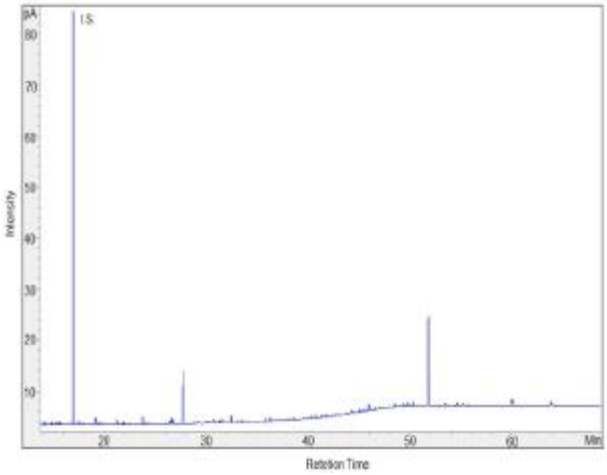

Sample CRA 23 R3

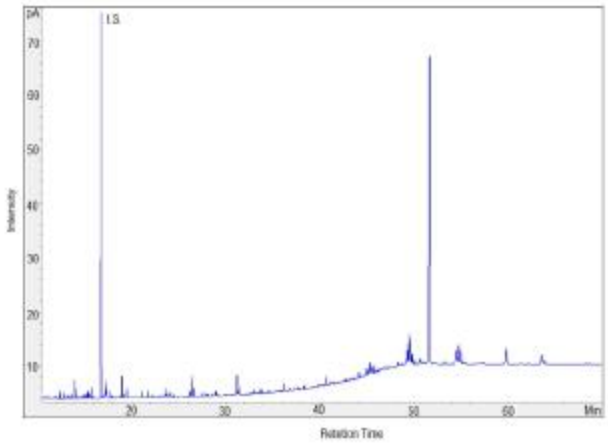

Sample CRA 26 R8

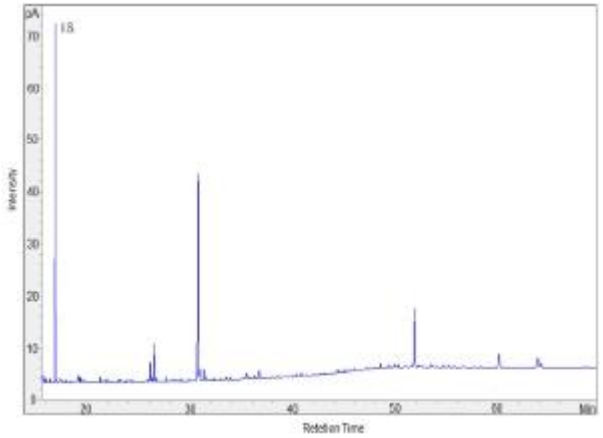

Sample CRA 24 R1

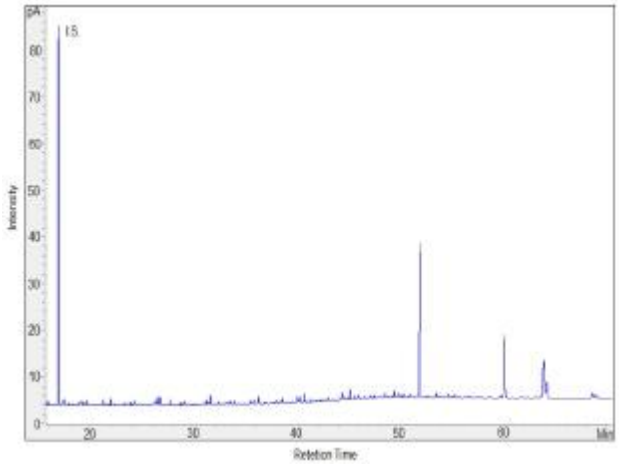

Sample CRA 29 R1

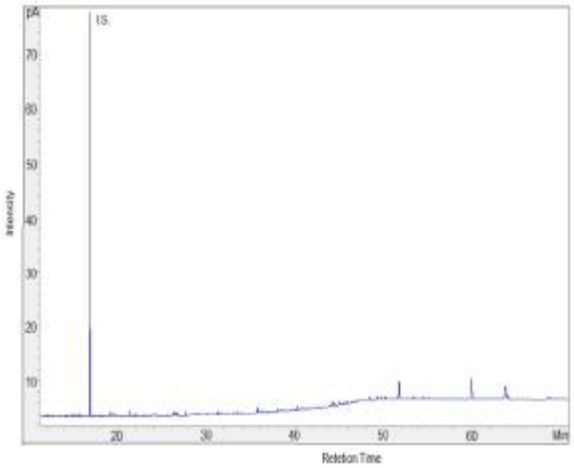

Sample CRA 30 R5

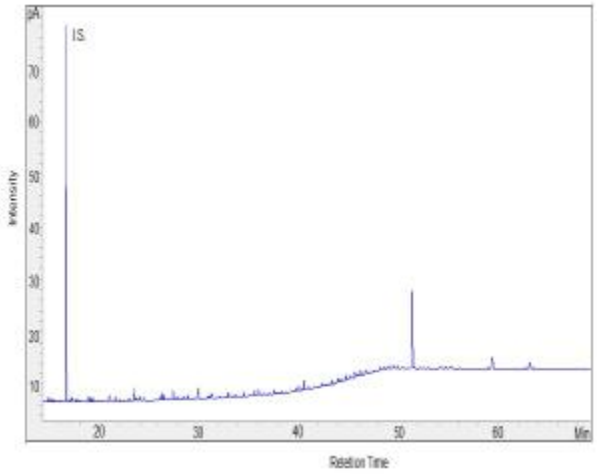

Sample CRA 36 R7

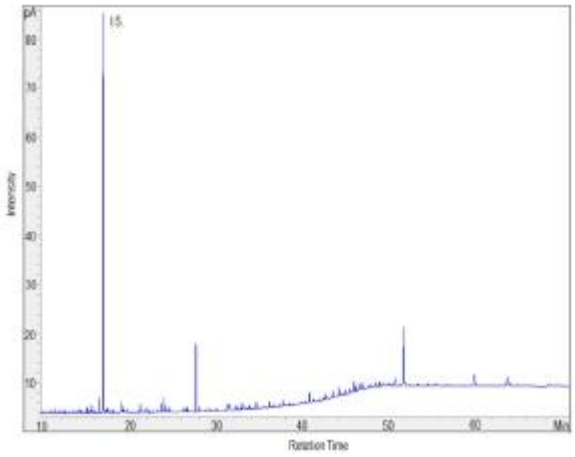

Sample CRA 32 R1

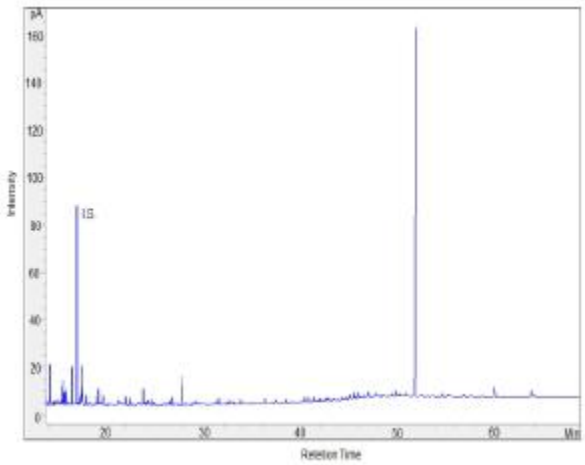

Sample CRA 39 R4

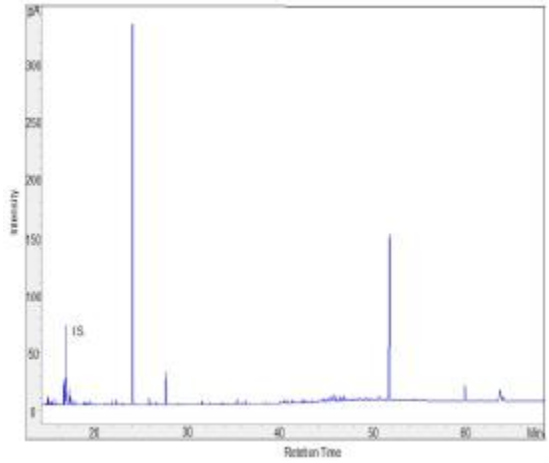

Sample CRA 33 R6

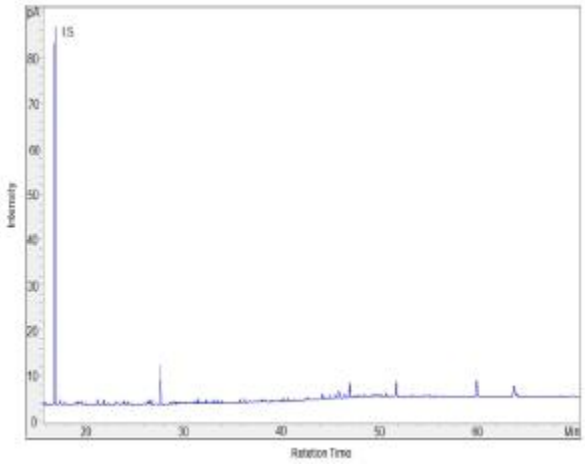

Sample CRB 2 H3

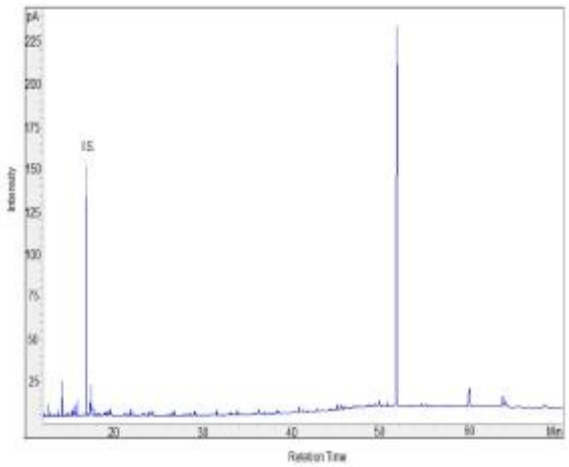

Sample CRB 2 R6

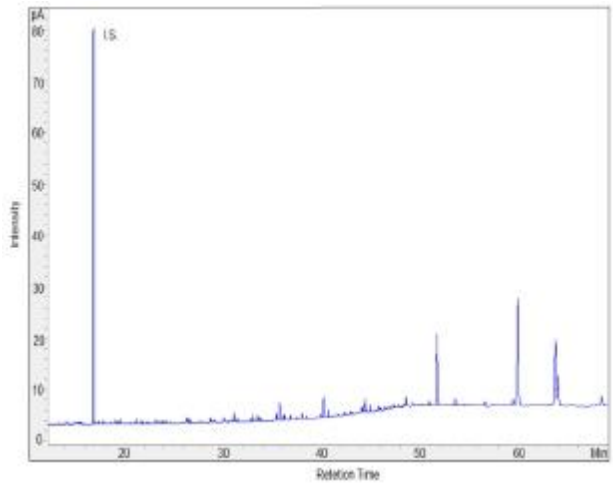

Sample CRB 5 H3

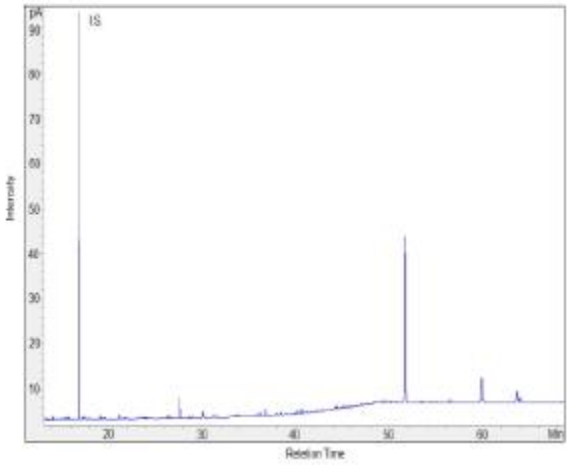

Sample CRB 3 H4

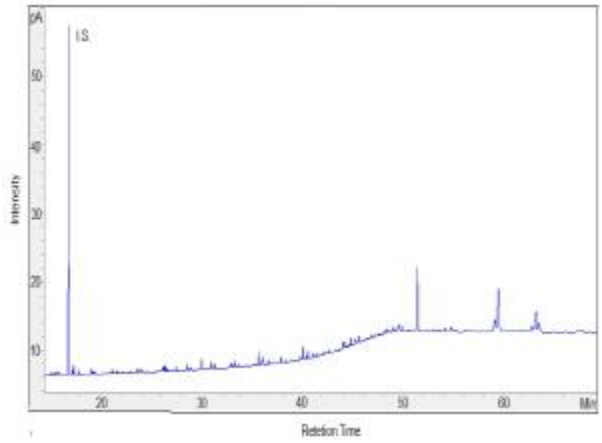

Sample CRB 5H6

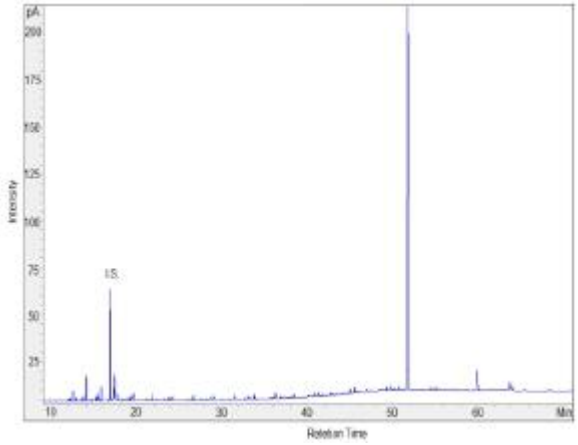

Sample CRB 4H3

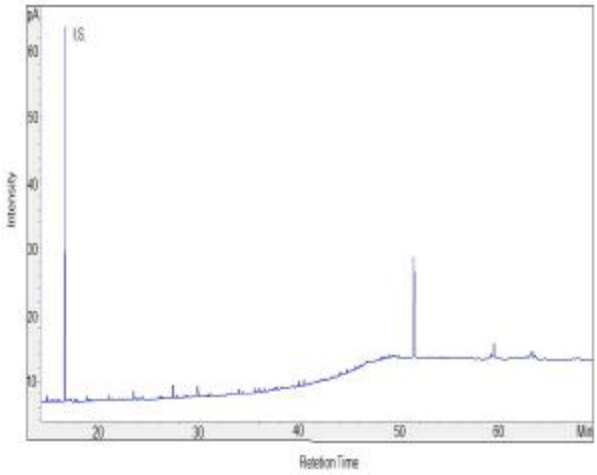

Sample CRB 6H4

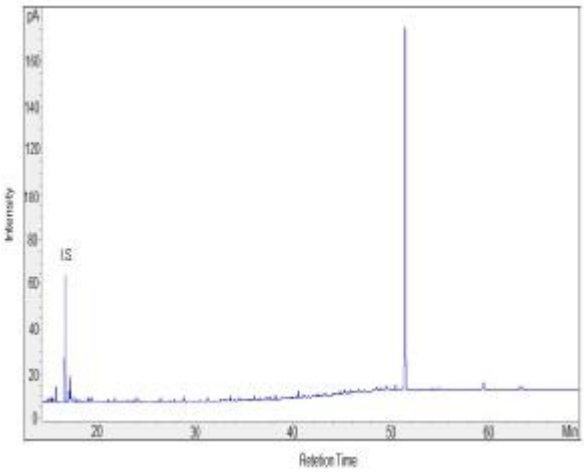

Sample CRB 7H1

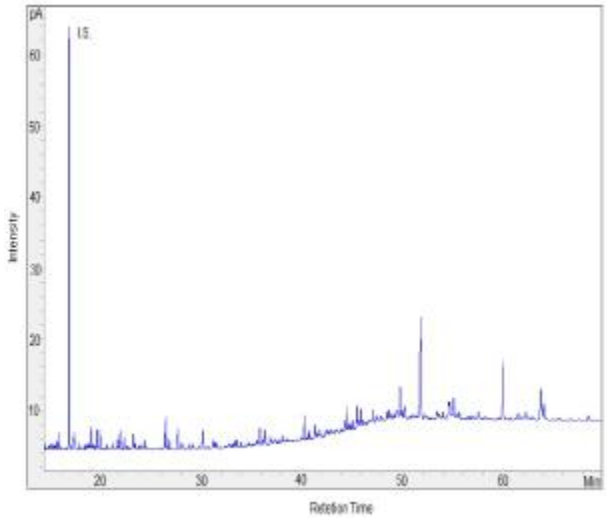

Sample CRB 8H3

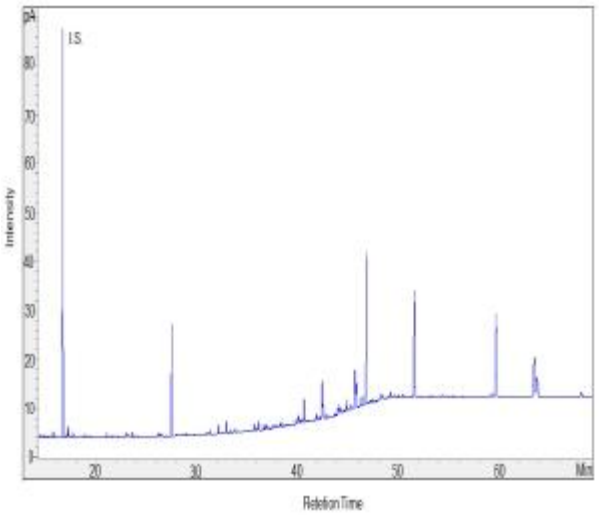

Sample CRB 7H3

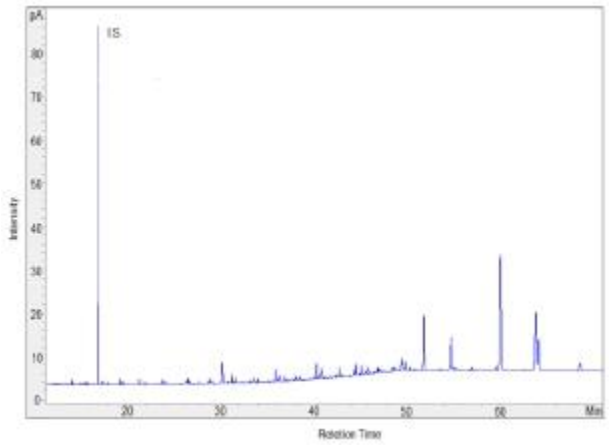

Sample CRB 9H3

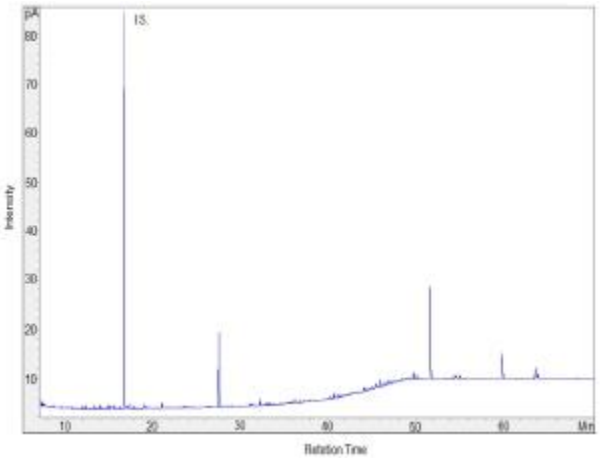

Sample CRB 7H5

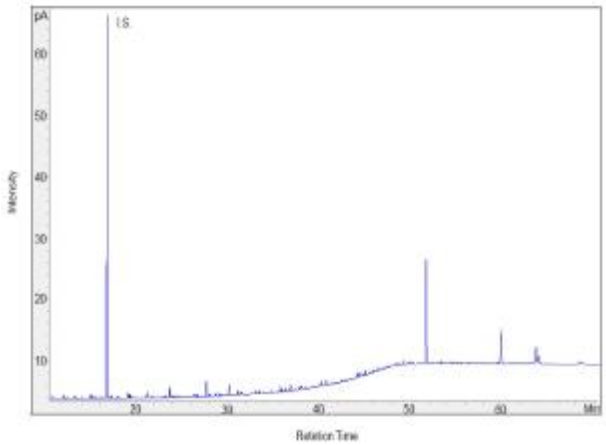

Sample CRB 10H3

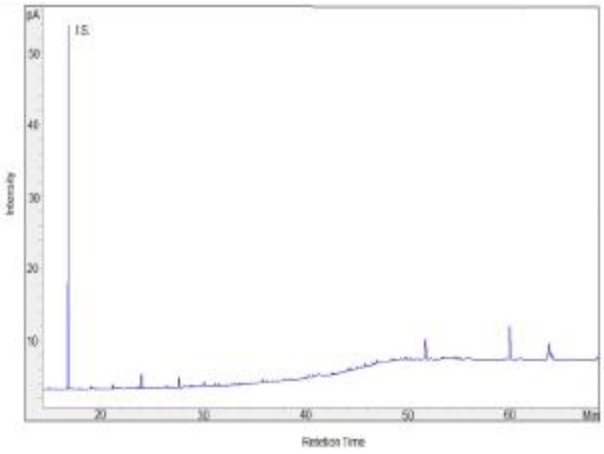

Sample CRB 11 H3

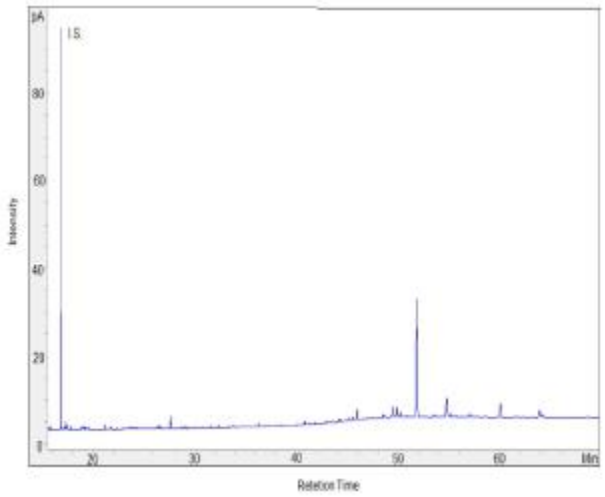

Sample CRB 13H5

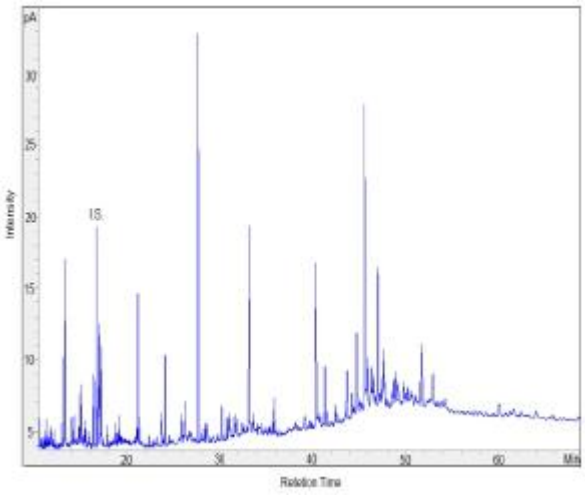

Sample CRB 11H6

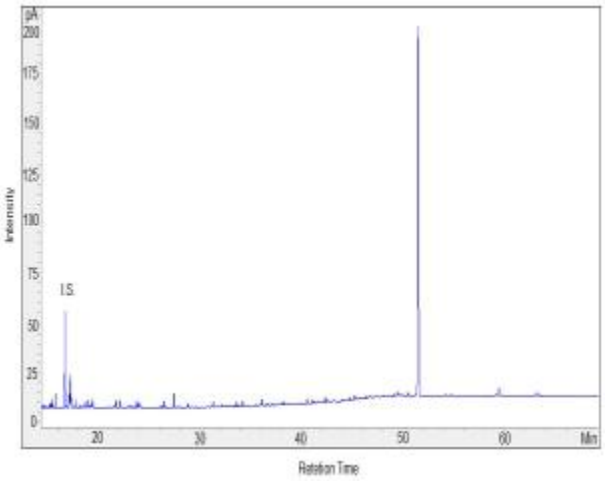

Sample CRB 14 H3

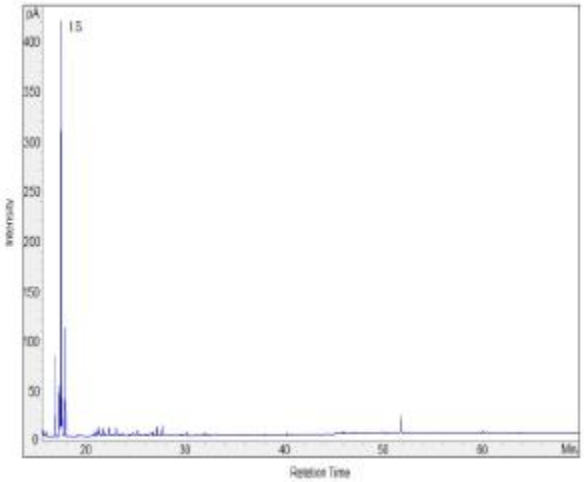

Sample CRB 12 H4

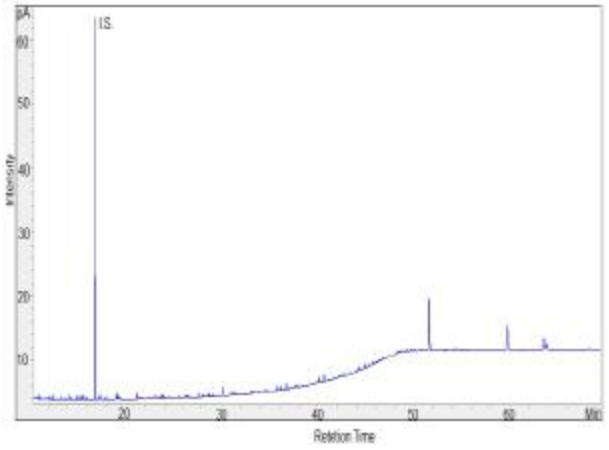

Sample CRB 15 H2

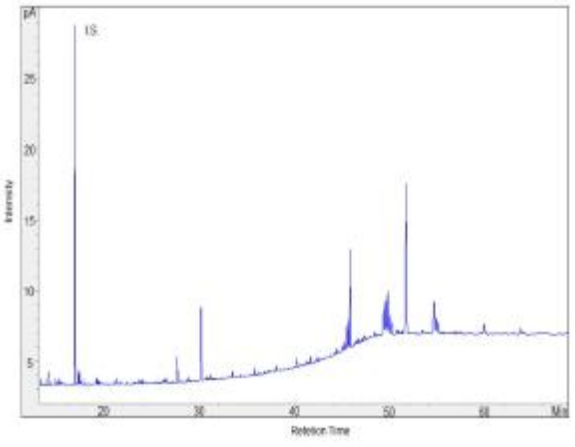

Sample CRB 16 H3

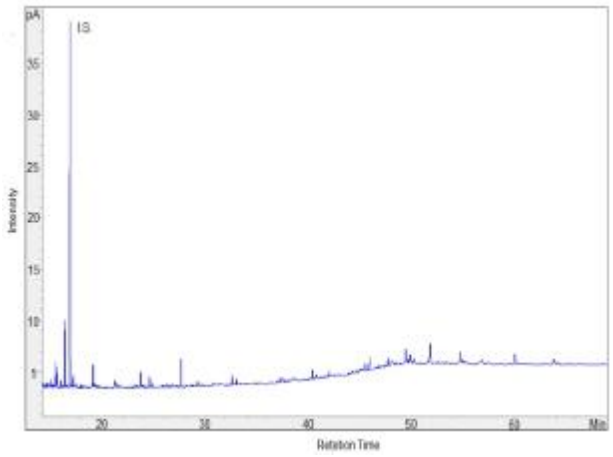

Sample CRB 18 H3

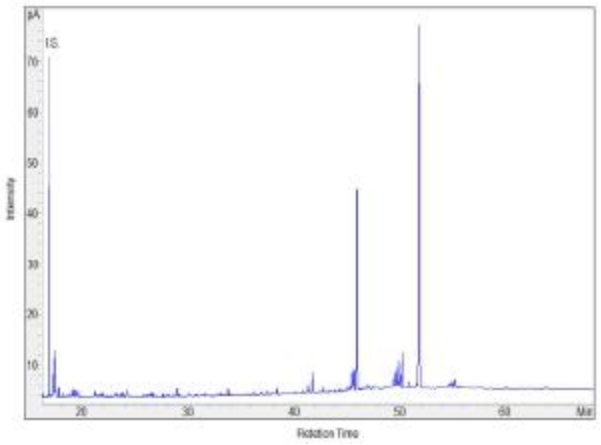

Sample CRB 17 H1

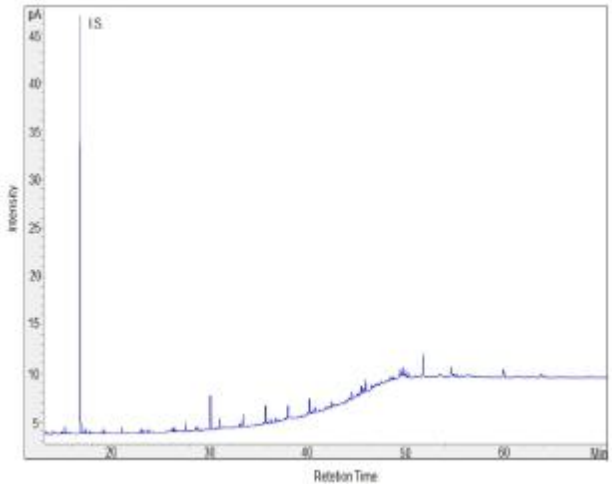

Sample CRB 19 H3

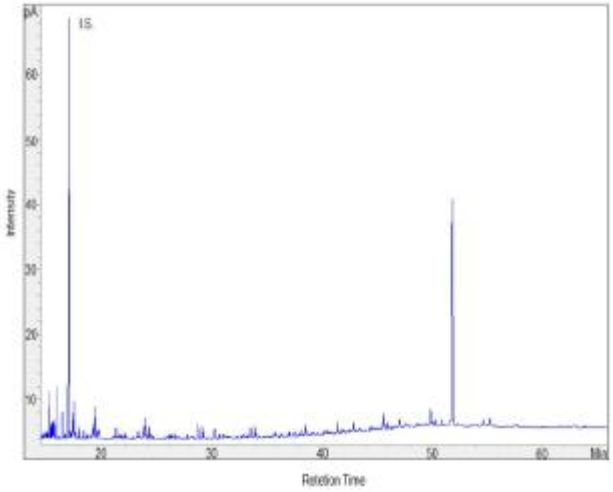

Sample CRB 17 H5

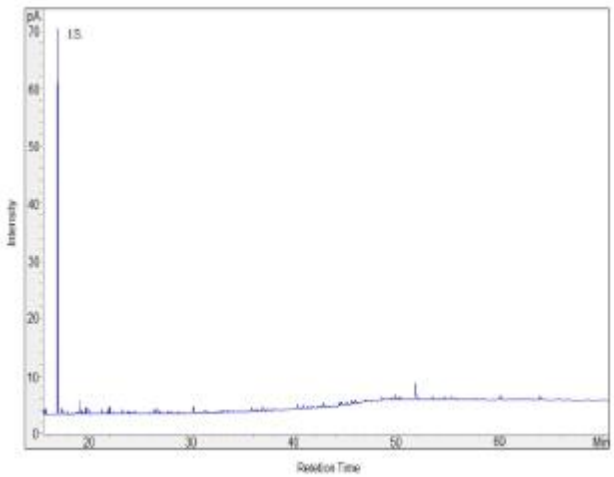

Sample CRB 19 H6

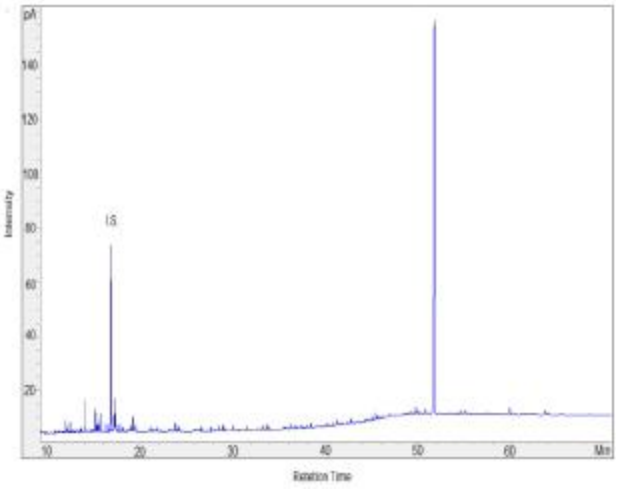

Sample CRB20 H6

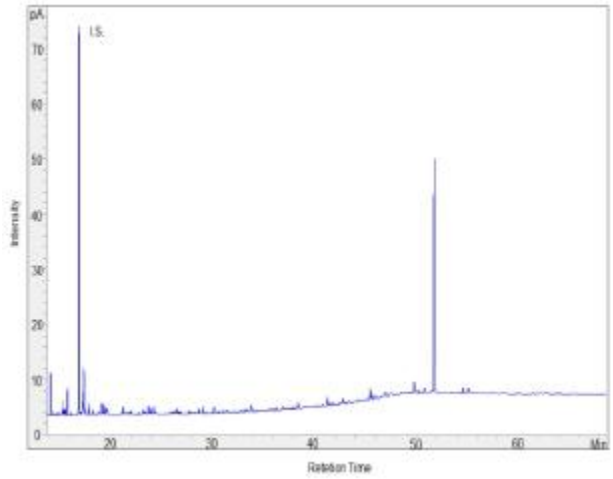

Sample CRB 22 H7

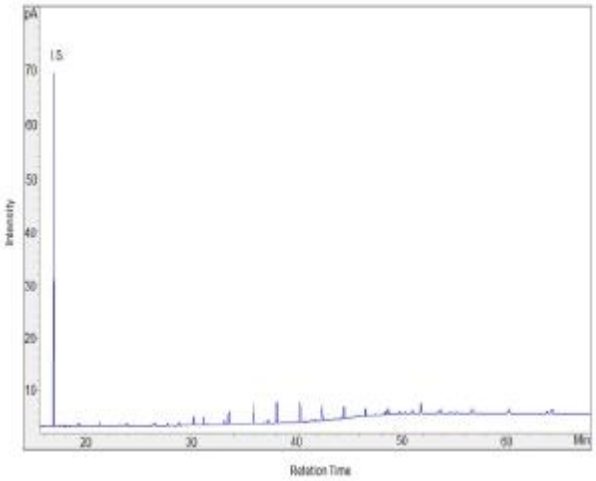

Sample CRB 21 H3

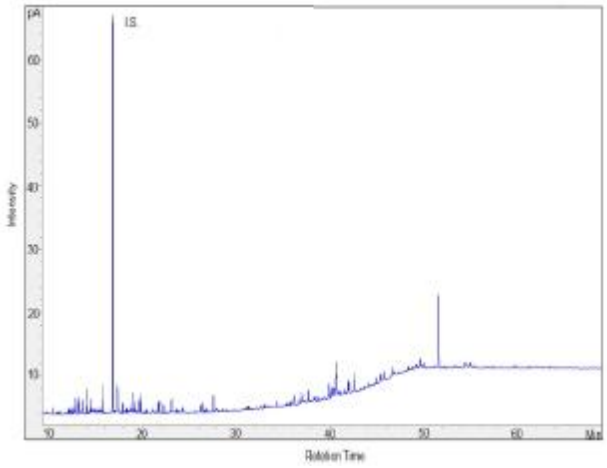

Sample CRB 23 H5

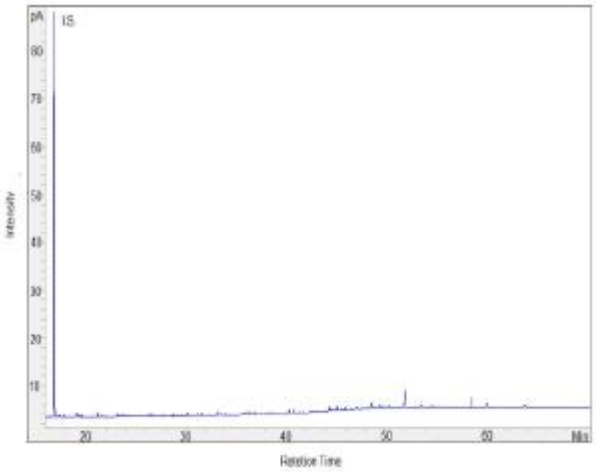

Sample CRB 21 H7

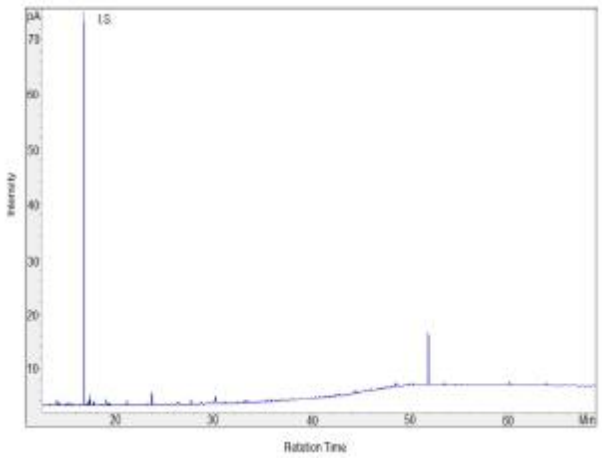

Sample CRB 24 H3

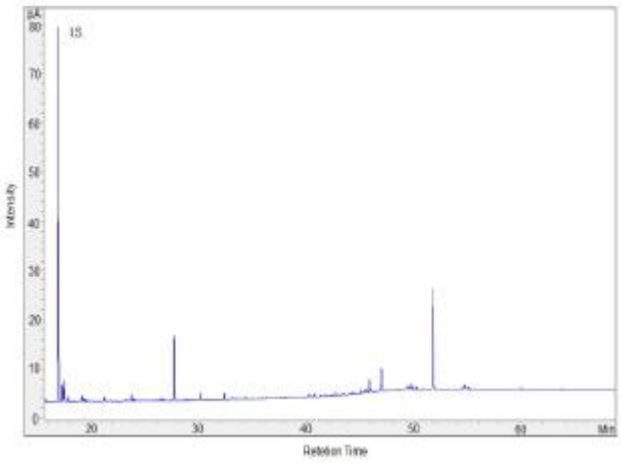

Sample CRB 25 H2

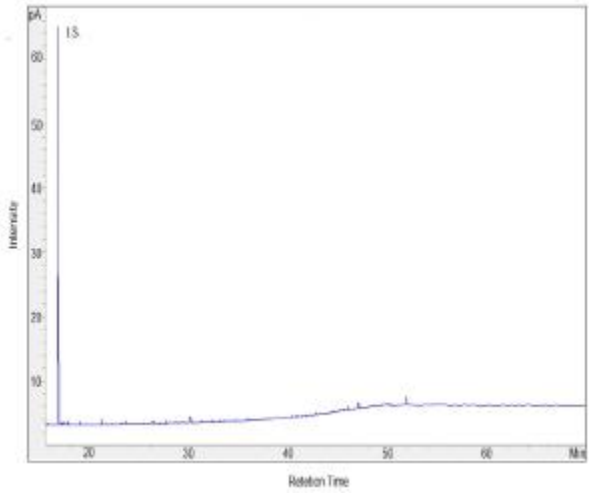

Sample CRB 26 H6

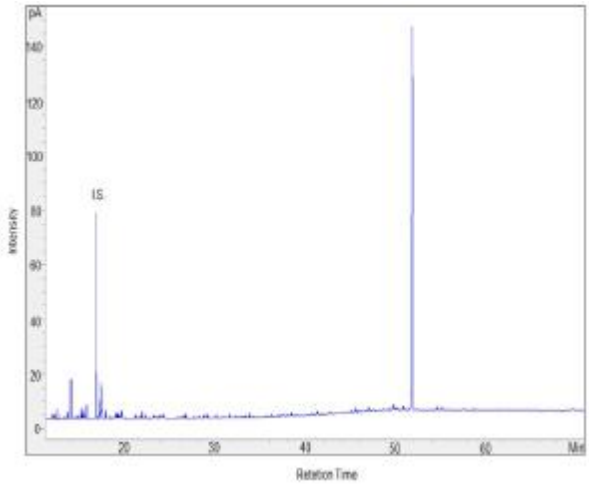

Sample CRB 25 H7

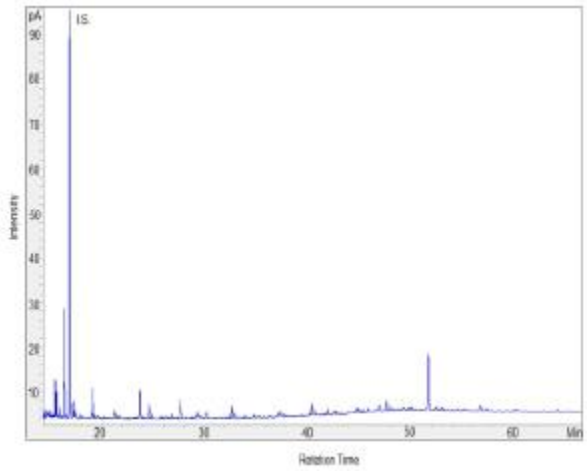

Sample CRB 27 H4

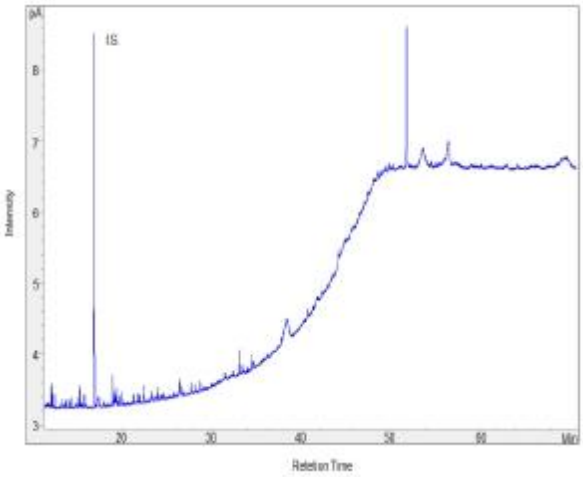

Sample CRB 26 H3

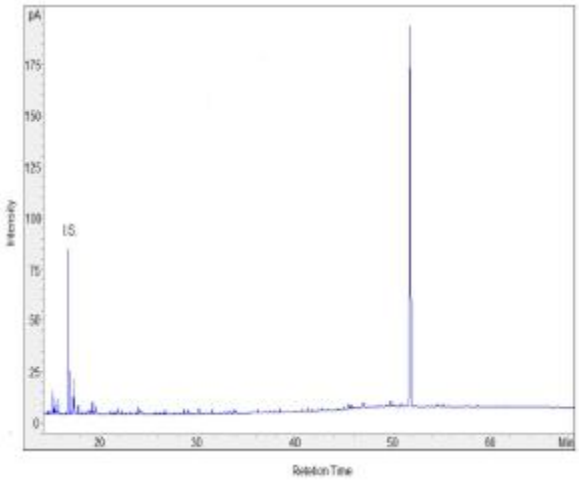

Sample CRB 27 H7

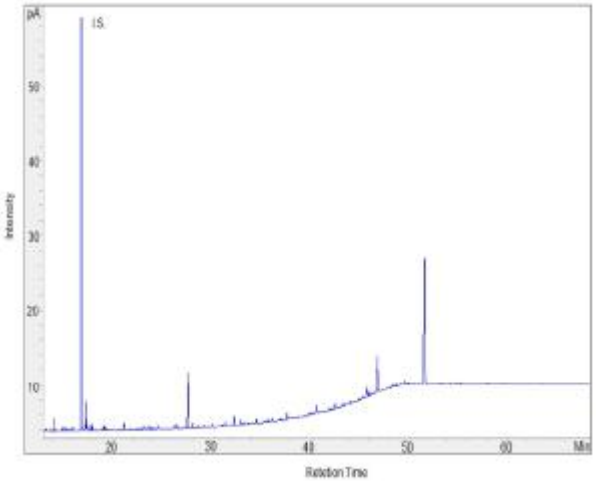

Sample CRB 28 H3

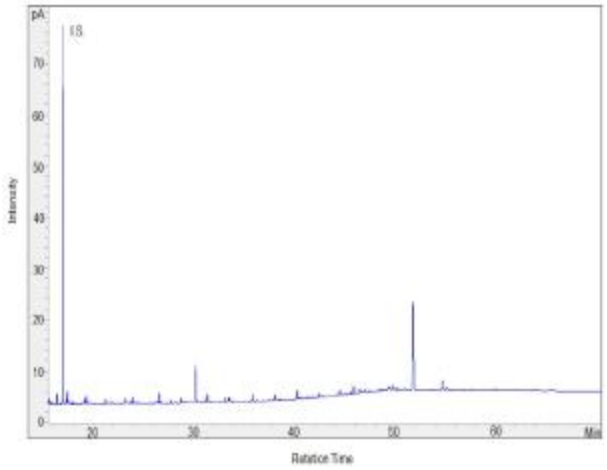

Sample CRB 30 H3

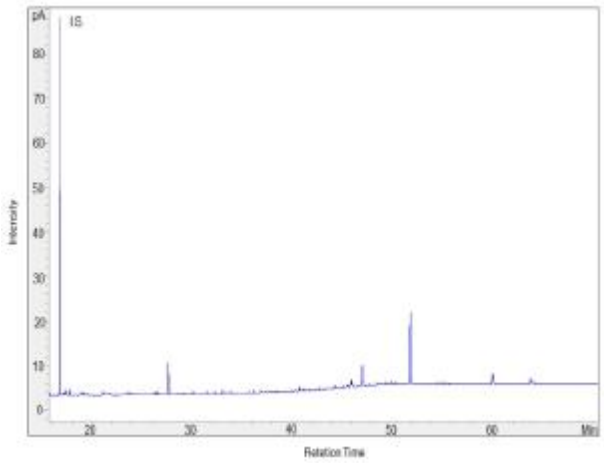

Sample CRB 28 H7

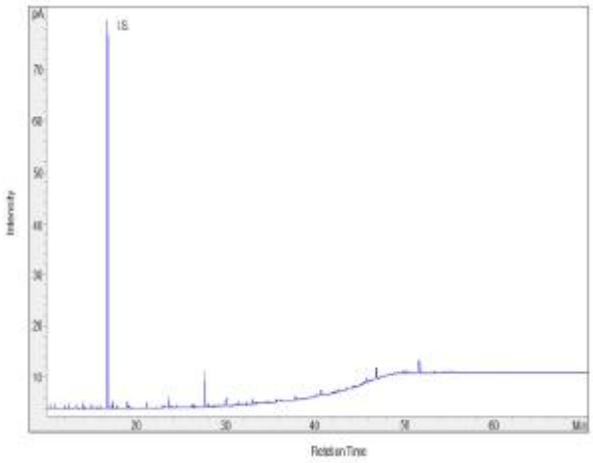

Sample CRB 30 H7

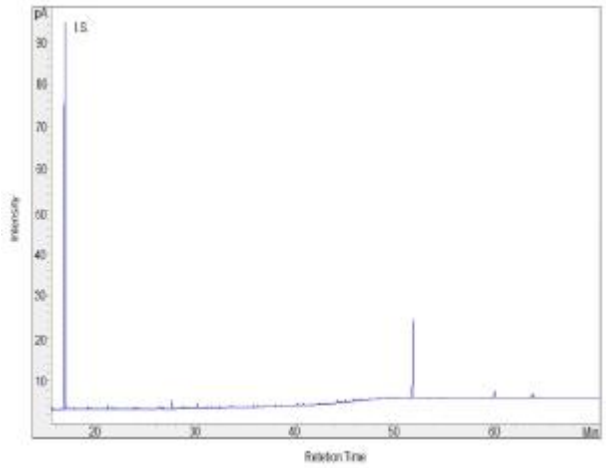

Sample CRB 29 H4

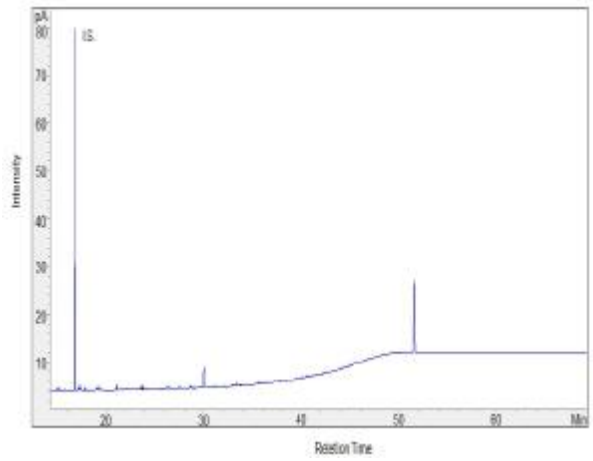

Sample CRB 31 H4

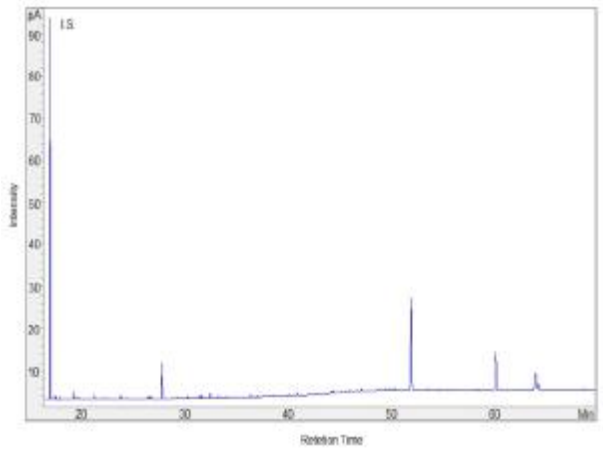

Sample CRB 32 H3

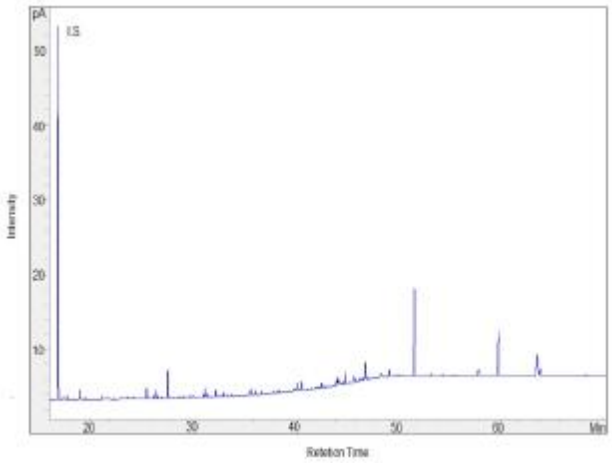

Sample CRB 32 H7

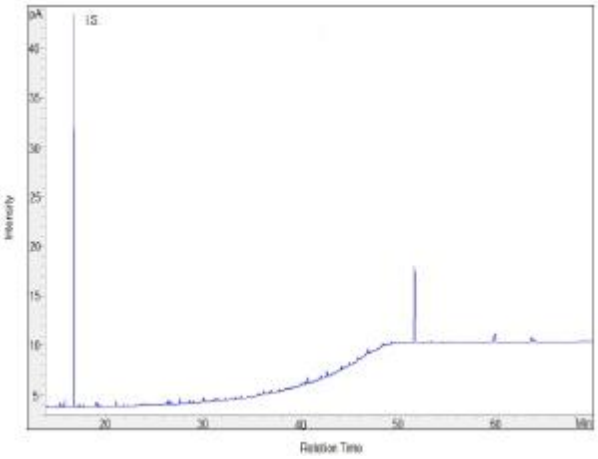

Sample CRB 33 H7